NUCLEAR IMPORT OF PURIFIED INFLUENZA A VIRAL RIBONUCLEOPROTEINS

by

YING-HUA BETTY SUN

B.Sc., The University of British Columbia, 2003

A THESIS SUBMITTED IN PARTIAL FULFILMENT OF
THE REQUIREMENTS FOR THE DEGREE OF

MASTER OF SCIENCE

in

THE FACULTY OF GRADUATE STUDIES

(Zoology)

THE UNIVERSITY OF BRITISH COLUMBIA

April 2006

ABSTRACT

The influenza A viral ribonucleoprotein (vRNP) is a macromolecular complex composed of nucleoproteins (NPs), heterotrimetric polymerase complexes (PA, PB1, PB2) and a single stranded viral RNA. Numerous nuclear localization signals (NLSs) have been identified on the vRNP proteins, including two on NP: a classical bipartite NLS (NPcNLS) and a classical nonconventional NLS (NPnNLS). However, the NLS responsible for vRNP nuclear import is not known. Previous studies have demonstrated that NP supports the nuclear import of *in vitro* assembled vRNA-NP complexes, but, whether NP also supports the nuclear import of authentic vRNPs is not known. Authentic influenza A vRNPs are assembled in the host nucleus and is complete with all four types of vRNP proteins. Unlike *in vitro* assembled vRNA-NP complexes, authentic vRNPs can, in theory, enter the nucleus using the NLS from any one of the four types of vRNP proteins. I have studied the nuclear import mechanism of authentic vRNPs in mammalian cells in order to determine the functional NLS responsible for vRNP nuclear import. My hypothesis is that authentic vRNPs enter the nucleus using a NP NLS. To test my hypothesis, I have purified authentic vRNPs from influenza A virus. The vRNPs had good structural integrity when visualized by high resolution electron microscopy. Using immunogold electron microscopy, I have shown that both NPnNLS and NPcNLS were exposed on the outer surface of authentic vRNPs; however, more exposed NPnNLS were found in comparison to NPcNLS. Both NLSs were functionally characterized using peptide competition and antibody inhibition experiments in digitonin-permeabilized cells and microinjected live cells. Only the microinjection studies provided consistent and convincing results. The digitonin-permeabilized cells were incompatible with purified vRNPs, as vRNPs bound strongly to nonspecific sites in the cytoplasm of the digitonin-permeabilized cells. Results from the microinjection studies

showed that nuclear import of authentic vRNPs could be inhibited by interfering with the NPnNLS nuclear import pathway, by either introducing excessive NPnNLS peptides or NPnNLS specific antibodies. By contrast, interfering with the NPcNLS nuclear import pathway using similar methods did not inhibited the nuclear import of vRNPs. In these studies, the vRNPs were visualized by indirect immunofluorescence using a monoclonal antibody against NP, because direct labeling of vRNPs to the cy3^{TM} fluorochrome abolished the vRNP nuclear import function. The results presented in this thesis demonstrated that while two NP NLSs are exposed on the surfaces of authentic vRNPs, the NPnNLS is the functional NLS responsible for vRNP nuclear import. These results show, for the first time that authentic vRNPs, purified from the influenza A virus, enter the nucleus of mammalian cells using the NPnNLS nuclear import pathway. This makes influenza A vRNP the second example, after the splicesomal uridine-rich small nuclear RNP (U snRNP), that an RNA-protein complex enters the nucleus by one of its protein NLS. Using the new results presented in this thesis, I have proposed a model for the nuclear import mechanism of influenza A vRNPs. These results open the possibility of using NPnNLS as a novel target for anti-viral therapeutics.

TABLE OF CONTENTS

LIST OF TABLES

LIST OF FIGURES

ABBREVIATIONS

3D:	three-dimensional
BSA:	bovine serum albumin
BRL:	buffalo rat liver
CCD:	charge-coupled device
CLAP:	chymostatin, leupeptin, antipoin and pepstatin
cNLS:	classical nuclear localization signal
cRNA:	complementary ribonucleic acid
DAPI:	4',6-diamidino-2-phenylindole
DTT:	dithiothreitol
EGTA:	ethylene glycol-O,O'-bis-[2-amino-ethyl]-N,N,N',N',-tetraacetic acid
EM:	electron microscopy
GDP:	guanosine diphosphate
GTP:	guanosine triphosphate
GBX:	green/blue/x-ray
HA:	hemagglutinin
HC:	HeLa cytosol
hnRNP:	heterogeneous nuclear ribonucleoproteins
H_o:	hypothesis

HRP: horse radish peroxidase

HVE: high volume extract

importin α1: karyopherin α2, RAG cohort 1, Rch1, NPI-3, SRP1α, IPOA1, QIP2

importin α5: karyopherin α1, NPI-1, SRP1, RCH2, IPOA5

kDa: kilodalton

LVE: low volume extract

M1: matrix 1

M2: matrix 2

m_3G: 5'-2,2,7-terminal trimethylguanosine

MDa: megadalton

MES: 2-(N-morpholino) ethanesulfonic acid

min: minute

MVM: minute virus of mice

NA: neuramidase

ncpl: nucleoplasmin

NE: nuclear envelope

NEP: nuclear export protein (also known as NS2)

NL: nuclear localization

NLS: nuclear localization signal

NP: nucleoprotein

NPC: nuclear pore complex

NPcNLS: NP classical bipartite nuclear localization signal (^{198}KRGINDRNFWRGENGRKTR)

NPNAS: NP nuclear accumulating signal (^{326}QLVWMACHSAAFEDLRVLS)

NPnNLS: NP non classical nuclear localization signal (^{1}MASQGTKRSYEQM)

NS1: non-structural protein 1

NS2: non-structural protein 2 (also known as NEP)

Nups: nucleoporins

p: probability

PA: polymerase A (A for acidic)

PB: polymerase B (B for basic)

PBS: phosphate saline buffer

PFA: paraformaldehyde

PMSF: phenylmethylsulphonylfluoride

RB: running buffer

RNP: ribonucleoprotein

rpm: revolution per minute

RRL: rabbit reticulocyte lysate

SB:	sample buffer
SD:	standard deviation
SDS:	sodium dodecyl sulphate
SDS PAGE:	SDS polyacrylamide gel electrophoresis
STAT:	signal transducers and activators of transcription
SV40:	simian virus 40
TBS:	Tris buffer saline
TEM:	transmission electron microscopy
TTB:	Towbin transport buffer
U snRNP:	uridine-rich small nuclear RNP
vRNA:	viral ribonucleic acid
vRNP:	viral ribonucleoprotein
χ^2	chi squared

ACKNOWLEDGEMENTS

First and foremost, I would like to thank my supervisor, Dr. Nelly Panté, for giving me the opportunity to purse a graduate degree in the University of British Columbia. Her knowledge and research expertise had shaped the research described in this thesis. I am gracious for her decision to finance the construction of expensive, custom anti-peptide antibodies used in my research, and to purchase a digital camera, which had made it possible to image live cell microinjections.

To my two committee members, Dr. Linda Matsuuchi and François Jean, I salute to you for providing me with such useful suggestions, and for giving me the motivation, support and encouragements when they are most needed.

I would also like to take the opportunity to thank Christiane Rollehagen, who had coached me at the beginning of my project, and Dr. Mike Whitlock for offering his expertise in statistical analysis. I would like to thank the UBC Bioimaging Facility and its entire EM support team: Dr. Elaine Humphrey, Garnet Martens, and Derrick Horne, for assisting me on the TEM. In particular, I would like to thank Dr. Elaine Humphrey, who generously allowed me to work on the TEM after working hours; thus, enabled me to gather some of the important data present in this thesis.

Finally, I would like to thank my parents, for giving me unconditional love and support from the start. It is because of them, that I have strived to be the best I can be and achieved all that I have achieved.

1 INTRODUCTION

A fundamental difference between eukaryotic and prokaryotic cell is that, the genetic contents of eukaryotic cell at interphase are stored in a nucleus enclosed by a double membrane nuclear envelope (NE). Consequently, communication between the nucleus and the cytoplasm is mediated by the nuclear pore complex (NPC). Protein nuclear transport has been well studied. However, the nuclear transport of supramolecular complexes, such as ribonucleoproteins (RNPs) is largely unknown.

The influenza A virus genome is segmented into eight helical viral RNPs (vRNPs). Each vRNP is made up of an RNA and four classes of proteins. During the influenza virus life cycle, the vRNPs must undergo bi-directional nuclear transport, such that, incoming vRNPs are imported into the nucleus and newly assembled progeny vRNPs are exported out of the nucleus. Nuclear import of influenza proteins has been well studied. However, very little is known about the nuclear import of influenza vRNPs. For this reason, this thesis is devoted to understand the nuclear import of influenza vRNPs, specifically, the nuclear localization signal (NLS) involved in this process.

1.1 NUCLEAR PORE COMPLEX STRUCTURE AND COMPOSITION

The NPC is a magnificent structural assembly. Its molecular mass is 55 megadalton (MDa) in yeast and 125 MDa in vertebrates. It has a functional diameter of 39 nm (Pante and Kann, 2002) and regulates all nuclear-cytoplasmic transport. It is one of the largest known biological machineries and its structure has been thoroughly reviewed (Pante and Aebi, 1994; Pante and Aebi, 1996b; Pante and Aebi, 1996a; Allen et al., 2000; Fahrenkrog and Aebi, 2003; Fahrenkrog et al., 2004). In addition, three-dimensional (3D) reconstructions of the NPC have been completed in vertebrate (Akey and Radermacher, 1993; Stoffler et al., 2003), yeast (Yang et al.,

1998) and *Dictyostelium* (Beck et al., 2004, reviewed by Pante, 2004). These reconstructions show that the overall NPC structure is conserved among eukaryotes.

The overall NPC structure appears as an octagonal cylindrical assembly composed of a cytoplasmic domain, a basic framework or spoke complex, and a nuclear domain (Figure 1A). Eight 35-50 nm long filaments extend from a 70 nm ring at the cytoplasmic domain (Figure 1A). Similarly, at the nuclear domain, eight 50-100 nm long filaments extend from a 70 nm nuclear ring and converge at a 30 nm terminal ring to form a nuclear basket (Figure 1A). In the center, a 52 MDa basic framework, sandwiched between the cytoplasmic and nuclear domain, is embedded in the NE. This basic framework is 90 nm tall (Stoffler et al., 2003) and has outer and inner diameters of 125 and 45 nm respectively (Figure 1A). Together, about 30 different nucleoporins (Nups), a total of approximately 400 individual proteins, form this elaborate assembly (Rout et al., 2000; Cronshaw et al., 2002, and Figure 1B).

The NPC is a nuclear gatekeeper (for review see Wente, 2000). Although small molecules under 9 nm and 20-40 kDa can diffuse through the NPC by passive diffusion, larger cargoes (folded proteins, protein complexes, RNAs and RNA-protein complexes) must travel through the NPC by signal-receptor mediated active transport (for reviews see Pante and Aebi, 1994; Gorlich and Kutay, 1999).

1.2 The Classical Nuclear Localization Signal Pathway

The number of identified nuclear transport pathway is rapidly growing (Figure 2, for review see Fried and Kutay, 2003). Among these, the classical nuclear localization signal (cNLS) pathway, which imports cargoes carrying a cNLS, is the best characterized. The cNLS is characterized by a patch of essential lysine (K) and arginine (R) amino acids and can be divided into two classes: (1) monopartite and (2) bipartite. The monopartite cNLS, exemplified in the simian virus 40

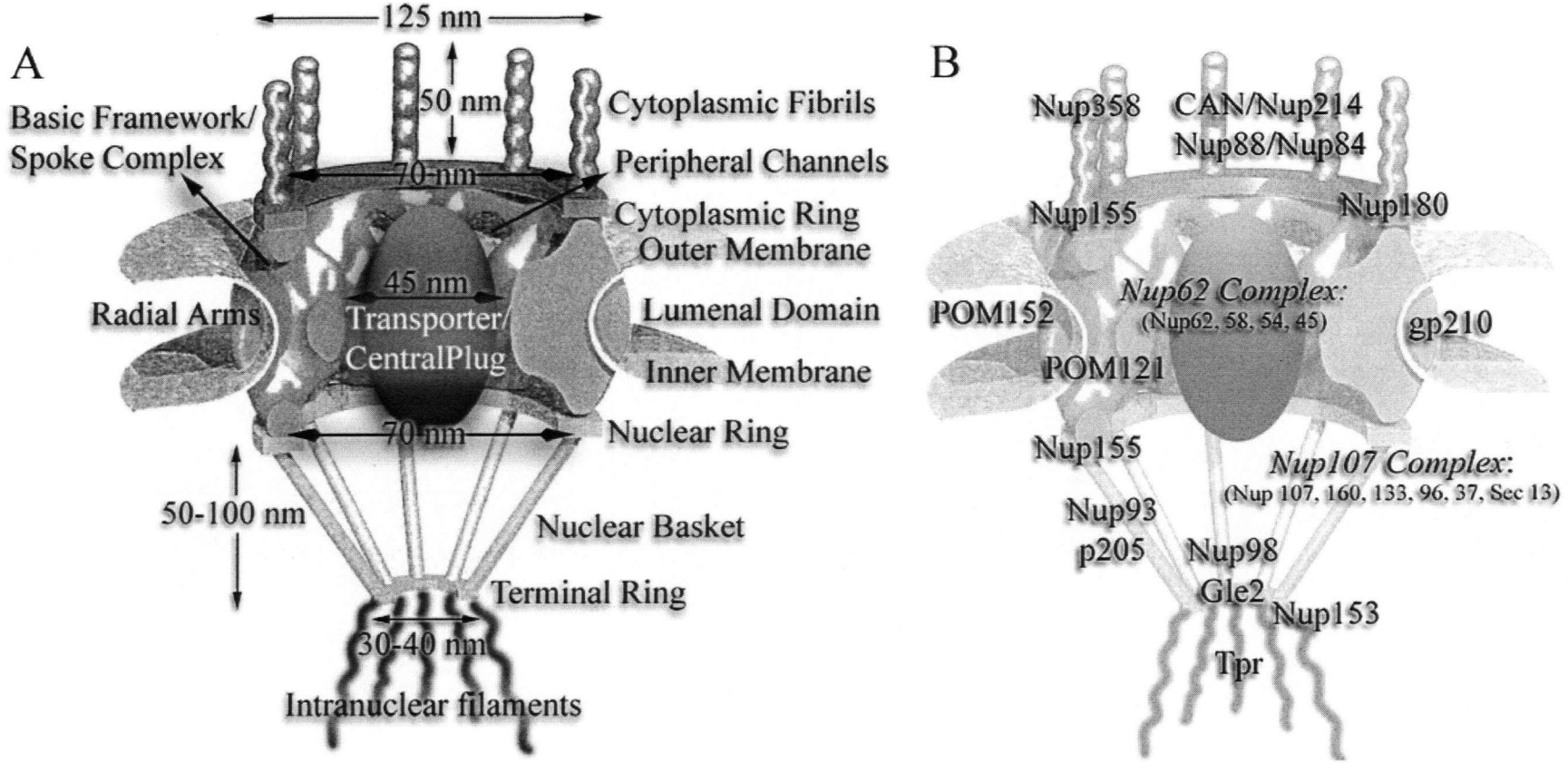

Figure 1: Structure of the NPC. (A) The architecture of the NPC and its major structural components. (B) Localization of the vertebrate nucleoporins (Nups). Figures adapted from Pante and Aebi, 1994 (courtesy of Nelly Panté). Note: A colored copy of this figure is available in the department of zoology at the University of British Columbia on 6270 University Boulevard, Vancouver, British Columbia, V6T 1Z4.

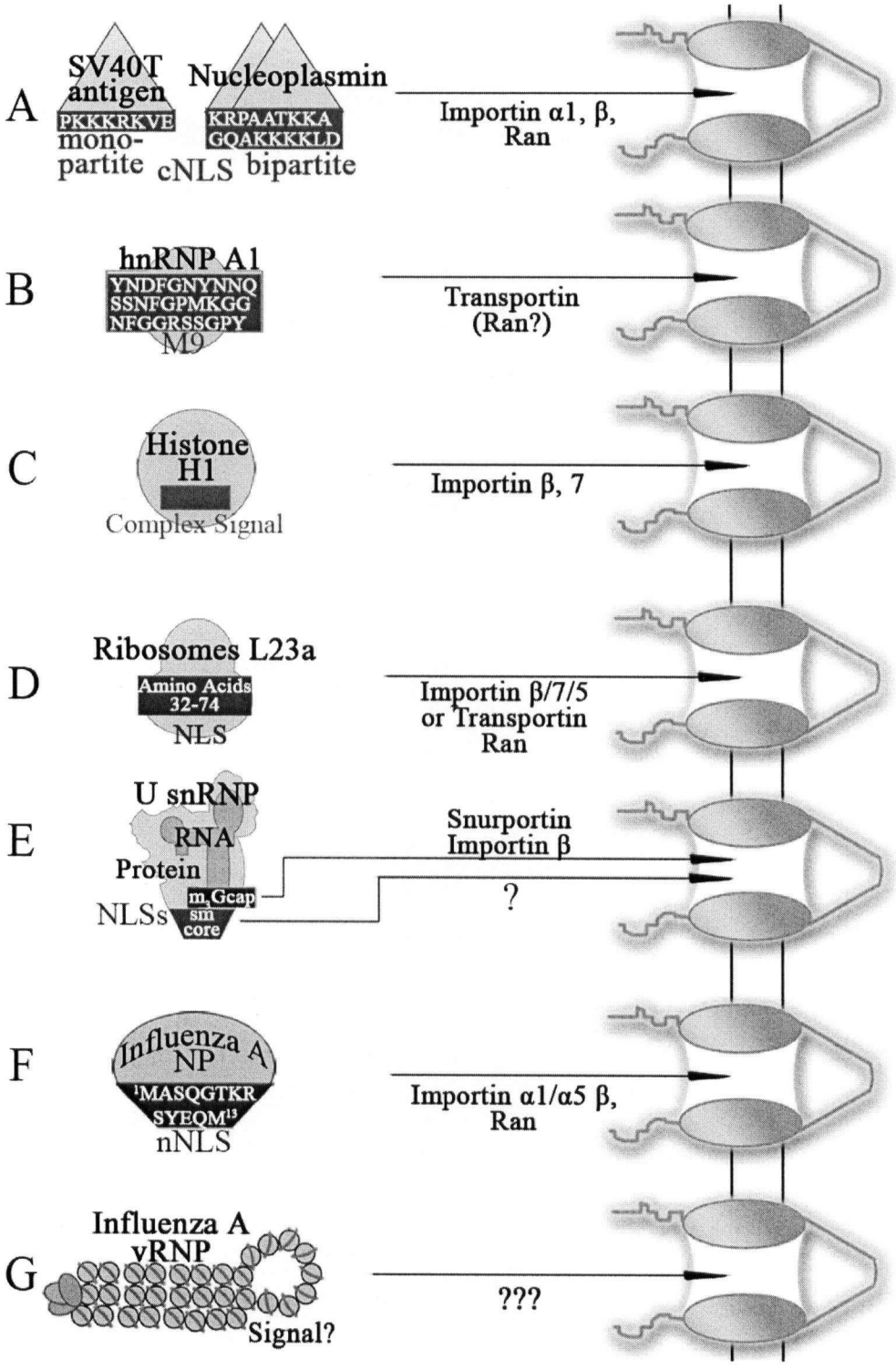

Figure 2: Nuclear import pathways. A schematic diagram that summarizes the signals and transport receptors for six different import pathways. (See text for details). Note: A colored copy of this figure is available in the department of zoology at the University of British Columbia on 6270 University Boulevard, Vancouver, British Columbia, V6T 1Z4.

(SV40) T antigen, has one stretch of amino acids rich in K and R (Figure 2A). In contrast, the bipartite cNLS, exemplified in the nucleoplasmin, has two stretches of essential K and R rich amino acids separated by a stretch of nonessential amino acids (Figure 2A).

The transport receptor for the cNLS pathway is importin β. It binds to the cNLS-carrying cargo through an adaptor molecule, importin α1. Once bound to importin α1, importin β interacts with the phenylalanine (F) glycine (G) repeats on the Nups and docks the cargo onto the NPC. The directionality of nuclear transport is established by a Ran-GTP/GDP concentration gradient: Ran-GTP is abundant in the nucleus while Ran-GDP is primarily present in the cytoplasm. Importin β uses this gradient to mediate cargo nuclear import. In the cytoplasm, in the presence of Ran-GDP, importin β forms a cargo-importin α1-importin β transport complex. When the complex is transported into the nucleus, it dissociates in the presence of Ran-GTP. At the end of this process, the cargo is released into the nucleoplasm while importin β, α1 and Ran are recycled to the cytoplasm.

1.3 Other Nuclear Import Pathways

To date, over 20 importin β-like transport receptors have been identified in higher eukaryotes (Fried and Kutay, 2003) and at least 6 different importin α isoforms (α1, α3-7) are found in humans (Macara, 2001). These transport receptors recognize and mediate the nuclear import of a wide range of NLS-containing cargoes, some of which I have summarized in Figure 2. Despite the overwhelming complexity that is often associated with individual nuclear import pathways, three common themes are emerging: (1) pathway diversity, (2) signal-receptor specificity and (3) signal-receptor redundancy.

Unlike the cNLS nuclear import pathway, some pathways, such as the uridine-rich small nuclear RNP (U snRNP) nuclear import pathway, are Ran-GTP independent (Figure 2E, and

Huber et al., 1998). Other pathways such as the heterogeneous nuclear RNP (hnRNP) A1 protein nuclear import pathway, have no adaptor molecule to bridge the cargo to the nuclear import receptor (Figure 2B, and Pollard et al., 1996). Instead, the glycine (G) rich NLS (M9) binds directly to the transport receptor, transportin, during hnRNP A1 protein nuclear import.

Nuclear import of macromolecules is also highly specific, and signal-receptor specificity in nuclear import is achieved in part by combinatorial diversity. Importin β, for example, has affinity for many different importin αs, each specific for its complementary NLSs. By pairing to different importin αs, importin β adopts the specificity required to transport a diverse range of cargoes (Goldfarb et al., 2004). As another example, importin β and importin 7, two receptors belonging to the importin β family of nuclear transport receptors, each can nuclear import several different cargoes (for reviews see Pemberton and Paschal, 2005); however, as a heterodimer, specifically imports H1 histones into the nucleus (Figure 2C, and Jakel et al., 1999; Bauerle et al., 2002).

Signal-receptor specificity is also enhanced by receptor functionality partition, where different domains on the same receptor receive different signals, allowing for multiple specificity to be obtained from the same receptor. The classic example is importin β, as illustrated above. However, another, lesser known example is importin α. This important family of adaptor molecule posses two discrete cNLS binding sites, one at the 2-4 armed repeats and another at the 7-8 armed repeats (Dingwall and Laskey, 1998; Melen et al., 2003). The elegant structural design provides a given importin α, such as the importin α1, the versatility of binding to either one bipartite cNLS, such as in nucleoplasmin, or simultaneously to two different monopartite cNLSs, such as the SV40 T antigen and the STAT1 transcription factor antigen (Sekimoto et al., 1997 and reviewed in Dingwall and Laskey, 1998; Gorlich and Kutay, 1999). Thus, allowing the same importin α to specifically transport several different cargoes at a time.

Signal redundancy, where a single cargo possesses more than one NLS, each sufficient for nuclear import, is common in nuclear import pathways. The U snRNP, for example, possesses two independent, functional NLSs, one located on the RNA m_3G cap (Fischer and Luhrmann, 1990) and a second, on the sm core protein (Figure 2E, and Fischer et al., 1993; Bordonne, 2000). Both NLSs are sufficient in transporting the U snRNP into the nucleus. Presently, the adaptor molecule and the nuclear import receptor for the NLS on the sm core protein is not known, but, the corresponding molecules for the NLS on the m_3G cap are identified to be snurportin and importin β respectively.

Similarly, receptor redundancy, where a single NLS can be transported into the nucleus by several distinct nuclear import pathways because it is recognized by several different transport receptors, is also common. This is illustrated for the ribosome protein L23a and the influenza A nucleoprotein (NP) nuclear import pathway (Figure 2D and F). For the L23a nuclear import pathway, either importin β, 7, 5 or transportin can recognize the L23a NLS and transport it into the nucleus (Figure 2E, and Jakel and Gorlich, 1998). Likewise, the influenza A NP nonconventional NLS (NPnNLS) can be recognized by either importin α1 or α5 to follow the cNLS pathway into the nucleus (Figure 2F, and Wang et al., 1997).

As illustrated in Figure 2, different cargoes use different pathways for nuclear import. At the moment, it is still unclear what is the nuclear import pathway used by the influenza A vRNP (Figure 2G). This is the central question that I will address in my thesis.

1.4 The Structure of Influenza A Virus and its Ribonucleoprotein Complex

The influenza A virus is the causal agent for the common flu. It is an orthomyxovirus containing eight segmented, single stranded viral RNAs (vRNAs) and is enclosed in a viral envelope (Figure 3A). The negative sense vRNAs are individually packaged into eight individual vRNP

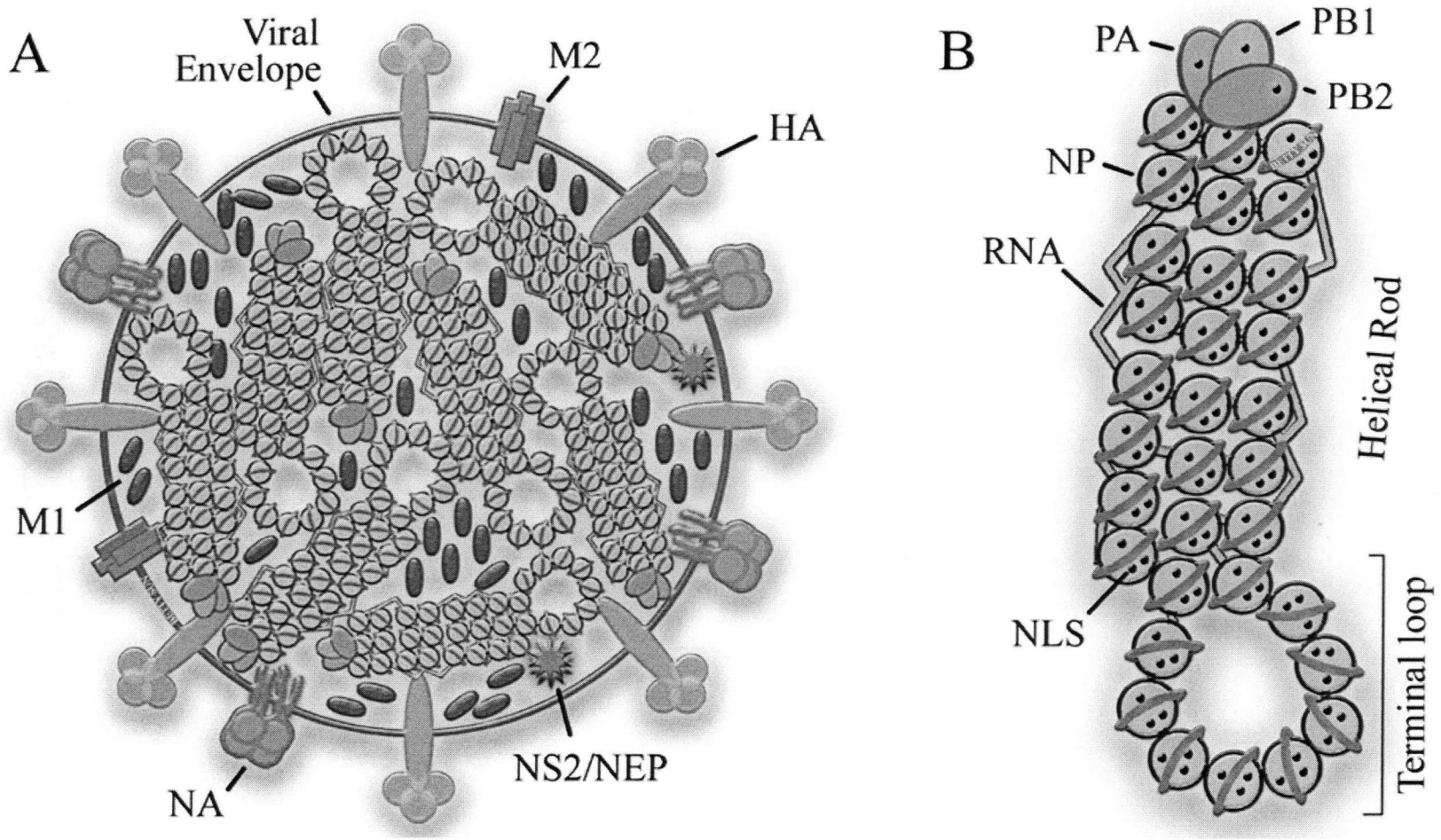

Figure 3: Structures of the influenza virus and its vRNP complex. (A) Cartoon of the influenza virus with labeled key viral structures and proteins. (B) Cartoon of the influenza vRNP. Putative NLS on vRNP proteins are indicated as black dots. Note: A colored copy of this figure is available in the department of zoology at the University of British Columbia on 6270 University Boulevard, Vancouver, British Columbia, V6T 1Z4.

with four viral proteins: the NP (56 kDa) and the heterotrimeric RNA polymerases PA (82 kDa), PB1 (86 kDa) and PB2 (86.5 kDa) (Figure 3B).

Electron micrographs of purified, negative stained, vRNP complexes reveal a circular terminal loop coiled into a helical rod (Jennings et al., 1983). The terminal loop has a constant diameter of 15-20 nm, while the length of the helical rod varies between 50 and 130 nm depending on the length of the vRNA (Pons et al., 1969). Recently, a mini recombinant vRNP of 248 nucleotides (a size that is 3-9 times smaller than authentic vRNPs) has been reconstructed in 3D (Area et al., 2004). This reconstruction resolves the terminal loop and the polymerase complex that normally sits on the tip of the helical rod (Murti et al., 1988; Martin-Benito et al., 2001; Area et al., 2004). However, the reconstruction, limited by the length of the vRNA, is unable to resolve the helical rod.

The influenza vRNP morphology is analogous to the "beads on a string" model of the nucleosomes. Specifically, the sugar-phosphate backbone of the vRNA associates with the RNA binding regions on NP (Albo et al., 1995) so that the RNA wraps around the protein with the bases exposed to the outside (Baudin et al., 1994). Approximately 25 nucleotides wraps around each NP (Jennings et al., 1983). Thus, given that each influenza vRNA is approximately 890-2341 nucleotides long (Nagata et al., 2002), each vRNP has approximately 36-94 NP associated to it.

The influenza vRNP is anchored to the viral envelope by matrix 1 (M1) proteins (Figure 3A). This 28 kDa, multifunctional protein, is the most abundant protein in the virus and each virion is estimated to have 3000 copies. Structurally, M1 is expected to form helical fibers in the virion (Harris et al., 2001). Furthermore, the protein has an N-terminal membrane binding domain and a C-terminal vRNP binding domain (Baudin et al., 2001) as well as two RNA

binding sites, a Zinc finger motif and a N-terminal NLS (Elster et al., 1997; Ye et al., 1999). These structure motifs allow M1 to link the vRNP to the viral envelope.

The non-structural protein (NS2) or later renamed to be the nuclear export protein (NEP) is 14.5 kDa in size, and can bind to the vRNP via M1. It has been postulated that, during vRNP nuclear export, a putative nuclear export signal, located on the N-terminal of the NEP, interacts with a number of Nups in order to mediate vRNP nuclear export (O'Neill et al., 1998; Neumann et al., 2000).

Influenza A virus has three membrane proteins (Figure 3A). They are the 58 kDa type I transmembrane glycoprotein, hemagglutinin (HA), the 11 kDa proton ion channel, matrix 2 (M2) and the 50 kDa type II transmembrane glycoprotein, neuramidase (NA). These three membrane proteins are essential for viral entry, uncoating and budding respectively.

Of the ten distinctive proteins synthesized in the host cell, one protein, the 26 kDa RNA binding protein, NS1, is not packaged into the mature virion (Figure 3A). NS1 is the interferon α/β antagonist and resides strictly in the host cell (for review see Garcia-Sastre, 2001).

1.5 The Influenza A Virus Life Cycle

The influenza A virus life cycle has been well studied (for reviews see Fodor and Brownlee, 2002; Nagata et al., 2002). I will outline here the key and well-understood steps in the viral life cycle, with an emphasis on nuclear transport.

The influenza A virus attaches to the host plasma membrane by means of HA-sialic acid glycoprotein association. It then enters the cell via receptor mediated endocytosis and internalizes into a host endosome (Figure 4, step 1, and Matlin et al., 1981; Sieczkarski and Whittaker, 2002). Inside the endosome, M2 mediates the acidification of the virion and leads to M1-vRNP dissociation. In addition, the endosome acidification activates the HA fusion peptide

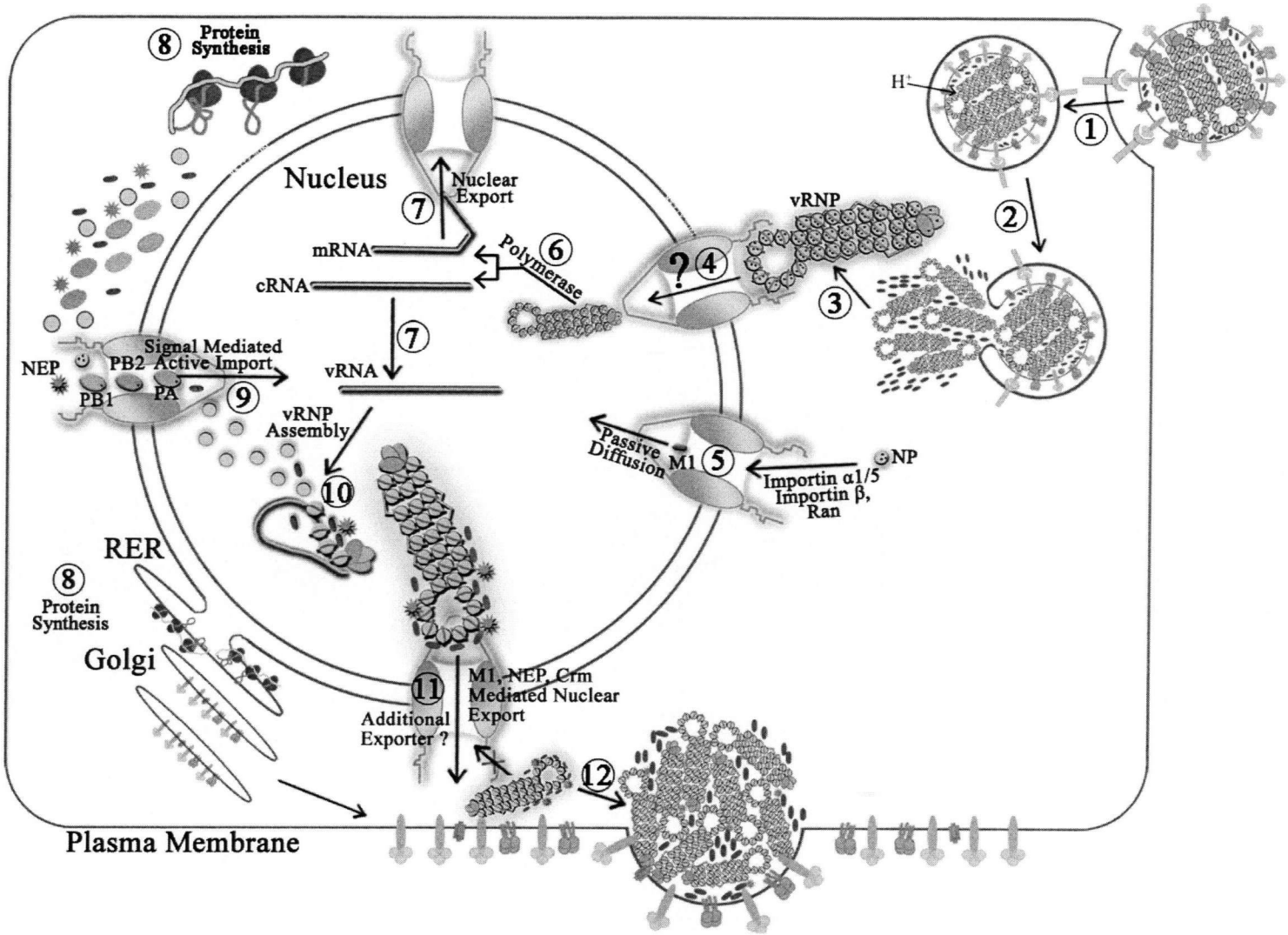

Figure 4: Influenza A virus life cycle. See text for details. For simplicity, in some of the steps, only 3 of the 8 vRNPs are shown. Black dots represent putative NLS and are illustrated in step 4, 5, and 9. Note: A colored copy of this figure is available in the department of zoology at the University of British Columbia on 6270 University Boulevard, Vancouver, British Columbia, V6T 1Z4

and stimulates HA mediated membrane fusion (Figure 4, step 2, and Doms et al., 1985), releasing the vRNPs, free of M1, into the cytoplasm (Figure 4, step 3). The influenza A virus is an unique RNA virus because, unlike the rhabdoviruses for example, the synthesis of influenza mRNA takes place in the host nucleus (Hsu et al., 1981). Consequently, one of the key steps in virus replication is to import the vRNPs into the nucleus (Figure 4, step 4). Currently, the details of this step are not known. For example, it is not known which vRNP component(s) is (are) involved in nuclear import, or which NLS(s) and host receptor(s) is (are) involved in this process. It is also not known whether the vRNP complex undergoes any degrees of disassembly prior to nuclear import. Addressing these questions is key to understanding the virus' life cycle.

Other viral proteins, including NP and M1 also undergo immediate nuclear import (for review see Whittaker et al., 1996b). Incoming NP enters the host nucleus via the cNLS pathway using the NPnNLS (Figure 4, step 5, and Wang et al., 1997, Cros et al., 2005). Incoming M1, on the other hand, is believed to enter the nucleus by passive diffusion (Figure 4, step 5).

Inside the nucleus, the viral polymerase uses the negative sense viral template to synthesize two types of single stranded, positive sense RNAs: the messenger RNAs (mRNAs) and the complementary RNAs (cRNAs) (Figure 4, step 6; for reviews see Fodor and Brownlee, 2002; Toyoda et al., 2002). The mRNAs are selectively exported into the cytoplasm to participate in viral protein synthesis while the cRNAs resides in the nucleus and function as the secondary template for genomic vRNA synthesis (Figure 4, steps 7 and 8).

vRNP assembly takes place in the nucleus. For this reason, shortly after their synthesis, NP, PA, PB1 and PB2 are imported into the nucleus via the cNLS pathway (Figure

4, step 9). Other viral proteins such as M1 and NEP, which function in the nuclear export of newly assembled vRNP, are also imported into the nucleus (Figure 4, steps 9). Once assembled (Figure 4, step 10), the vRNPs are exported to the cytoplasm (Figure 4, step 11) and are prevented from re-entering the nucleus by associating to M1. Details in the viral assembly process are not fully understood. A putative model involves assembled vRNPs migrating to regions of the host plasma membrane with inserted viral membrane proteins (Figure 4, step 12), and packaged into virions. Finally, NA cleaves the sialic acids on host glycoproteins, mediating the release of mature virions from the host.

In summary, during its life cycle, the influenza A virus utilizes the NPC at four individual occasions: (1) the nuclear import of incoming vRNPs and viral proteins, (2) the nuclear export of newly synthesized viral mRNAs, (3) the nuclear import of newly synthesized viral proteins and (4) the nuclear export of newly assembled vRNPs. This thesis addresses the first of the four nuclear trafficking steps, the nuclear import of incoming vRNPs.

1.6 Influenza A vRNP Nuclear Import

Structural and fluorescence studies support that assembled influenza A vRNPs are imported into the host nucleus (Martin and Helenius, 1991a; Martin and Helenius, 1991b; Kemler et al., 1994). The vRNP complex has at least six putative NLSs (Figure 5, and section 1.7). The complex is long, but is smaller than the 39 nm functional diameter of the NPC in diameter and height (section 1.4); thus, it can theoretically fit through the NPC. Using anti-NP antibodies, immunofluorescence studies have demonstrate that vRNPs localize to the host nucleus after being microinjected into the cytoplasm of tissue culture cells (Kemler et al., 1994). More recently, single particle tracking studies have captured the trajectory profile of a

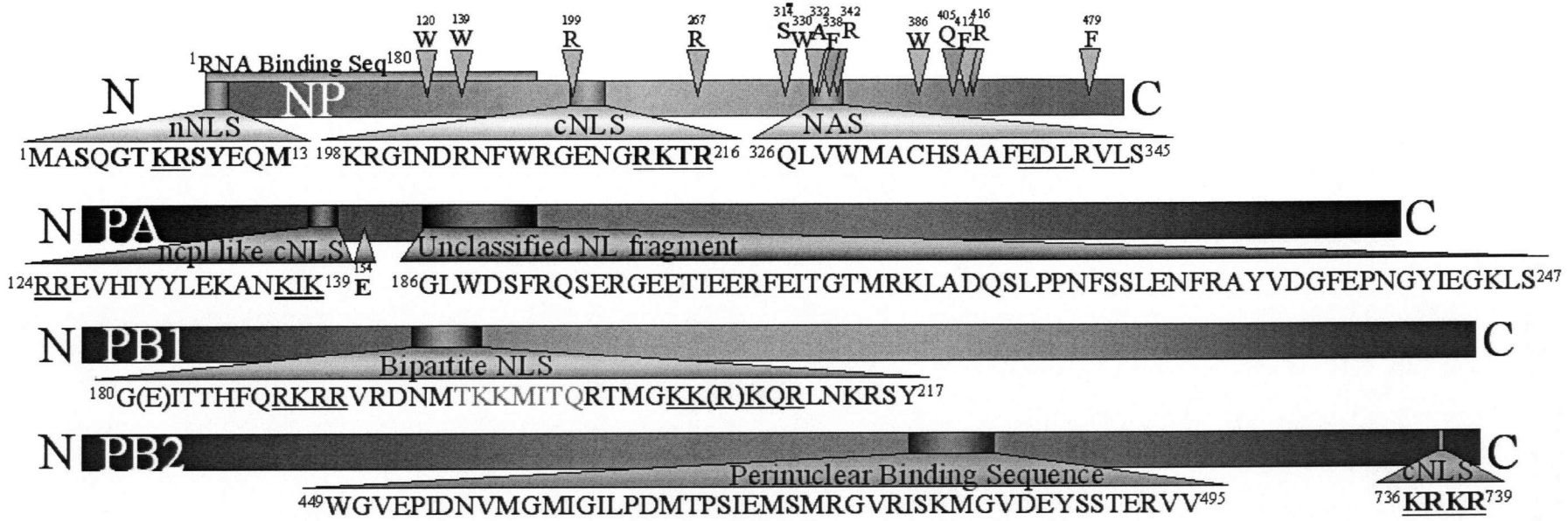

Figure 5: Schematic representation of the NLS and other key binding regions on the vRNP proteins. The protein sequence is based on influenza A virus, strain X:31. Superscript numbers indicate positions of the adjacent amino acid. Amino acids in bold have been demonstrated to be essential for nuclear import. Amino acids underlined are basic amino acids suspected to be important for nuclear import. Amino acids in brackets are amino acids different from the X:31 strain but are part of the NLS. Amino acids in grey are nonessential amino acids for nuclear import. On NP, yellow triangles indicate essential RNA binding amino acids, orange triangles indicate essential NP binding amino acids, and blue triangles indicate essential actin binding amino acids. The figure is a summary of the following papers: NP: Davey et al., 1985; Nieto et al., 1994; Albo et al., 1995; Neumann et al., 1997; Wang et al., 1997; Weber et al., 1998; Elton et al., 1999b; Medcalf et al., 1999; Bullido et al., 2000; PA: Nieto et al., 1994; PB1: Nath and Nayak, 1990; PB2: Mukaigawa and Nayak, 1991. The following abbreviations are used: NL=nuclear localization, ncpl=nucleoplasmin. (See text for details). Note: A colored copy of this figure is available in the department of zoology at the University of British Columbia on 6270 University Boulevard, Vancouver, British Columbia, V6T 1Z4.

single, fluorescently labeled vRNP, as it makes its way from the cytoplasm into the nucleus, in real time (Babcock et al., 2004).

Studies have also demonstrated that NP can mediate vRNA nuclear import. O'Neill et al. (1995) mixed fluorescently labeled influenza vRNA with recombinant NP at a 4.8NP:1vRNA molar ratio *in vitro*, a proportion that is 10 fold lower than what was estimated for authentic vRNPs (see section 1.4). Nevertheless, the authors found the fluorescently labeled vRNA to enter the nucleus of digitonin-permeabilized cells when supplemented with recombinant importin α1 and β. By contrast, in the absence of NP, fluorescently labeled vRNA was largely excluded from the nucleus. These results demonstrate that *in vitro* assembled vRNA-NP complex is imported into the nucleus using the cNLS pathway in an NP dependent process (O'Neill et al., 1995). Since then, it has been assumed that NP drives influenza vRNP nuclear import.

Very recently, this group has used the same approach to show that the nuclear import of *in vitro* assembled vRNA-NP complex is mediated by one of the NLS in NP (Cros et al., 2005). However, because the studies done by O'Neill et al. (1995) and Cros et al. (2005) use *in vitro* assembled vRNA-NP complexes, it is not know whether authentic vRNPs, assembled *in vivo*, also use this pathway.

Authentic influenza vRNPs is defined here as vRNPs that possess the same characteristics as those found in the active virus. That is, vRNPs with all four vRNP proteins (Figure 3B), assembled in the host nucleus in a M1 and vRNA mediated process, and forms a characteristic helical rod and terminal loop (Figure 3B and Huang et al., 2001). These key characteristics are absent in the *in vitro* assembled vRNA-NP complexes studied by O'Neill et al. (1995) and Cros et al. (2005). The vRNA-NP complexes have no polymerases and therefore their roles in vRNP nuclear import were not addressed. The vRNA-NP complexes were assembled in

the absence of M1 and the ultrastructure of the complex is not known. Finally, the recombinant NP used to form the *in vivo* complex was modified with a 37 N-terminal residue and a C-terminal histine tag. The impacts of these modifications are not known, but they open the possibility that the vRNA is carried into the nucleus by a few, loosely bound NPs.

Another approach to study vRNP nuclear import is indirect immunofluorescence microscopy using anti-NP antibodies (Martin and Helenius, 1991a; Martin and Helenius, 1991b; Kemler et al., 1994; Whittaker et al., 1996a; Neumann et al., 1997). The advantage of using anti-NP antibodies to visualize vRNP localization is that, unlike direct labeling methods such as GFP tagging and fluorochrome conjugation, no modification will be made to the vRNP itself. Thus, the intrinsic nuclear import characteristics of vRNP will be studied. However, this method limits from visualizing vRNP transport in real time. Furthermore, this method requires the assumption that vRNP localization can be inferred from NP localization.

Supporting the validly of using anti-NP antibodies to visualize vRNP localization is an elegant immunogold electron microscopy (EM) study done by Martin and Helenius (1991b). The authors showed that, at high resolution, anti-NP antibodies detected imported vRNPs as clusters of NPs in the nucleus, and not freely dispersed NP proteins. This suggest that NPs enter the nucleus in the form of assembled vRNP complexes and, more importantly, that these vRNPs can be visualized using anti-NP antibodies (Martin and Helenius, 1991b).

Several pieces of evidence suggest that M1 inhibits vRNP nuclear import and acid mediated M1 dissociation in endosomes eliminates this inhibitory effect (Martin and Helenius, 1991a; Kemler et al., 1994; Bui et al., 1996; Whittaker et al., 1996a). However, how M1 prevents vRNP nuclear import is not known. It is not known whether M1 blocks essential vRNP signals or whether the added size from M1 fibers wrapping around the vRNP in the cytoplasm exceeds the functional diameter of the NPC. Also, M1 is essential for vRNP stability; therefore an interesting

question to pose is: how does vRNP balance between structural stability and nuclear import activity?

1.7 NLSs On Influenza A vRNP Proteins

All four vRNP proteins have at least one NLS. As illustrated in Figure 5, some are cNLS but others are not. NP contains two cNLSs: a nonconventional (Neumann et al., 1997; Wang et al., 1997; Weber et al., 1998) and a bipartite cNLS (Neumann et al., 1997; Wang et al., 1997; Weber et al., 1998), abbreviated here as the NPnNLS and NPcNLS, respectively. The NPnNLS is 13-amino acid long and is located on the N-terminal (Figure 5). It has been demonstrated to be the dominating NP NLS on numerous occasions (Neumann et al., 1997; Wang et al., 1997; Weber et al., 1998), and very recently, it has been demonstrated to be the dominating NLS on *in vitro* assembled vRNA-NP complexes (Cros et al., 2005). In this last study, the authors showed that NPnNLS peptides can successfully inhibit the nuclear import of fluorescently labeled vRNA-NP complex in digitonin-permeabilized cells.

Two different importin αs can associate to the NPnNLS. They are importin α1, which binds the sequence ^{3}SxGTKRSYxxM^{13}, and importin α5, which binds the sequence ^{6}KRSYxxM^{13} (Wang et al., 1997); amino acids are abbreviated using the single letter amino acid code and 'x' can represent any amino acid. In the case of importin α5, the association is through the C-terminal NLS binding site (Melen et al., 2003).

The NPcNLS is 19-amino acid long and is located between amino acids 198 and 216 (Figure 5, and Weber et al., 1998). It is a weaker NLS, thought to be overshadowed by the NPnNLS, and only reveals its nuclear import properties when the NPnNLS is non-functional (Wang et al., 1997; Weber et al., 1998; Bullido et al., 2000). Details of this signal, including its nuclear import mechanism, have not been evaluated. Furthermore a paper by Cros et al. (2005)

has recently brought up some controversy. Using a similar approach as previous investigators (Wang et al., 1997; Weber et al., 1998; Bullido et al., 2000), Cros et al. (2005) replaced key residues in the NPnNLS with alanine. However, they did not find any nuclear import function in the NPcNLS. These new results directly contradict previous findings, and have placed the role of the putative NPcNLS up for reinvestigation.

Finally, a 19-amino acid long nuclear accumulating signal (NPNAS) near the C-terminus has long been a subject of debate (Figure 5). To date, the precise function of the NPNAS is not known. In *Xenopus* oocytes, the NPNAS clearly possesses nuclear accumulating properties (Davey et al., 1985); however, this nuclear accumulating property could not be demonstrated in mammals (Neumann et al., 1997; Wang et al., 1997; Bullido et al., 2000). For this reason, in this thesis, the NPNAS will not be classified with the other NP NLSs.

PA has two independent NLSs: a nucleoplasmin-like NLS between amino acids 124 and 139, and an unclassified NLS between amino acids 186 and 247, plus a critical glutamine residue at position 154 (Figure 5, and Nieto et al., 1994). Presently, the unclassified NLS is believed to be within a 62-amino acid long fragment, but the exact identity of this NLS is not known.

The other two polymerases each have one NLS: a 38-amino acid long bipartite NLS on PB1 (Nath and Nayak, 1990) and a 4-amino acid long monopartite NLS on PB2 (Mukaigawa and Nayak, 1991) (Figure 5). In addition, a 47-amino acid protein segment has been found on PB2 and is essential for perinuclear binding (Figure 5, and Mukaigawa and Nayak, 1991).

In addition to existing vRNP protein NLSs, novel NLSs can be present when the proteins assemble on the RNA and/or at the vRNP protein interface or on the influenza A vRNA. Currently, it is not known what is (are) the functional NLS(s) exposed on the surfaces of influenza A vRNPs.

1.8 NP NUCLEAR IMPORT

Of all vRNP proteins, the nuclear import of NP, particularly the NPnNLS pathway, is the best characterized (Figure 2F). First, NP binds to importin β via either importin α1 or α5 using the NPnNLS (O'Neill et al., 1995; Wang et al., 1997). Then, it docks onto the NPC, and is transported into the nucleus as in any other classical nuclear import pathway (Figure 4, step 5, and O'Neill et al., 1995). The NPnNLS is regulated by phosphorylation. A dephosphorylated serine at the 3rd amino acid in the NPnNLS mediates NP nuclear import while a phosphorylated serine at this position inhibits nuclear import (Figure 5, and Arrese and Portela, 1996; Bullido et al., 2000). NPnNLS phosphorylation is tightly regulated by the host kinases and phosphatases (Neumann et al., 1997; Bui et al., 2002) and the phosphorylation can be mimicked by substituting serine 3 for a negative amino acid such as, a asparate or a glutamate (Bullido et al., 2000).

Still other NP nuclear import pathways are present. Several studies have shown that the NPcNLS can nuclear import NP in the absence of the NPnNLS, suggesting that it is an independent pathway (Wang et al., 1997; Weber et al., 1998; Bullido et al., 2000). In addition, the adaptor importin α3 binds to NP at a presently unidentified site (Melen et al., 2003). Whether this suggests the presence of yet another NP nuclear import pathway has to be elucidated. Finally, the role of NPNAS is puzzling. The NPNAS is the dominating NLS in *Xenopus* oocytes (Davey et al., 1985). A deletion of this signal results in a 96% reduction from full nuclear import capacity in *Xenopus* oocytes, compared with a 67% reduction or 2% reduction of nuclear import for a deletion of the NPcNLS or NPcNLS plus NPnNLS respectively (Davey et al., 1985). However, this signal has no role in NP nuclear import in mammalian cells. Whether this difference is due to variations in the nuclear transport receptors subtypes between the mammalian and amphibian systems is not clear.

1.9 THESIS GOAL

Although many NLSs have been identified on vRNP proteins, the NLS(s) used by authentic vRNPs is (are) not known. As described in section 1.6, previous studies have shown that the influenza vRNA, when bound to the NP at 4.8NP:1vRNA molar ratio, can enter the nucleus of digitonin-permeabilized cells (O'Neill et al., 1995) using the NPnNLS (Cros et al., 2005). It is not known whether the NPnNLS also plays a vital role in the nuclear import of authentic vRNPs or whether other NP NLSs, such as the NPcNLS, mediate this process instead. For these reasons, **the goal of this thesis is to determine the functional NLS responsible for the nuclear import of authentic vRNPs.**

To achieve this goal, two NP NLSs, namely the NPnNLS and the NPcNLS are chosen to investigate their functional roles in vRNP nuclear import in mammalian cells. The NPNAS is not included in this investigation because, while the NPNAS is important in NP nuclear import in amphibolies oocytes (Davey et al., 1985), its role in mammalian cells has yet to be demonstrated (Neumann et al., 1997; Wang et al., 1997; Bullido et al., 2000). In contrast, both the NPnNLS and the NPcNLS are shown to be involved in NP nuclear import in mammalian cells (Neumann et al., 1997; Wang et al., 1997; Weber et al., 1998). Therefore, given that vRNP nuclear import will be studied in mammalian cells here, only the NPnNLS and NPcNLS will be studied.

SPECIFIC HYPOTHESIS: Authentic influenza A vRNP uses NP NLS for nuclear import.

SPECIFIC OBJECTIVES:

I) To biochemically purify authentic vRNPs that have good structural integrity from the influenza A virus (section 3.1).

II) To demonstrate that biochemically purified vRNPs are nuclear import competent in mammalian cells (section 3.2).

III) To determine whether putative vRNP NLSs (NPnNLS and NPcNLS) are exposed on the surfaces of authentic vRNPs using anti-NPnNLS and anti-NPcNLS antibodies by immunogold EM (section 3.3). (Note: Because mammalian cells will be used to assay vRNP nuclear import here, NPNAS was not studied.)

IV) To characterize vRNP nuclear import and the functions of putative vRNP NLSs using peptide competition and antibody inhibition experiments in digitonin-permeabilized cells (section 3.4) and in live mammalian cells (section 3.5).

1.10 Experimental Approaches

I) *Biochemical Purifications*: The methods for purifying influenza A vRNPs have been developed previously (Rochovansky, 1976; Kemler et al., 1994). It involves (1) disruption of the viral envelope with mild detergents to release viral proteins and vRNPs; (2) separation of the vRNPs from the rest of viral contents by ultracentrifugation in a glycerol density gradient; (3) fractionation of the gradient and assaying each fraction for vRNP; (4) pooling fractions containing vRNPs together and concentrating the purified vRNPs. In this thesis, vRNPs was purified following the same general procedure.

II) *Authenticity and Structural Validation:* Authenticity, as in the presence of every protein element, of biochemically purified vRNPs was validated by comparing the purified vRNP proteins to their known molecular mass by sodium dodecyl sulphate (SDS) polyacrylamide gel electrophoresis (PAGE) and by immunoblots using antibodies against specific vRNP proteins. Integrity, as in the fulfillment of all key structural characteristics, of purified vRNPs was validated by high resolution transmission electron microscopy (TEM) to show that, for example, purified vRNPs are not disassembled or degraded.

III) *Immunogold Labeling*: In order to identify which putative vRNP NLSs (NPnNLS and NPcNLS) are exposed on the surface of authentic vRNPs, purified vRNPs was immunolabeled using specific anti-NP NLS antibodies and colloidal gold-conjugated secondary antibodies. Then, vRNPs was visualized by high resolution TEM to determine whether the colloidal gold particles were bound to the purified vRNPs.

IV) *In Vitro Nuclear Import Assay*: Digitonin-permeabilized cells are a powerful tool widely used to study nuclear import. These cells have partially permeabilized plasma membranes but intact NE, allowing researchers to study the nuclear import processes *in vitro* (Figure 6A). This assay has been used to successfully characterize a number of nuclear import pathways in the past (Gorlich et al., 1994; O'Neill et al., 1995; Pollard et al., 1996; Jakel and Gorlich, 1998; Cros et al., 2005), and it was used to characterize the vRNP nuclear import pathway in this thesis.

5) *In Vivo Nuclear Import Assay:* Microinjection of purified cargo into cultured cells is another powerful method to study nuclear transport pathways (Figure 6B). In contrast to digitonin-permeabilized cells, microinjection studies use live, intact cells. For this reason, microinjection studies will give a closer representation of the normal conditions during nuclear import. In this thesis, HeLa cells, which have large cell size and are readily available in the laboratory, were used for the microinjection studies.

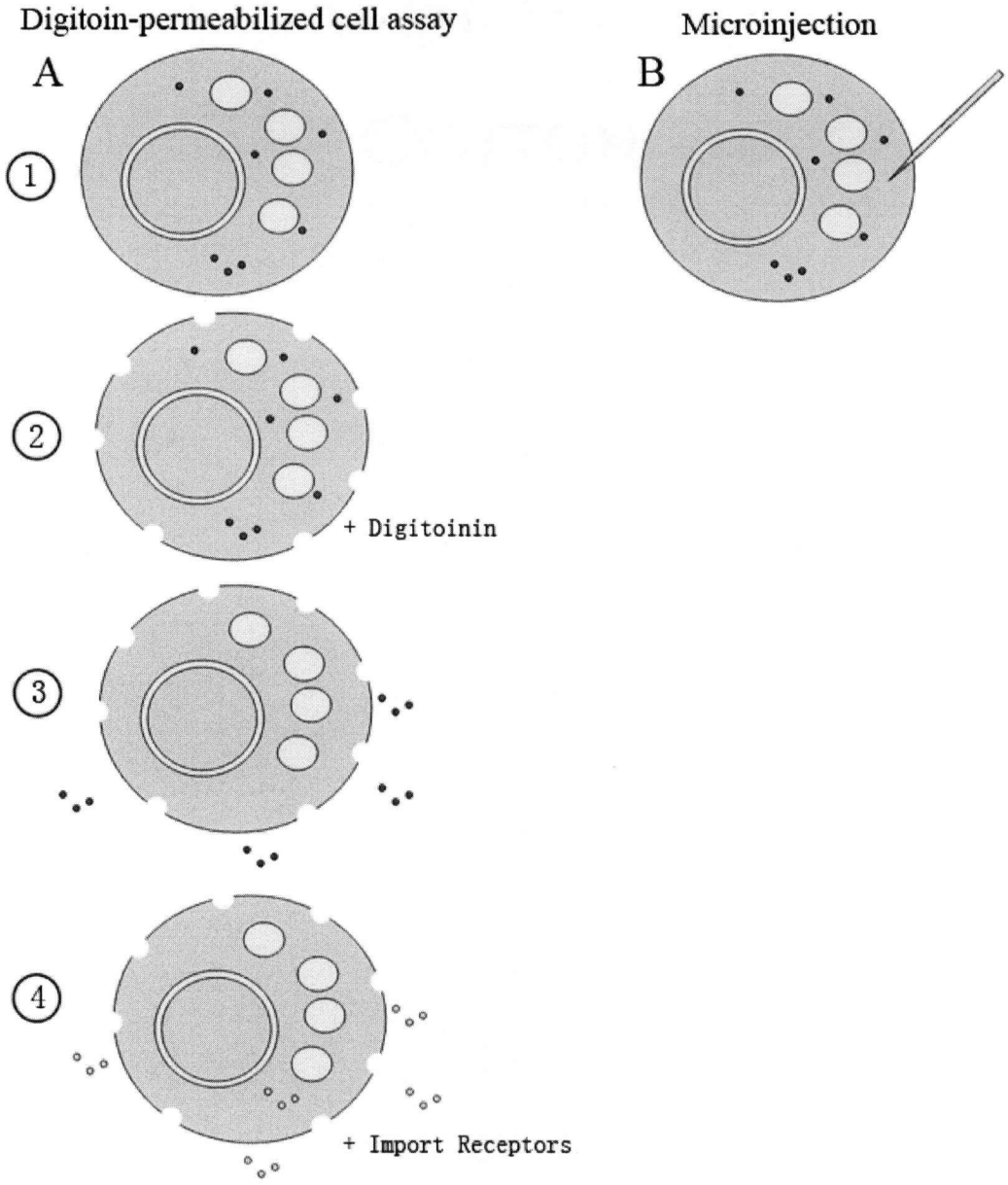

Figure 6: Schematic diagram of *in vitro* and *in vivo* nuclear import assay. (A) Intact cells (step 1) are selectively permeabilized at the plasma membrane in the presence of digitonin (step 2). Digitonin-permeabilized cells release their cytosolic proteins (red circles, step 3). Introduced cargos (yellow circles) in the presence of specific import receptors can be imported into the nucleus of digitonin-permeabilized cells (step 4). (B) Intact cells can be microinjected live, using a fine needle filled with the cargo (green). The cargo can be imported into the nucleus of microinjected cells if its specific nuclear import receptors are expressed in the cell. Note: A colored copy of this figure is available in the department of zoology at the University of British Columbia on 6270 University Boulevard, Vancouver, British Columbia, V6T 1Z4.

2 MATERIALS AND METHODS

2.1 CELL AND VIRUSES

HeLa cells were grown in standard culture medium [Dulbecco's modified eagle's medium with 4500 mg/L glucose (Hyclone, Logan, UT) with 7% fetal bovine serum (Sigma, St. Louis, MD), 1% penicillin-streptomycin (Sigma), 1% sodium pyruvate (Cellgro, Herndon, VA), 1% glutamine (Cellgro)] at 37°C with 5% CO_2 and were passaged weekly. Purified influenza A virus, H3N2, strain X:31 were purchased from Charles River Laboratories (Wilmington, MA) and were stored at -80°C.

2.2 PEPTIDES AND ANTIBODIES

Influenza A, X:31 NPnNLS (^{1}MASQGTKRSYEQMC) and NPcNLS (^{198}KRGINDRNFWRGENGRKTRC) peptides were synthesized by Pacific Immunology (Ramona, CA) along with a peptide (^{35}SDAAAKEHDEAYDQYIKSGKNC) from the minute virus of mice (MVM); amino acids are denoted according to the single letter amino acid code. The SV40 cNLS (CGGGPKKKRKVED^{134}) peptide was synthesized and conjugated to BSA by Sigma Genosys (Woodlands, TX), at a ratio of 5 cNLS to BSA. The antibodies used in this thesis are summarized in Table 1.

2.3 BIOCHEMICAL PURIFICATION OF AUTHENTIC INFLUENZA A VRNP

2.3.1 DISRUPTION OF THE INFLUENZA VIRUS

Influenza vRNPs were biochemically purified using one of the two vRNP purification protocols tested: a low volume extract (LVE) protocol, adapted from Kemler et al., 1994, and a high volume extract (HVE) protocol, adapted from Rochovansky, 1976. In the LVE protocol, 1 mg virus was diluted in 4 volumes of 10% (w/v) sucrose/MNT [20 mM 2-(N-morpholino) ethanesulfonic acid (MES), 150 mM NaCl, 30 mM Tris-HCl, pH 7.5] and centrifuged at 35,000

Table 1: Optimum antibody conditions. Antibodies were purchased from the indicated vendor and used in the following concentrations unless described otherwise. Abbreviations: Western blot (WB), dot blot (DB), immunofluorescence (IF), immunogold labeling by TEM (EM), incompatible (IC), not applicable (-), not tested (NT), affinity purified (ap), horse radish peroxidase (HRP) and rhodamine (Rho).

Primary Antibodies		**Concentration Used**			
Name	Vendor	WB	DB	IF	EM
mouse anti-NP	Acris	IC	1:100,000	1:10,000	1:5
mouse anti-M1	Acris	1:100,000	1:100,000	-	NT
rabbit anti-NPnNLS*	Pacific Immunology	1:1,000	1:10,000	NT	NT
rabbit anti-NPcNLS*	Pacific Immunology	NT	1:10,000	NT	NT
rabbit anti-NPnNLS* (ap)	Pacific Immunology	NT	NT	NT	1:100
rabbit anti-NPcNLS* (ap)	Pacific Immunology	NT	NT	NT	1:1

Secondary Antibodies		**Concentration Used**			
Name	Vendor	WB	DB	IF	EM
HRP-goat anti-mouse	Sigma	1:5,000	1:5,000	-	-
HRP-goat anti-rabbit	Sigma	1:5,000	NT	-	-
Rho-goat anti-mouse	Molecular Probes	-	-	1:5,000	-
Rho-goat anti-rabbit	Molecular Probes	-	-	NT	-
10 nm gold-goat anti-mouse	Aurion	-	-	-	1:50
10 nm gold-goat anti-rabbit	Aurion	-	-	-	1:50

* The antibodies were custom made to recognize the indicated NP NLS peptides.

rpm in a Beckman SW50.1 rotor for 40 min at 4°C. The virus pellet was thoroughly resuspended in 0.1 ml of disruption buffer [100 mM Tris-HCl, pH 8.1, 100 mM KCl, 5 mM $MgCl_2$, 5% (w/v) glycerol, 18 mg/ml octyl glucoside, 14 mg/ml lysolecithin, 1.5 mM dithiothreitol (DTT)] and lysed for 35 min in a thermomixer (Eppendorf, Westbury, NY) at 31°C. In the HVE protocol, the virus was pelleted as in the LVE protocol, but it was then resuspended in 1 ml, not 0.1 ml, of disruption buffer [100 mM Tris-HCl, pH 8.1, 100 mM KCl, 5 mM $MgCl_2$, 5% (w/v) glycerol, 14.6 mg/ml octyl glucoside, 10 mg/ml lysolecithin, 1.5 mM DTT], and was lysed for 25 min in a thermomixer at 31°C.

2.3.2 Purification and concentration of the influenza vRNPs

For both LVE and HVE protocols, the lysate was loaded onto an ice-cold step glycerol gradient [1 ml of 70%, 0.7 ml of 50%, 0.375 ml of 40%, 1.8 ml of 33% (w/v) glycerol in 50 mM Tris-HCl, pH 7.8 and 150 mM NaCl]. The gradient was centrifuged at 45,000 rpm in a Beckman SW50.1 rotor for 4 hours at 4°C. After centrifugation, the gradient was separated manually into 300 μl fractions and the fractions were analyzed by SDS PAGE stained with Coomassie brilliant blue.

Fractions containing vRNPs, judged by the presence of NPs, were pooled together, washed and concentrated either by ultracentrifugation or filtration. When vRNPs were concentrated by ultracentrifugation, the fractions containing vRNPs were diluted in 4 volumes of phosphate buffered saline (PBS) [9.1 mM $Na_2(HPO_4)$, 1.7 mM $Na(H_2PO_4)$, pH 7.4 and 150 mM NaCl] and centrifuged at 35,000 rpm in a Beckman SW50.1 rotor for 2.5 hours at 4°C. Supernatants were carefully withdrawn and the pellet was resuspended in a minimal volume of the remaining PBS buffer. When vRNPs were concentrated by filtration, the fractions containing vRNPs were pooled into a 30K Amicon Ultra-4 filtration device (Millipore, Bedford, MA). The excess glycerol was washed with saline buffer [10 mM Tris, pH 8.0 and 120 mM NaCl] and then

centrifuged at 3,000 g in 10-minute (min) intervals until the final volume was approximately 100 μl. vRNP concentration was estimated from its absorbance at 280 nm using an Ultrospec 2100 pro UV/visible spectrophotometer (Biochrom, Cambridge).

2.4 Electrophoresis, Western Blot and Dot Blot

2.4.1 SDS polyacrylamide gel electrophoresis

Samples were diluted in 4X Laemmli Sample Buffer (SB) [4% SDS, 50% glycerol, 0.02% bromophenol blue in 0.12 M Tris-HCl, pH 6.8 with 10% of freshly added β-mercaptoethanol] at 3:1 ratio and boiled in a thermomixer at 98°C for 5 min. The samples were briefly centrifuged and then loaded into 10% polyacrymide gels [10% Acrylamide/Bisacrylamide 40:1, 0.1% SDS, 0.1% ammonium persulfate 0.1% TEMED, 0.4 M Tris, pH 8.8]. SDS polyacrylamide gels fully immersed in Running Buffer (RB) [19.2 mM Glycine, 0.01% SDS 2.5 mM Tris, pH 8.3] ran at 150 V, 100 mA for 1 hour in a Protean 3 minigel chamber (Biorad, Hercules, CA). Gels not used for Western blots were stained with Coomassie blue [0.025% Coomassie Brilliant blue R 250, 40% methanol, 7% acetic acid] overnight and destained in 40% methanol and 7% acetic acid for a day. Stained gels were air dried using Cellophane (Biorad).

2.4.2 Western blot

Protein transfer was performed on a Trans-Blot® Semi-Dry Electrophoretic Transfer Cell (Biorad) as described by the instructions provided by the manufacture. Briefly, the polyacrymide gel and nitrocellulose paper (Pall BioTrance^{NT}, Pensacola, FL) were soaked in Towbin Transfer Buffer (TTB) [25 mM Tris, pH 8.3, 192 mM glycine. 20% methanol] and sandwiched between 2 TTB soaked, extra thick filter paper. The gel was transferred at 20 V for 1 hour. Transferred nitrocellulose blots were stained with Ponceau stain [0.1% Ponceau S (w/v) in 5% acetic acid (v/v)] briefly to mark the positions of the molecular mass markers, and to monitor the transfer

efficiency. The blots were then blocked with 5% milk powder in Tris-Buffer Saline (TBS) [20 mM Tris-HCl pH 8.8, 140 mM NaCl] with 0.1% Tween 20 for 1 hour at room temperature on an ATR Labatron bench top shaker (Laurel, MD) followed by brief washing in TBS-Tween [0.1% Tween 20 in TBS]. Incubation with primary antibody was at room temperature for 1 hour while shaking on a bench top shaker. The antibodies were diluted in TBS-Tween with 2% bovine serum albumin (BSA). The blots were then washed twice with TBS-Tween before subjected to incubation with secondary antibodies. The antibody dilutions used is indicated in Table 1, unless specified otherwise.

Antibodies were detected by the enhanced chemiluminescence Western blot detection system (Amersham, Piscataway, NJ). This was performed according to the prescribed manufacturer's instructions. Briefly, the blots were washed twice with TBS-Tween and twice with TBS-TritonX-100 [1% TritonX in TBS]. Excess solution was absorbed off and the blots were incubated for 1 min in the enhanced chemiluminescence solution. Excess detection reagents were blotted off and the blot was exposed to a Biomax MR film (Kodak, Rochester, NY) in the dark. The films were developed manually in a GBX developer and replenisher (Kodak) for 1 min, washed in cold water, then fixed in GBX fixer and replenisher (Kodak) for 1 min and washed thoroughly in running water in the dark.

2.4.3 Dot blot

Dot blots were performed as Western blot, except that 0.5 to 5 μl samples were dotted and absorbed onto a piece of dry nitrocellulose. The antibody dilutions used is indicated in Table 1, unless specified otherwise.

2.5 Electron Microscopy

EM processing was done according to standard conditions and EM samples were visualized using a Hitachi H7600 TEM. TEM images were taken with a AMT Advantage HR Digital CCD Camera.

2.5.1 Negative staining

Samples were absorbed onto a 200 or 400 mesh copper EM grid (Ted Pella, Redding, CA). The grid was film coated with 2% parlodion in amyl acetate, carbon coated with the Med 020 coating system (Bal-tec, Reading) for 10 seconds and glow discharged under vacuum (Biowerk) for 1 min. Each grid was inverted onto a 5-10 μl drop of concentrated sample for 10 min. Excess sample was wicked off using a hardened Whatman filter paper (W & R Balston, Florham Park, NJ) and the grid was stained with 2% aqueous uranyl acetate (Ted Pella) for 1 min. The solution of uranyl acetate was centrifuged in a benchtop centrifuge (Eppendorf) at maximum speed for 5 min to separate precipitate. Stained grid was carefully wicked dry, stored and visualized in a Hitachi H7600 TEM.

2.5.2 Immunogold labeling

Immunogold labeling using the anti-peptide antibodies were performed using a modified method from Murti et al. (1988). The 400 mesh copper grids, pretreated the same way as for negative staining, were incubated onto a 5 μl drop of concentrated vRNP for 20 min. Excess vRNP were wicked off and the grids were rinsed once in 5 μl of PBS. In a moist incubation chamber, the grids were blocked 2 times, 5 min each, with 2% BSA in PBS that was filtered with 0.2μm Acrodisc Syringe Filters (Pall, East Hills, NY). The grids were then incubated for 4 hours in 10 μl of affinity purified primary antibody diluted in 0.2% BSA in filtered PBS. Excess antibodies were washed with 0.2% BSA in filtered PBS in 4 sequential 5-minute steps. The grids were then

incubated with 10 μl of gold conjugated secondary antibodies diluted in 0.2% BSA in PBS for 1 hour and washed 3 times with filtered PBS, 5 min each. Antibody-protein interactions were fixed with 1% glutaraldehyde in PBS for 5 min, washed with a continuous stream of filtered distilled water and then stained with 2% aqueous uranyl acetate for 1 min. Grids were dried and viewed in a Hitachi H7600 TEM. The antibody dilutions used are indicated in Table 1.

Immunolabeling using the anti-NP monoclonal antibody was performed similar to anti-peptide antibodies, with the following exceptions. The vRNPs were absorbed onto the grid for 5 min and incubated with 10 μl of primary antibody for 2 hours, washed with filtered PBS 3 times, and incubated in secondary antibody for 1 hour. The grids were then washed with 1% BSA in PBS 3 times, 5 min each, fixed, washed, and stained with 2% uranyl acetate. The antibody dilutions are indicated in Table 1.

2.6 Fluorescently Labeling of Import Probes

Probes for nuclear import studies (purified vRNP or cNLS (CGGGPKKKRKVED) conjugated BSA (cNLS to BSA ratio of 5) (Sigma Genosys)) were labeled with cy3 Bis-Reactive dye (Amersham) according to the prescribed protocol and similar to Babcock et al. (2004). First, probes were prepared by washing in 4 ml of 0.1 M Na_2HCO_3/NaH_2CO_3 pH 9.3 in a 30K Amicon Ultra-4 filtration device and centrifuged as above. Then the probes were labeled in a thermomixer shielded from the light for 1 hour with prescribed concentration of cy3. Unlabeled cy3 was separated from labeled probe with 4 sequential washes in PBS, pH 7.4, in the Amicon filter. Fluorescently labeled vRNP underwent another 5-minute centrifugation at 4°C in a Microcon YM-100 filtration unit (Millipore) at 500 g to exclude any dissociated vRNP proteins. The labeling efficiency and the concentration of the labeled probe were estimated from their absorbance at 280 nm and 552 nm.

2.7 DIGITONIN PERMEABILIZATION IMPORT ASSAY

2.7.1 IMPORT ASSAY

Digitonin permeabilization assays were carried out as described by Adam et al. (1990) with minor modifications. Specifically, HeLa cells were seeded to 80% confluent on sterile coverslips (Fisher, Nepean, ON). Seeded cells were immersed in fresh medium before each experiment and incubated for 2 hours at 37°C. Cells were then washed with fresh import buffer [20 mM Hepes-KOH, pH7.3, 2 mM magnesium acetate, 5 mM sodium acetate, 1 mM EGTA (Ethylene glycol-O,O'-bis-[2-amino-ethyl]-N,N,N',N',-tetraacetic acid), 110 mM potassium acetate, 2 mM DTT, supplemented with a protease inhibitor cocktail CLAP (10 μg/ml chymostatin, 10 μg/ml leupeptin, 10 μg/ml antipain, 10 μg/ml pepstatin)] and permeabilized with digitonin (Sigma) at 40 μg/ml in ice-cold import buffer for 5 min. Permeabilized cells were washed 3 times in import buffer at 10-minute intervals with gentle rocking.

Coverslips with digitonin-permeabilized cells (with preserved NE but devoid of soluble cytosolic contents) were gently blotted off of any excess of import buffer and inverted onto a drop of 50 μl transport mixture on parafilm and incubated for 45 min at 37°C inside a humidified chamber. A standard transport mixture contained active cytosol (10 μl of rabbit reticulocyte lysate (Promega, Madison, WI) or the optimum volume of purified HeLa cytosol (HC)), 18 U/ml creatine phosphokinase (Sigma), 4.5 mM creatine phosphate (Sigma), 0.40 mM ATP, 0.45 mM GTP, 1.6 mg/ml BSA, 1-3 μg of the import probe and import buffer. For antibody inhibition experiments, import probes were incubated at 2:1 antibody:NP molar ratio for 1 hour in the dark at room temperature. For competition inhibition experiments, import probes were mixed at 700:1 peptide (or BSA):NP molar ratio before assayed in digitonin-permeabilized cells.

Transport reactions were terminated by three 10-minute washes in import buffer. Cells were fixed in 4% paraformaldehyde (PFA) in import buffer for 10 min at room temperature.

Fixed cells were rinsed in import buffer and mounted onto glass slides using a slowfade antifade kit with DAPI (Molecular Probes, Burlington, ON). Coverslips were sealed with clear nail polish and observed in an Axioplan-2 fluorescence microscope (Zeiss, Toronto, ON) using a 100 W fluorescent bulb. All images were taken digitally using a Q imaging Retiga 1300 camera and the Northern Eclipse 6.0 software.

2.7.2 Purification of HeLa cytosol

HC was purified from HeLa cells as previously described (Paschal and Gerace, 1995). Ten cell culture plates (diameter, 10 cm) of confluent HeLa cells were washed with PBS and incubated in 1 ml of trypsin (1mg/ml, Sigma) at 37°C for 5 min. After the HeLa cells were detached from the plates, the cells were combined and diluted in 10 volumes of culture medium and centrifuged at 500 g for 5 min at 4°C. Cells were then washed 2 times with iced PBS and then 1 time with fresh, iced cold transport buffer (20 mM Hepes, pH 7.4, 110 mM potassium acetate, 2 mM magnesium acetate, and 0.5 mM EGTA with 2mM DTT) at 500 g for 5 min at 4°C.

Two volumes of ice-cold lysis buffer [5 mM Hepes, pH 7.4, 10 mM potassium acetate, 2 mM magnesium acetate, 1 mM EGTA, CLAP, 5 mM DTT, and 0.1 mM phenylmethylsulphonylfluoride (PMSF)] were added to the pellet. The cells were swelled for 15 min on ice then lysed in an iced cold, tight-fit glass douce homogenizer, with 15 strokes. The cell lysate added with 0.1 volumes 10X transport buffer was centrifuged at 40,000 g for 30 min. The supernatant was centrifuged a second time at 150,000 g for 60 min. The clear supernatant was snap froze in liquid nitrogen and stored at -80°C. Each HC purification was tested in an import assay using cy3-labeled cNLS-conjugated BSA (cy3-cNLS-BSA) to determine its activity and optimum volume for the import assay.

2.8 IMMUNOFLUORESCENCE MICROSCOPY

Immunofluorescence microscopy was performed according to standard procedures. Cells on coverslips were fixed with 4% PFA in import buffer for 5 min, washed with PBS and permeabilized with 0.1% TritonX-100 in PBS for 6 min. Permeabilized cells were then washed with PBS-Tween [0.05% Tween-20 in PBS] and sequentially blocked with 1% BSA in PBS-Tween for three 5-minute intervals. Incubation with primary antibodies took place at room temperature for 1 hour. The primary antibodies were diluted in 1% BSA in PBS-Tween. Unbound antibodies were thoroughly washed with PBS-Tween for three 5-minute intervals. Secondary incubation took place at room temperature in the dark for 1 hour using fluorescently conjugated secondary antibodies diluted in 10% goat serum (Sigma) in PBS-Tween. Unbound antibodies were washed 5 times with PBS-Tween as before. Antibody-protein bindings were fixed with 4% PFA for 5 min then washed with PBS-Tween. Cells that underwent the digitonin permeabilization assay were mounted and observed as above. Cells that underwent the microinjection assay were observed directly in a Axiover 200 inverted fluorescence microscope (Zeiss). The antibody dilutions used here are indicated in Table 1.

2.9 MICROINJECTION

Microinjection experiments were performed using the FemptoJet microinjection system (Eppendorf) and monitored on the Axiover 200 inverted fluorescence microscope. Prior to microinjection, HeLa cells were seeded onto glass bottom Petri dishes to 60% confluent. Fresh medium was added 2 hours at the beginning of each experiment and the cells were incubated at 37°C. For immunofluorescence experiments, during this incubation, an orientation map, containing the location of a field of cells to be injected, was constructed. This is achieved by capturing low magnification digital images of the cells to be injected at 37°C on the inverted

microscope and digitally joining the images using Adobe Photoshop 7.0.1.

HeLa cells were injected live, at 37°C, using FemptoJet connected to a Femptotip II needle (Eppendorf). Between 0.1-0.5×10^{-3} nl of sample were injected into each cell. Given each HeLa cell has a cell volume of 5×10^{-3} nl, between 1/50 to 1/10 of the cell volume is injected into each cell. All samples used for microinjection were centrifuged at 13,000 rpm (Biofuge fresco, Heraeus) for 5 min at 4°C to exclude aggregates. A typical injection setting showed an injection pressure (Pi)=150, injection time (t)=0.1s, constant pressure (Pc)=50. The needle was manipulated using the InjectMan (Eppendorf) and injection was monitored on a DC monitor (Sony) through a CMA02 Camera (Sony). For fluorescently labeled samples, the injected cells were imaged immediately after injection in the inverted fluorescence microscope. For samples that require immunofluorescence labeling, each injection was recorded digitally on the orientation map. Any cells that did not survive the injection were also recorded. For immunofluorescence experiments, approximately 100 cells were injected per sample.

Furthermore, for immunofluorescence experiments, during the primary incubation step, a second orientation map containing the same field of cells injected was created. By merging the first and second orientation map digitally, the number of cells that survived the fixation and permeabilization step was monitored. After immunofluorescence labeling, all injected cells were imaged in the inverted fluorescence microscope and recorded on the orientation map.

3 RESULTS

3.1 PURIFIED VRNPS WERE AUTHENTIC AND HAD STRUCTURAL INTEGRITY

Previously, NP has been shown to import influenza vRNA into the nucleus of digitonin-permeabilized cells (O'Neill et al., 1995) using the NPnNLS (Cros et al., 2005). However, it is not known whether NP can also import authentic vRNPs. To study the nuclear import of authentic vRNPs, vRNPs were purified from influenza A virus. Purified vRNPs were analyzed for protein authenticity and structural integrity.

3.1.1 TWO PURIFICATION METHODS: LVE AND HVE

Using established biochemical protocols it was found that authentic vRNP could be purified (Rochovansky, 1976; Kemler et al., 1994). Two versions of the purification protocols, HVE and LVE, with varying virus disruption steps, were tested. In HVE, 1 ml of disruption buffer was used, while in LVE, 0.1 ml was used. It was found that both HVE and LVE produced similar purifications, as judged by sampling the purified fractions using SDS PAGE and Western blots (Figure 7, A-D). Peak NP fractions, as judged by both Coomassie blue staining and anti-NPnNLS antibody staining, were in the 40% glycerol fractions (Figure 7, A-B, fractions 8-9 and Figure 7, C-D, fractions 10-11). In contrast, peak M1 fractions, as judged by both Coomassie blue and anti-M1 antibody staining, were in the low-density glycerol fractions (Figure 7A, fractions 1-3, and C, fractions 1-6). Trace amounts of M1 co-fractionated with vRNPs, as detected using anti-M1 antibodies (Figure 7D, fractions 10-11). But, it was found that at this low concentration, M1 did not interfere with vRNP nuclear import (section 3.2).

Polymerases could be identified in SDS polyacrylamide gels stained with Coomassie blue from vRNP fractions purified using HVE (Figure 7C, fractions 9-12, at approximately 80 kDa). Nine purifications were done, and polymerases bands were visible with Coomassie blue every

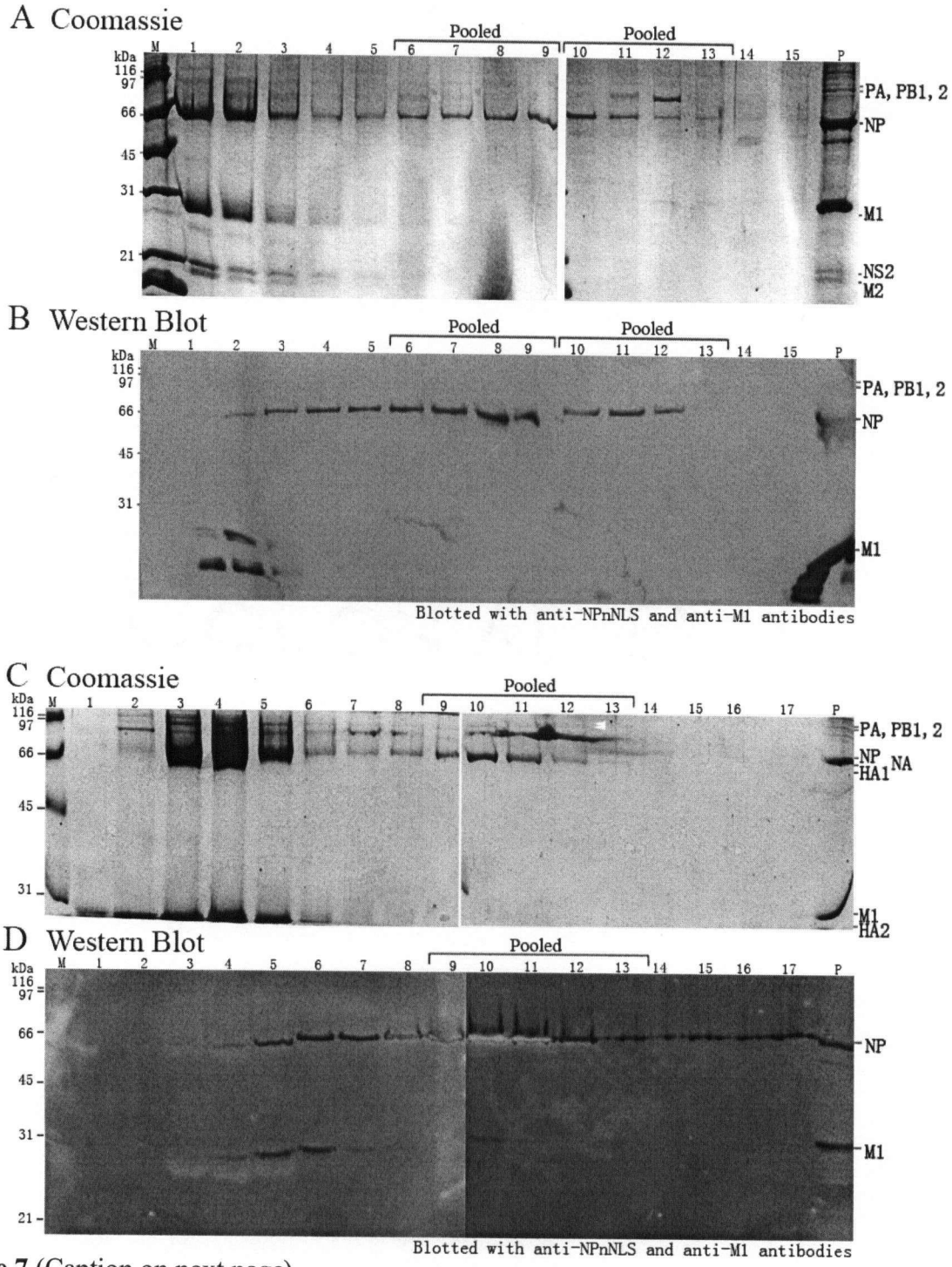

Figure 7 (Caption on next page)

Figure 7: Comparison of the two vRNP purification protocols.
(A-B) Low volume extraction (LVE) purification. Influenza A virus was lysed in 100 μl of disruption buffer according to Kemler et al. (1994) and separated in a glycerol gradient. (A) 18 μl from each fraction, numbered according to increase in glycerol density, were analyzed by 10% SDS PAGE. 5% of the pellet (P), which contained partially disrupted virus, was also analyzed. The pellet lane indicates the degree of lysis and provides a reference for influenza A protein migration patterns. Molecular mass markers (M) and their mass in kDa are indicated to the left of each panel. The position of vRNP proteins are indicated to the right of each panel. Pooled vRNP fractions are indicated above each panel. Gels were stained with Coomassie blue. (B) 18 μl from each fraction were analyzed by Western blot using a mixture of anti-M1 and anti-NPnNLS antibodies. 5% of the pellet was also analyzed.
(C-D) High volume extraction (HVE) purification. Influenza A virus was lysed in 1 ml of disruption buffer according to Rochovansky (1976) and separated in a glycerol gradient as in (A). (C) 16 μl from each fraction were analyzed by 10% SDS PAGE and stained with Coomassie blue. 5% of the pellet (P) was also analyzed. (D) 16 μl from each fraction was analyzed by Western blot along side with 5% of the pellet as in (B). The position of the polymerases, when visible is indicated by white arrow heads. Note: the four gels were separated for slightly different lengths of time.

time (data not shown). These results provided evidence to support biochemically purified vRNPs are complete with all four vRNP proteins.

The ability to detect polymerases by Coomassie blue was the only major difference found between purifications using HVE and LVE (compare Figure 7, A and C). Consequently, HVE was the preferred method to purify influenza vRNPs. However, the exact reason for this difference is not known. For one, the yield of vRNPs was the same for each method: a typical purification using either HVE or LVE yielded approximately 100 μg of vRNP proteins, as estimated from vRNP absorbance at 280 nm. Secondly, aside from a difference in virus disruption buffer volume, the two methods were nearly identical. One hypothesis is that at a low volume, the virus disruption buffer partially disrupts the viral envelope, leaving some viral proteins, such as the polymerases, partially attached to the viral envelope. After ultracentrifugation, these vRNP proteins, along with the rest of the partially disrupted virus, are collected in the pellet (compare the pellet lane of Figure 7A with C). By contrast, a large volume of virus disruption buffer volume can completely disrupts the viral envelope, leading to a cleaner separation. Consequently, more polymerases remain assembled in the vRNPs after separation, and few are collected in the pellet.

3.1.2 VERIFICATION OF THE AUTHENTICITY AND INTEGRITY OF PURIFIED VRNP

To verify the authenticity of purified vRNPs, the vRNP fractions were analyzed by dot blot and Western blot using anti-NP antibodies (Figure 7, B and D, and data not shown). Consistent with the findings from SDS PAGE, the results from dot blot and Western blot showed that peak NP fractions appeared in the 40% glycerol fractions (Figure 7). The results from Western blot also verified that the 56 kDa band present in the polyacrylamide gels belonged to NP, while the double band at ~80 kDa did not. This ruled out the possibility that the double band could be a

dimerized form of NP and supported the above notion that the ~80 kDa bands belonged to the polymerases.

To verify the structural integrity of the purified vRNPs, vRNP were negatively stained and then visualized by TEM. It was found that, consistent with previous observations (Jennings et al., 1983), the purified vRNPs had an elongated helical rod with variable lengths and a terminal loop, which was visible when the vRNP was positioned in the correct orientation (Figure 8A). To quantify the amount of intact vRNPs present, the length of 329 vRNPs was measured, and it was found that 88% was longer than 40 nm, indicating that the majority of the purified vRNPs were intact.

In addition, the structural integrity of cy3-labeled vRNPs (cy3-vRNPs) was also analyzed by negative staining and then visualized by TEM. Cy3-vRNPs was used to characterize vRNP nuclear import in direct fluorescent studies (see section 3.4 and 3.5) therefore, it was vital to ensure that purified vRNPs did not undergo structural disassembly after labeling with cy3. It was found that the ultrastructure of negative stained cy3-vRNPs was indistinguishable from that of unlabeled vRNPs (Figure 8B): the terminal loop and helical rod of cy3-vRNPs could be identified, and from the lengths of 144 cy3-vRNPs measured, 86% was found longer than 40 nm. These results strongly suggest cy3 labeling did not destroy the vRNP ultrastructure.

Together, the biochemical and EM studies confirmed that purified vRNPs were authentic, they had all four vRNP proteins, and they included all the structural features present in vRNPs.

3.2 Purified vRNP Were Nuclear Import Competent

Using live HeLa cells, it was demonstrated that freshly purified vRNP (Figure 9A) localized to the cell nucleus after cytoplasmic microinjection (Figure 9C). The vRNPs were visualized by indirect immunofluorescence microscopy using a monoclonal anti-NP antibody and a rhodamine

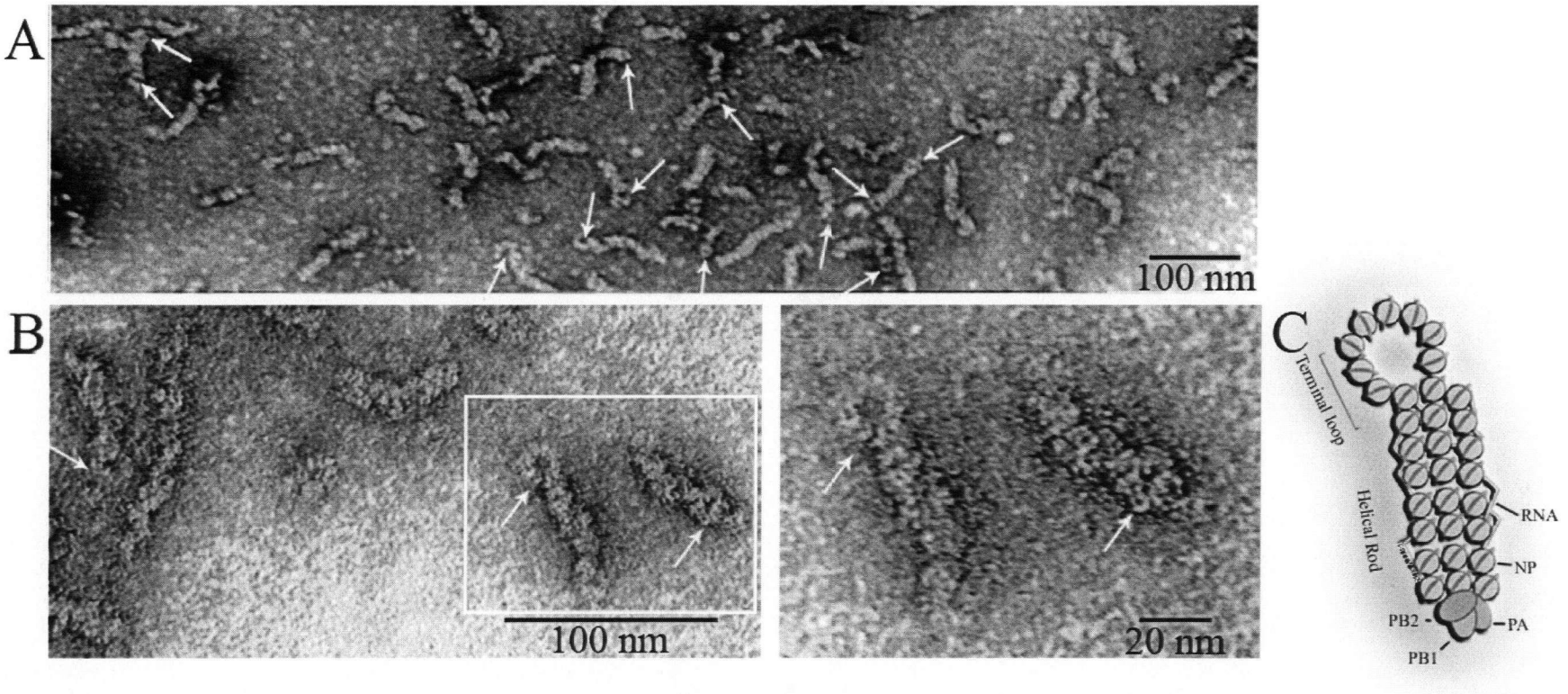

Figure 8: Negative stained vRNPs. (A) Biochemically purified vRNPs or (B) cy3-labeled vRNPs (cy3-vRNPs) were absorbed onto parlodion and carbon coated copper EM grids, and negative stained with 2% aqueous uranyl acetate for 1 min. Stained vRNPs were visualized in a Hitachi H7600 TEM. It was determined that 88% of the unlabeled vRNPs and 86% of the cy3-vRNPs had a length greater than 40 nm (the total number of vRNPs measured (n) were 329 and 144 respectively). The right image in (B) shows the magnified view of the bordered area on the left image. White arrows indicate the vRNP terminal loop. (B) A cartoon representation of a vRNP with its major structural components labeled. Note: A colored copy of this figure is available in the department of zoology at the University of British Columbia on 6270 University Boulevard, Vancouver, British Columbia, V6T 1Z4.

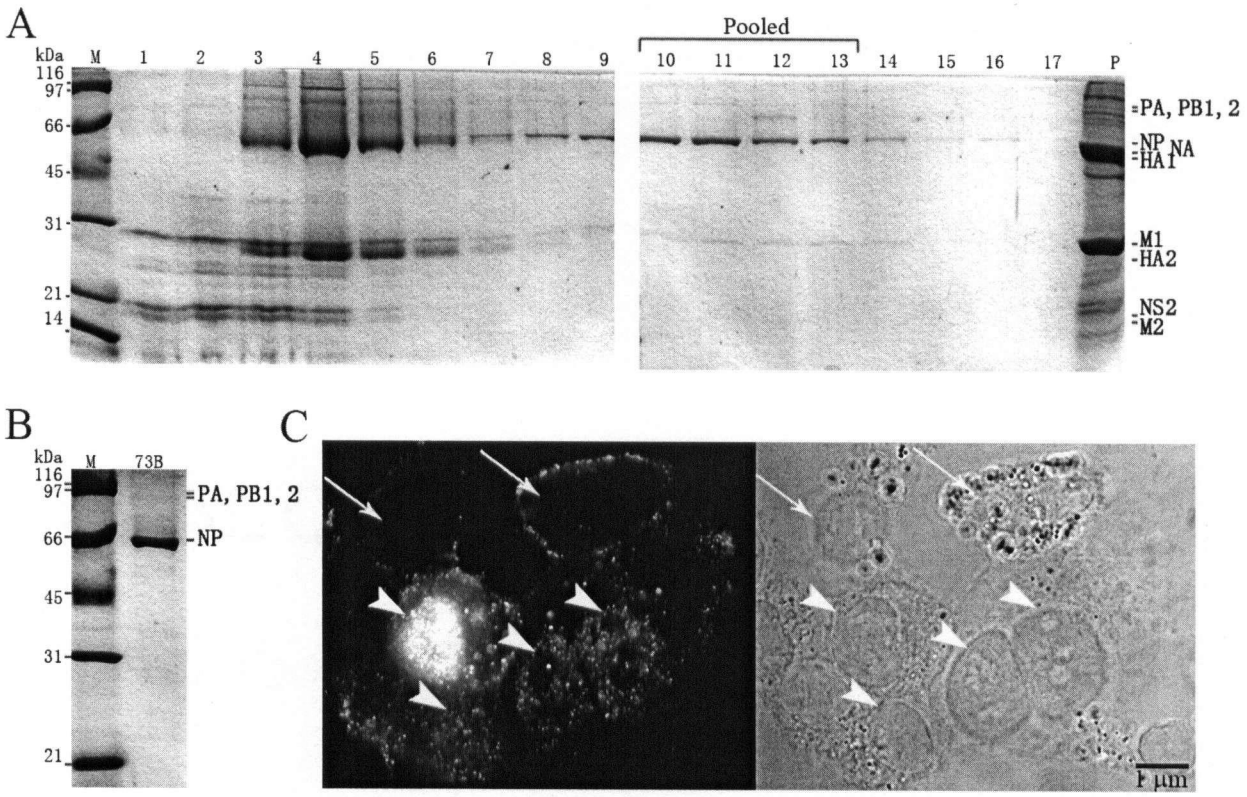

Figure 9: vRNP purified by the HVE protocol enters the nucleus of HeLa cells after microinjection.

(A-B) Purification of influenza A vRNP. (A) Influenza A virus was purified by the HVE protocol. Virus was lysed in 1 ml disruption buffer and separated in a glycerol gradient as described in Materials and Methods. Fractions rich in both NP and polymerases, as judged by 10% SDS PAGE, were pooled and concentrated. The migration positions of molecular mass markers (M) in kDa and vRNP proteins are indicated to the left and right sides of each panel respectively. (B) 5 μl of concentrated vRNP (purification N^{o} 73B) was reanalyzed by 10% SDS PAGE and stained with Coomassie blue.

(C) Purified vRNP entered the nucleus of HeLa cells *in vivo*. vRNP (73B, as in panel B) was microinjected into live HeLa cells (white arrowheads). Injected cells were incubated for 30 min at 37°C to allow for nuclear import. Nuclear import was stopped by fixation and cells were prepared for indirect immunofluorescence microscopy using an anti-NP monoclonal antibody and rhodamine-conjugated anti-mouse antibody. In this experiment, a total of 139 cells were injected, 101 cells survived the injection, 76 cells survived the immunofluorescence process and were available for observation. However, only 25 cells showed fluorescent signal, of which 19 (76%) had fluorescent nuclei. Representative fluorescent image (left) and bright field image (right) are shown. White arrows indicate uninjected cells, and arrowheads indicate injected cells.

conjugated secondary antibody under optimized conditions (1:10,000 anti-NP antibody and 1:5,000 secondary antibody). The monoclonal anti-NP antibody was purchase from Acris. The NP epitope that it binds to has not been determined by the vendor. The optimized labeling conditions produced in a 5-10 fold signal to background ratio difference as determined by varying primary and secondary antibody concentrations in digitonin-permeabilized cells in the presence (signal) or absence (background) of vRNPs (data not shown).

The microinjection study was done a total of eight times, using fresh vRNPs from a different purification each time. The purifications used in these microinjections were vRNP purification Nº 73B, 73C, 74A, 74B, 75A, 76A, 76B and 76C; each vRNP purification number designates an independent purification experiment. In every experiment, the microinjected vRNPs could enter the nucleus of live HeLa cells (Figure 9C, and Figure 10). Together, a total of 886 cells were injected, 591 cells survived the microinjection and the immunofluorescence protocol; of these, 307 cells were fluorescent and 278 had fluorescent nuclei. On average, the percent of cells with fluorescent nuclei was 91% (standard deviation (SD)=10%) (Figure 10C). These results demonstrated that the vast majority of the microinjected vRNPs entered the nucleus of HeLa cells and that purified vRNPs were import competent.

In addition, I had also observed that after vRNPs were microinjected into the cytoplasm and incubated for 10 min at 37°C, over 90% of the visualized cells had a nucleus fluorescence (data not shown), indicating that 10 min was sufficient for vRNP to enter the nucleus *in vivo*.

3.3 NP NLSs Were Exposed On Authentic vRNPs

To evaluate whether NPnNLS and NPcNLS are exposed on the outer surfaces of authentic vRNPs, vRNPs biochemically isolated from influenza A virus were immunolabeled using polyclonal antibodies against either peptides, and visualized using dot blot and

Figure 10 (Caption on next page)

Figure 10: A summary of microinjection studies from different vRNP purifications. Freshly purified vRNPs from eight different purifications (73B, 73C, 74A, 74B, 75A, 76A, 76B and 76C), each pooled from a glycerol gradient, were microinjected into HeLa cells and analyzed by immunofluorescence using an anti-NP antibody. The orientation and position of the cells were mapped digitally as described in the materials and methods (section 2.9). Only cells sure to be microinjected in the cytoplasm were analyzed. (A) Microscopic images of vRNP localization. Injected (white arrowheads) and uninjected (white arrows) cells were incubated for 10-60 min at 37°C, and analyzed by indirect immunofluorescence microscopy as indicated in Figure 9C. Fluorescent (left) and bright field (right) images are shown. (B) Quantification of vRNP nuclear import. Microinjected HeLa cells were mapped digitally, and the fluorescence signal was judged visually to be predominantly in the nucleus (Nuc), the cytoplasm (Cyt) or equally distributed between the nucleus and cytoplasm (Nuc-Cyt). Only injected cells with fluorescent signal stronger than the nearest uninjected cell were analyzed. The percentage of cells in each phenotypic class is represented in a histogram for each experiment. n indicates the total number of fluorescent cells. (C) Average of the eight experiments with SD illustrated as error bars and the number of independent experiments indicated as N. The probability (p) that the average percent of cells in one phenotype is the same as another phenotype is calculated using a two-tailed student t test. They are: Nuc=Nuc-Cyt ($p<<0.0001$), Nuc=Nuc-Cyt ($p<<0.0001$), and Nuc-Cyt=Cyt ($p=0.3607$), indicating that while the average percent of Nuc is significantly different from Nuc-Cyt and Cyt, the average percent of Nuc-Cyt is not significantly different from Cyt.

chemiluminescence or TEM. But first, each antibody was evaluated for specificity and binding efficiency using dot blot and chemiluminescence.

As seen in Figure 11A, when NP NLS peptides were dotted onto nitrocellulose, they were found reactive only to their corresponding antibody, demonstrating that each antibody was highly specific and cross reactivity was minimal. Furthermore, judging by the darkness of the dots, when the peptide was reacted with its specific antibody, it was determined that both antibodies bound equally well to its specific peptides.

When equal volumes of biochemically isolated vRNPs were dotted onto nitrocellulose, and the degree to which vRNPs could be immunolabelled was evaluated, it was found that the chemiluminescence of vRNPs in the presence of either anti-NPnNLS or anti-NPcNLS antibodies was stronger than the control (Figure 11A). This provided evidence that vRNPs could be immunolabelled using either anti-NP NLS antibodies. However, it was found that at the same antibody dilution, while anti-NPnNLS antibody was just as reactive to purified vRNPs as to NPnNLS peptides, anti-NPcNLS antibody was only marginally reactive to purified vRNPs (Figure 11A). From this, it was inferred that NPnNLS was densely dispersed on the surface of vRNPs, but NPcNLS were only sparsely dispersed. For this reason, subsequent immunogold TEM studies were performed using a higher anti-NPcNLS antibody concentration than the anti-NPnNLS antibody concentration.

When equal volumes of purified vRNPs were absorbed onto EM grids and analyzed by immunogold TEM using anti-NP NLS specific antibodies in combination with gold-conjugated secondary antibodies, it was found that the majority of the electron dense gold particles had associated to the vRNPs (Figure 11B). In contrast, when either anti-NP NLS antibody was absent, very little electron dense gold particles could be found.

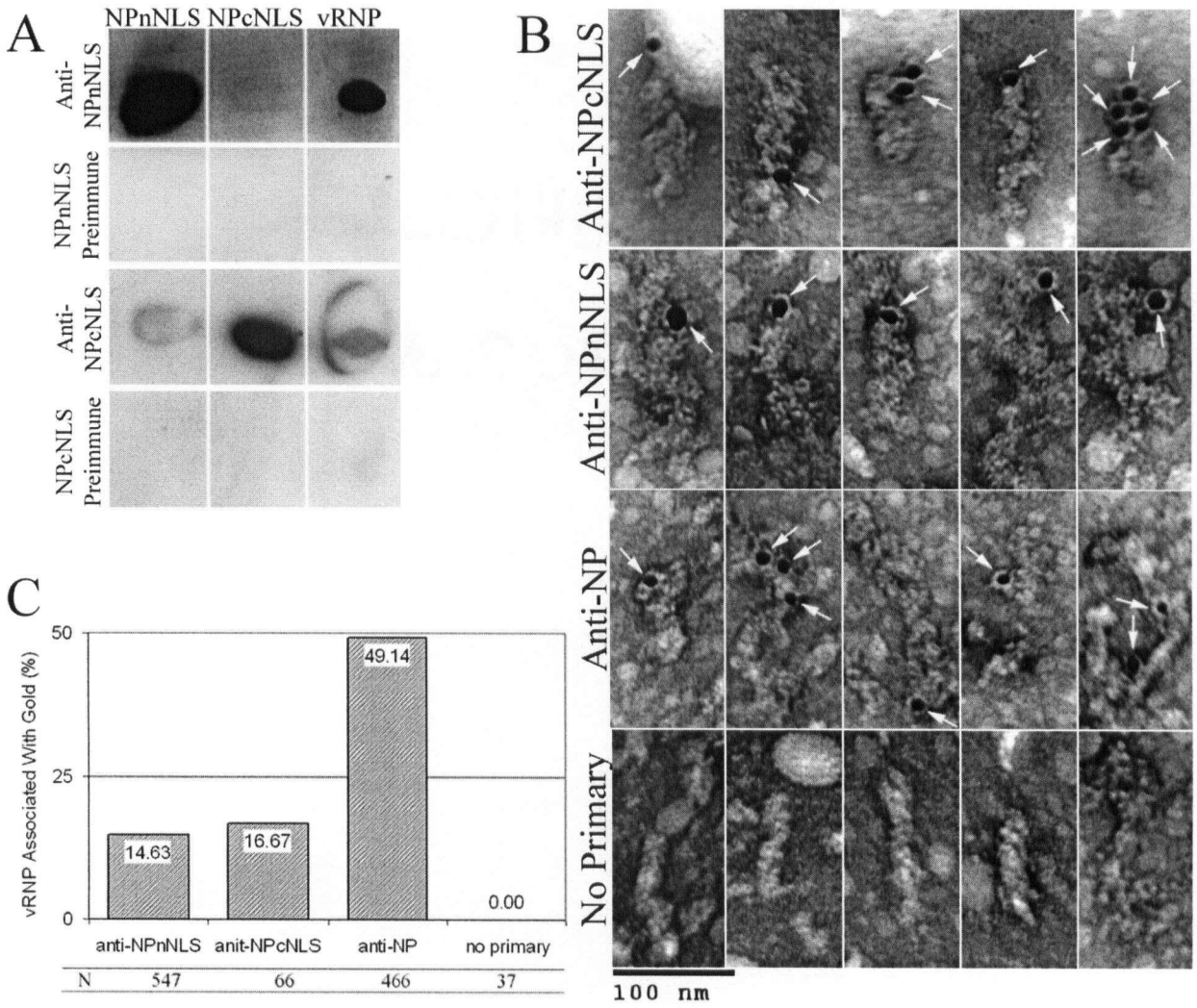

Figure 11: NPnNLS and NPcNLS are exposed on vRNPs. vRNPs were immunolabeled with anti-NPnNLS and anti-NPcNLS antibodies and visualized using dot blot and enhanced chemiluminescence (A) or immunogold EM (B-C).

(A) Dot blot. 0.2 μg of NPnNLS peptide, 0.2 μg of cNLS peptide and 0.5-1 μg of concentrated vRNP were dotted onto nitrocellulose and immunolabeled with anti-NPnNLS serum (dilution 1:10,000), NPnNLS preimmune serum (dilution 1:5,000), anti-NPcNLS serum (dilution 1:10,000) and NPcNLS preimmune serum (dilution 1:5,000). The preimmune serum is the serum extracted from the rabbit prior to immunization with the peptide.

(B-C) Immunogold TEM. (B) Image gallery and (C) quantification analysis of vRNP immunolabeled with the indicated antibody and the corresponding gold conjugated anti-primary antibody. The 10 nm colloidal gold particles were visualized as dense black dots (white arrows). Concentrations of the antibodies used are indicated in Table 1. The total number of vRNPs analyzed from each set of images is indicated (N). Please note that the number of pictures captured for each condition and the number of vRNP available for analysis was different. Also note that the immunolabeling experiments with anti-NP peptide antibodies were done on different days as the experiment with anti-NP antibodies, and using slightly different protocols (see section 2.5.2 of the thesis).

It was difficult to accurately quantify these immunolabeling studies because the immunogold labeling protocols lead to a compromised image resolution: not only was the vRNP loop no longer visualized, details in the helical rod was also lost (compare Figure 8 and 11B). This is consistent with previous studies that immunolabeled vRNPs (Murti et al., 1988). For this reason, the values reported in the following quantification analysis should be considered as approximations. It was found that, in the presence of either anti-NPnNLS or anti-NPcNLS antibodies, greater than 90% of the observed gold particles were next to a vRNP, providing evidence that (1) the majority of the purified NPs were assembled in vRNP complexes and (2) the degree of nonspecific immunolabeling was low. Quantification also showed that using 1:1 anti-NPcNLS antibody dilution (final concentration 0.5 mg/ml), approximately 17%, out of a total of 66 vRNPs counted had at least one gold particle associated to it (Figure 11C). Using 1:100 anti-NPnNLS antibody dilution (final concentration 0.01mg/ml), approximately 15% out of 547 vRNPs had at lease one gold particle associated to it. For comparison, at 1:5 anti-NP (monoclonal) antibody dilution (final concentration 0.2 mg/ml), approximately 49% out 466 vRNPs had at least one gold particle associated to it.

Together, the two immunolabeling studies showed that (1) both NPnNLS and NPcNLS were exposed on the assembled vRNP complex, (2) more NPnNLS were exposed than NPcNLS and (3) the population of free dissociating NP proteins was low. The implications of these results are explored in the discussion.

3.4 Characterization of vRNP Nuclear Import in an *In Vitro* Import Assay With Digitonin-Permeabilized HeLa Cells

3.4.1 Testing the in vitro import assay with fluorescently labeled cNLS-BSA

As described in section 1.10, digitonin-permeabilized cells are a powerful tool to test specific hypotheses in nuclear import pathways. Here, it will be used to characterize the nuclear import of

authentic vRNPs. Properties of the *in vitro* nuclear import assay were verified using cNLS conjugated BSA (cNLS-BSA), a standard probe for validating nuclear import assays. The cNLS-BSA was fluorescently labeled with cy3, ideally, in a 0.5-1 fluorochrome per protein ratio. However, deviations from this ratio did not impose major effects.

It was found that when cy3-cNLS-BSA was tested in digitonin-permeabilized HeLa cells in the presence of rabbit reticulocyte lysate (RRL) and an energy regenerating mixture (energy), it could enter the nucleus (Figure 12B). Thirteen individual experiments (n=13) were performed, and similar results were obtained. In contrast, in the absence of RRL and energy, cy3-cNLS-BSA was excluded from the nucleus (Figure 12B). This experiment was repeated ten times (n=10), all yielding similar results. These results confirmed that (1) digitonin-permeabilized cells had intact NE and functional NPCs, which selectively exclude macromolecules from entering the nucleus in the absence of cytosol or energy and (2) the RRL contained active transport receptors that could transport NLS-containing proteins into the nucleus.

3.4.2 NUCLEAR IMPORT OF CY3-VRNP IN DIGITONIN-PERMEABILIZED CELLS

The import assay with digitonin-permeabilized cells was then used to study nuclear import of vRNP. Purified vRNP was labeled with cy3 using the same protocol as for cNLS-BSA, but at a lower fluorochrome labeling efficiency. The fluorochrome labeling efficiency was set to approximately 0.16 fluorochrome per NP to minimize the adverse effects from cy3 modifications, particularly to the NP NLSs. Note here that because each vRNP is made up of approximately 36-94 NPs, it was estimated that each cy3-vRNP had between 5 to 15 fluorochromes bound. To be sure that cy3-vRNPs did not undergo disassembly, cy3-vRNPs were visualized by TEM, and their ultrastructure characterized. No visible difference was found between unlabeled and cy3-vRNPs (Figure 8 and section 3.1.2)

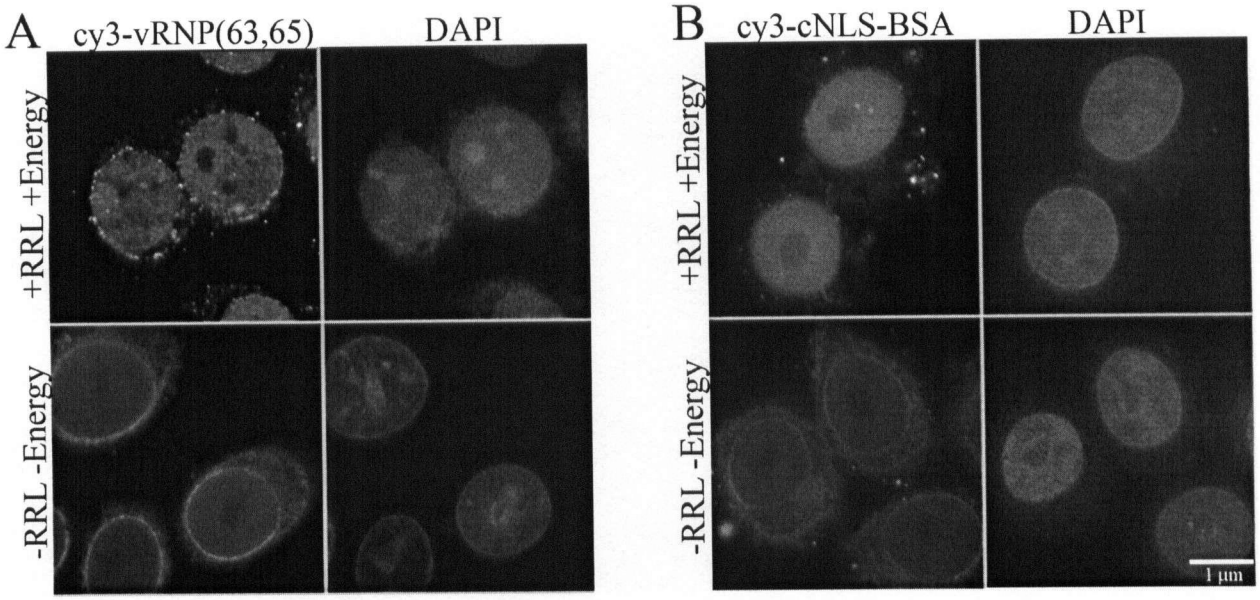

Figure 13: Cy3-vRNP enters the nuclei of digitonin-permeabilized HeLa cells. (A) Cy3-vRNP from purification Nº 63, A and B, and Nº 65, A and B (vRNP(63,65)) and (B) cy3-cNLS-BSA were assayed in digitonin-permeabilized HeLa cells as in Figure 12 and analyzed by fluorescence microscopy.

Next, cy3-vRNP was assayed in digitonin-permeabilized cells using the same condition as for cy3-cNLS-BSA. To our surprise, cy3-vRNP could not be imported into the nucleus of digitonin-permeabilized HeLa cells, *in vitro* (Figure 12A).

Approximately 38 independent digitonin permeabilization studies were performed, testing the nuclear import of vRNPs from approximately 50 independent purifications. It was found that purified vRNPs were consistently localized to the cytoplasm. Various conditions in the assay were systematically varied to improve vRNP nuclear import. They include, varying the cytosol (by increasing or decreasing the amount of RRL used, or using purified HeLa cytosol instead of RRL), varying cy3 labeling (by increasing or decreasing cy3:protein ratio, using other fluorochromes (Alexa 488^{TM} (Molecular Probes) and fluos^{TM} (Roche Diagnostics, Palo Alto, CA), or eliminating fluorescent labeling completely and visualizing vRNP using indirect immunofluorescence microscopy), varying the cell type (using LA9, a mouse fibroblast cell line, instead of HeLa cells), varying incubation times (30 min, 1 hour and 2 hours) and incubation temperatures (room temperature and 37°C), but none of these changes could improve vRNP nuclear import (data not shown). The effects of vRNP nonspecific binding were also explored by blocking permeabilized cells with tRNA or BSA, and preincubating vRNPs with the cytosol. It was found that none of these modifications could release the vRNPs from their nonspecific interactions. Finally, the vRNPs themselves were evaluated, by pooling the vRNPs at different fractions (earlier vs later fractions (see Figure 7A)), increasing or reducing the concentration of vRNPs used, choosing vRNPs completely freed of M1 (by Western blot evaluation) or pre-incubating the vRNPs with anti-M1 antibodies to inhibit M1 functions), and it was found, only one time, that complete nuclear import of cy3-vRNP could be observed (Figure 13A). In contrast to previous studies, in which the vRNP, was pooled at peak NP fractions (6-9) (data not shown),

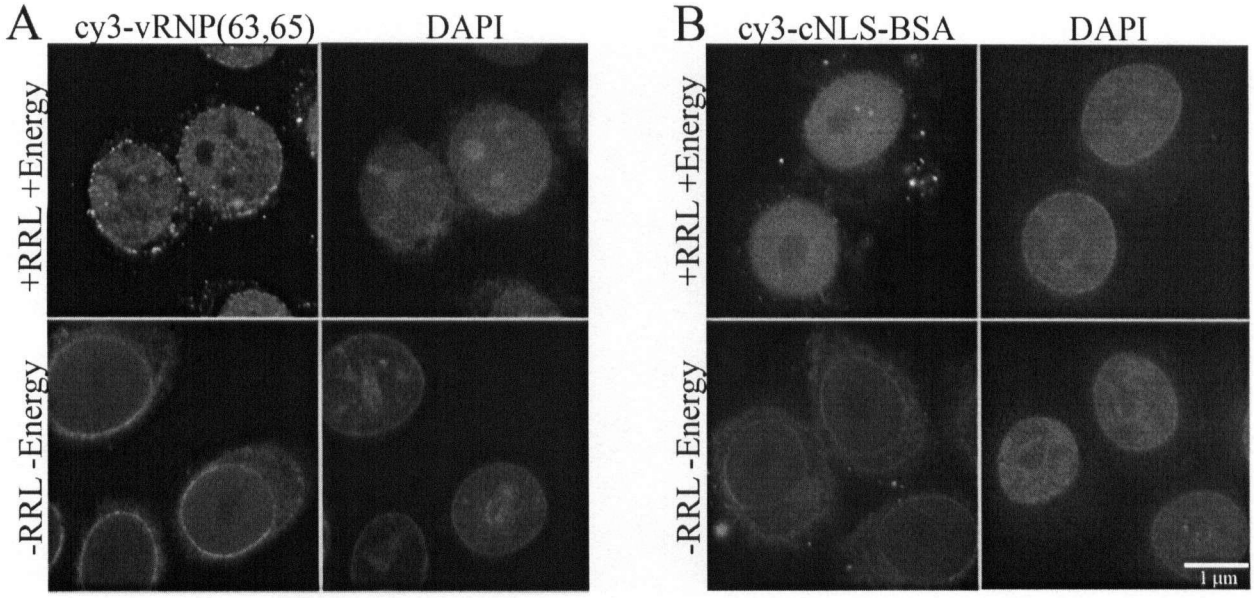

Figure 13: Cy3-vRNP enters the nuclei of digitonin-permeabilized HeLa cells. (A) Cy3-vRNP from purification Nº 63, A and B, and Nº 65, A and B (vRNP(63,65)) and (B) cy3-cNLS-BSA were assayed in digitonin-permeabilized HeLa cells as in Figure 12 and analyzed by fluorescence microscopy.

in this study, the vRNP was pooled from fractions 10-13. In addition, the vRNPs was pooled from a total of four different purifications, all of which had been stored at 4°C for approximately 2 months and then freshly labeled with cy3 prior to the *in vitro* assay. For this reason, these vRNPs were referred to as "aged" vRNP.

3.4.3 "AGED" CY3-VRNP USES THE NPNNLS NUCLEAR IMPORT PATHWAY

To characterize the NLS used by the "aged" cy3-vRNP, two studies were carried out: (1) inhibition studies using specific antibodies (including an anti-NP antibody and antibodies against the putative NLSs of NP) and (2) competition experiments using synthetic NP NLS peptides (NPcNLS and NPnNLS).

In the antibody inhibition experiments, cy3-vRNP nuclear import was tested using antibodies against NP (at a specific, but unknown epitope), M1, BSA, NPnNLS or NPcNLS. Antibodies were incubated with the cy3-vRNP (at 2:1 antibody:NP molar ratio) for 1 hour at room temperature in the dark and assayed in digitonin-permeabilized cells, as described in Materials and Methods, section 2.7.1. The results show that the anti-NP antibody inhibited the nuclear import of "aged" cy3-vRNP, while under the same conditions, the anti-BSA antibody and the anti-M1 antibody did not (Figure 14, and data not shown). These finding demonstrated that the NLS responsible for "aged" cy3-vRNP nuclear import was located on the NP proteins.

To pinpoint which NP NLS was responsible for vRNP nuclear import, anti-NPnNLS and anti-NPcNLS antibodies were used. It was found that in the presence of both anti-NPnNLS and anti-NPcNLS antibody, nuclear import of "aged" cy3-vRNP could be inhibited efficiently (Figure 14). However, individually, the anti-NPcNLS antibody could not effectively inhibit "aged" cy3-vRNP nuclear import, while the anti-NPnNLS antibody could (Figure 14). Theses results indicated that the signal responsible for "aged" cy3-vRNP nuclear import was the NPnNLS.

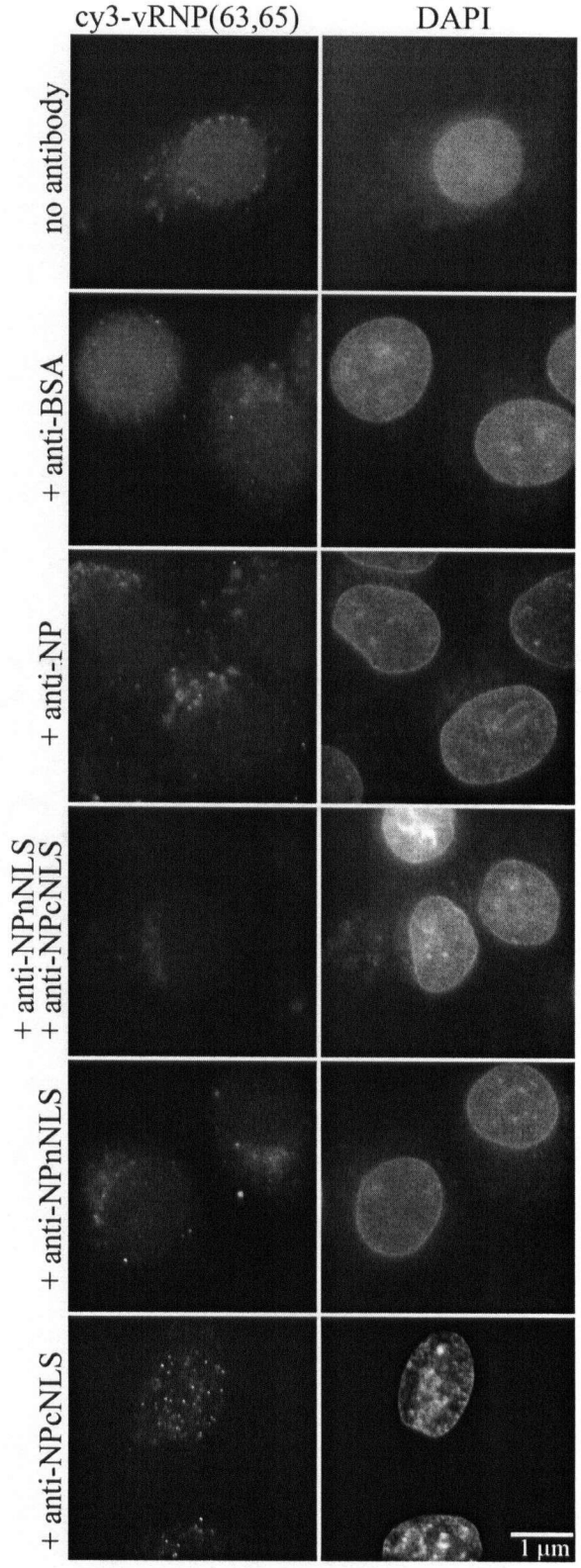

Figure 14 (Caption on next page)

Figure 14: "Aged" Cy3-vRNP nuclear import is inhibited by the anti-NPnNLS antibody but not by the anti-NPcNLS antibody. Cy3-vRNP was incubated with the indicated antibody at 2:1 antibody:NP molar ratio for 1 hour in the dark at room temperature. The cy3-vRNP antibody mixture was then assayed in digitonin-permeabilized HeLa cells in the presence of RRL and energy, as indicated in Figure 12. Cells were analyzed by fluorescence microscopy.

Competition experiments, in which cy3-vRNP was mixed with an excess of peptide (or BSA for control), at a ratio of 1:700 (NP:competitor), confirmed the above findings. In the presence of both NPnNLS and NPcNLS peptides, the nuclear import of "aged" cy3-vRNP was inhibited (Figure 15). However, the nuclear import of "aged" cy3-vRNP was not inhibited in the presence of NPcNLS alone, but it was in the presence of NPnNLS (Figure 15), demonstrating again, that the NPnNLS was the NLS responsible for "aged" cy3-vRNP nuclear import. As a positive control, excess BSA could not inhibit "aged" cy3-vRNP nuclear import under the same conditions (Figure 15).

3.5 Characterization of vRNP Nuclear Import In Live HeLa Cells By Microinjection

Despite large efforts to repeat the cy3-vRNP nuclear import assays with digitonin-permeabilized HeLa cells, it was found that vRNPs were consistently excluded from the nucleus in the presence of RRL and energy (section 3.4.2). Furthermore, it was decided that "aged" cy3-vRNP, being stored in at 4°C for a few months, could have underwent modifications causing it to behave differently from authentic vRNPs. Consequently, freshly purified vRNPs were studied in intact HeLa cells to characterize vRNP nuclear import. HeLa cells were microinjected live, and visualized by direct fluorescence microscopy or immunofluorescence microscopy using anti-NP antibodies.

3.5.1 Freshly purified vRNP could not enter the nucleus of intact HeLa cells after labeled with cy3

It was found, to our surprise that purified vRNPs, competent of nuclear import by microinjection (Figure 9C) could not enter the nucleus of live, intact, HeLa cells after labeled with cy3 (Figure 16C) (Note: both studies uses vRNPs from purification Nº 73B). In the direct fluorescence study, cy3-vRNPs were microinjected into the cytoplasm of HeLa cells. Eleven individual time lapse

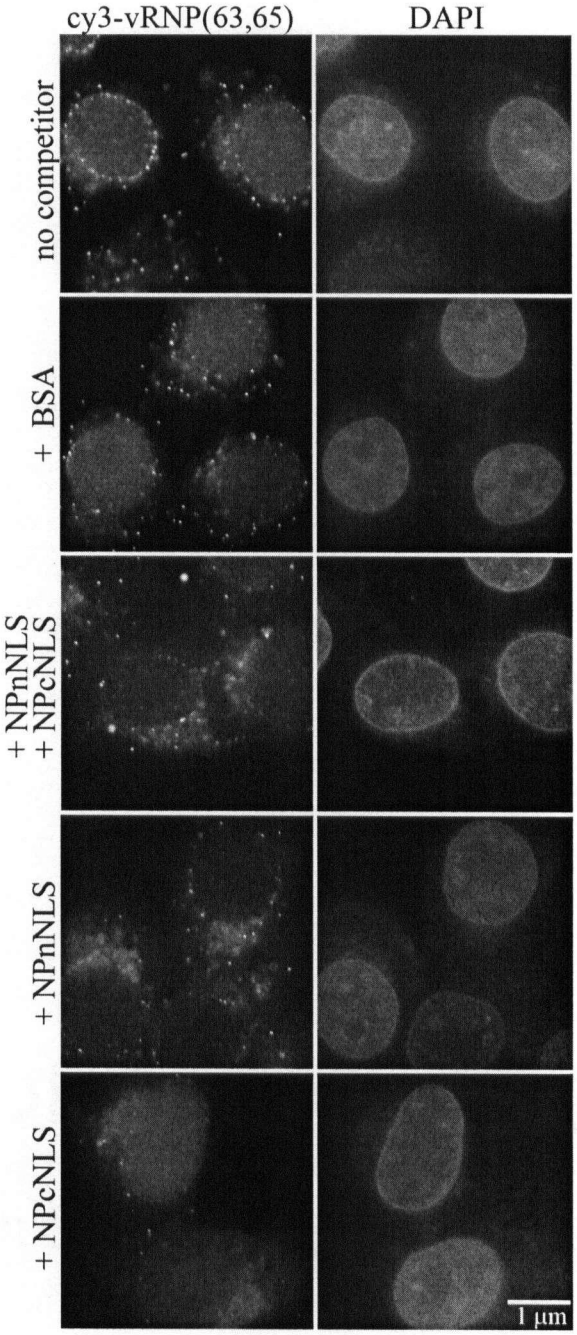

Figure 15: Cy3-vRNP nuclear import is inhibited by the NPnNLS peptide but not by the NPcNLS peptide. Cy3-vRNP was assayed in digitonin-permeabilized HeLa cells as in Figure 14 but in the presence of 700:1 peptide(or BSA):NP molar ratio, as indicated. Cells were analyzed by fluorescence microscopy.

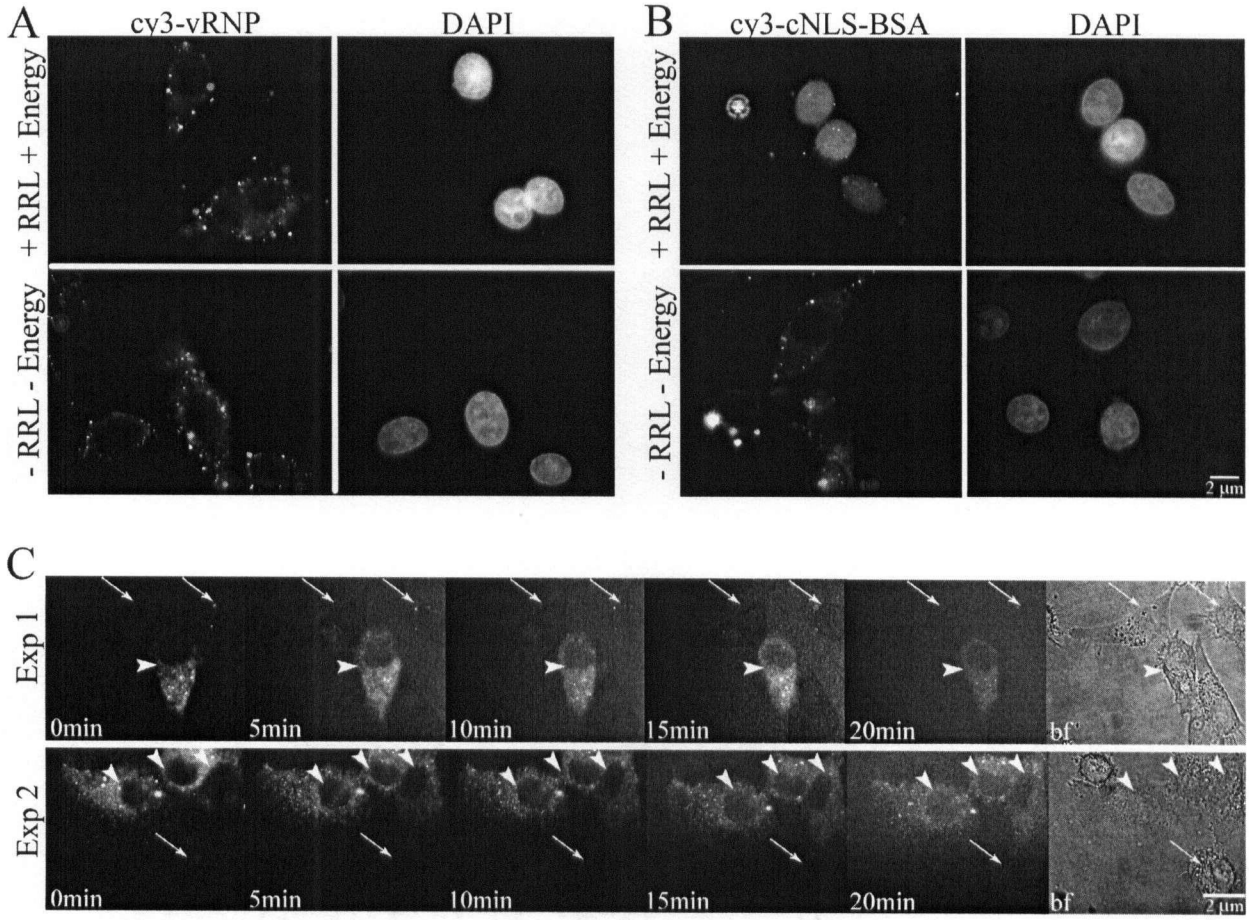

Figure 16: Cy3-labeled vRNP cannot enter the nucleus of microinjected or digitonin-permeabilized HeLa cells. The same vRNP (Purification 73B) previously demonstrated to be competent of nuclear import *in vivo* (see Figure 9C) was labeled with cy3 and its nuclear import was studied in digitonin-permeabilization assays and by microinjection.

(A-B) Digitonin-permeabilization assays. (A) Cy3-vRNP (73B) and (B) cy3-cNLS-BSA were assayed in digitonin-permeabilized HeLa cells and analyzed by fluorescence microscopy as in Figure 12.

(C) Microinjection. Cy3-vRNP (73B) was microinjected into HeLa cells and studied by live cell fluorescence imaging. Two representative time lapse series (Exp1 and Exp2) are shown here. The fluorescent images are shown on the left and the bright field images on the right. White arrowheads and white arrows indicate injected and uninjected HeLa cells respectively.

experiments were performed and where a total of 28 cells were microinjected. None of these injected cells showed any signs of cy3-vRNP nuclear import. In this study, all of the cells were followed up to 5 min, 22 cells up to 10 min, 11 cells up to 15 min and 4 cells up to 20 min (Figure 16C, and data not shown). It was found that cy3-vRNP could not enter the nucleus of the injected cells in all of the tested time intervals. The entire study was repeated using vRNP and cy3-vRNP from a different purification, and the results were similar (data not shown).

The same cy3-vRNP (purification Nº 73B) was also assayed *in vitro* (in the digitonin-permeabilized cell assay) for nuclear import. Consistent with previous studies, cy3-vRNP could not enter the nucleus of digitonin-permeabilized cells in the presence of RRL and energy (Figure 16B), while the control, cy3-cNLS BSA could (Figure 16B). These results demonstrated that cy3-vRNP could not be imported into the nucleus, and the results from the microinjection studies suggested that the vRNP nuclear import activity had been lost during the labeling process.

3.5.2 DIGITONIN-PERMEABILIZED HELA CELLS DID NOT SUPPORT NUCLEAR IMPORT OF FRESHLY PURIFIED VRNP

To test whether freshly purified, unlabeled vRNP can enter the nuclei of digitonin-permeabilized HeLa cells, the same, unlabeled vRNP (purification Nº 73B), found to be import competent in microinjected cells (Figure 9) was assayed in digitonin-permeabilized cells in the presence of RRL and energy. After incubating at 37°C for 30 min, the vRNP was detected by indirect immunofluorescence microscopy. It was found that in the presence of RRL and energy, unlabeled vRNP could not enter the nuclei of digitonin-permeabilized cells and resided primarily in the cytoplasm and the cell periphery (Figure 17A). In contrast, cy3-cNLS-BSA was able to enter the nuclei under the same conditions (Figure 17B).

To test whether vRNP nuclear import in digitonin-permeabilized cells was halted by the absence of essential nuclear transport receptors in RRL, HeLa cytosol (HC) was purified as

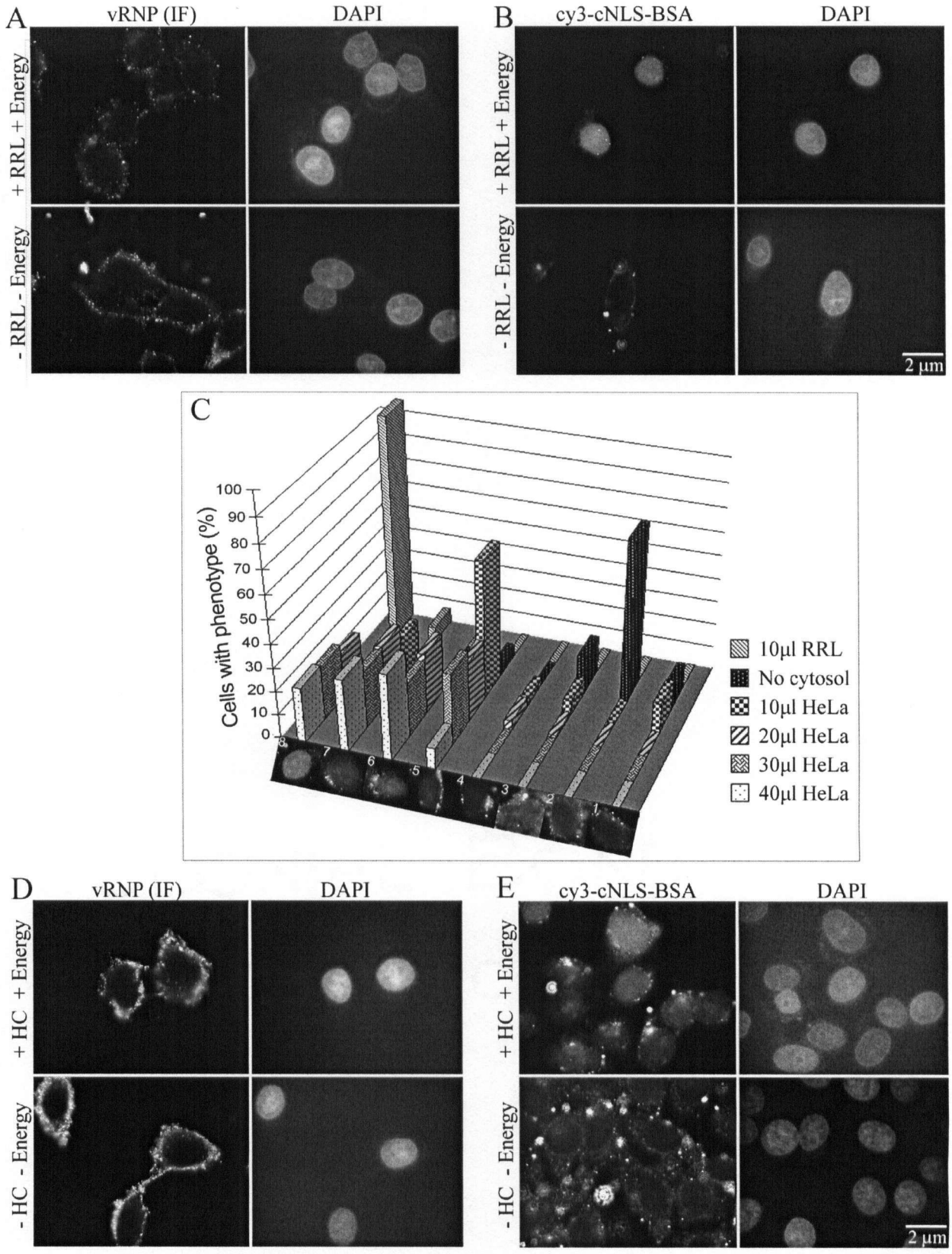

Figure 17 (Caption on next page)

Figure 17: vRNP cannot enter the nucleus of digitonin-permeabilized HeLa cells.
(A-B) Digitonin-permeabilization nuclear import assays with RRL. (A) vRNP (purification N^{o} 73B) competent in nuclear import as demonstrated *in vivo* (Figure 9C) and (B) cy3-cNLS-BSA were assayed in digitonin-permeabilized HeLa cells in the presence or absence of 10 μl RRL and an energy regenerating system (Energy). Cells were visualized by indirect immunofluorescence (IF) using an anti-NP monoclonal antibody (A) and direct fluorescence microscopy (B).
(C) Test of the nuclear import ability of commercial RRL and purified HeLa cytosol (HC). HC and RRL in the indicated volume were used to assay nuclear import of cy3-cNLS-BSA in digitonin-permeabilized HeLa cells. Eight common phenotypes were observed, to which all cells were classified into. The phenotypes range from completely fluorescent nuclei (8) to non-fluorescent nuclei (1) as shown in the guide.
(D-E) Digitonin-permeabilization nuclear import assays with HC. (D) vRNP competent in nuclear import as demonstrated *in vivo* (Figure 10) and (E) cy3-cNLS-BSA were assayed in the presence or absence of 30 μl HC and Energy and visualized by indirect immunofluorescence (D) and direct fluorescence microscopy (E).

previously described (Paschal and Gerace, 1995) and the import activity of HC was evaluated in digitonin-permeabilized cells using cy3-cNLS-BSA (Figure 17, C-E). The assay demonstrated that purified HC could support active nuclear import of cy3-cNLS-BSA, although, judging from the nuclear import profiles of the cy3-cNLS-BSA, the import activity of HC was inferior to that of RRL (Figure 17C). Nonetheless, import assays using digitonin-permeabilized HeLa cells and HC were done, but it was found that, like RRL, purified HC was not able to support vRNP nuclear import *in vitro* (Figure 17D).

To test whether vRNP nuclear import *in vitro* was halted due to nonspecific binding in the cell, vRNP or vRNP pre-incubated with HC for 40 min at 37°C was introduced into digitonin-permeabilized cells or digitonin-permeabilized cells that were blocked with 1% BSA in import buffer for three 5-minute intervals (Figure 18). The vRNP was then visualized using anti-NP antibody. It was found that none of these conditions were able to result in vRNP nuclear import. Consequently, digitonin-permeabilized HeLa cells were not used to characterize the nuclear import pathway of freshly purified vRNPs.

3.5.3 Nuclear import of vRNP in intact HeLa cells could be partially inhibited by NPnNLS peptides

Using live, intact HeLa cells, the question of which NLS on NP drives the nuclear import of vRNP was addressed. Freshly purified vRNP was microinjected into the cytoplasm of in intact HeLa cells in the presence of NPnNLS (^{1}MASQGTKRSYEQMC), NPcNLS (^{198}KRGINDRNFWRGENGRKTRC) or a control peptide (^{35}SDAAAKEHDEAYDQYIKSGKNC). The control peptide was readily available in the lab and it was a sequence from the minute virus of mice (MVM) that has no known nuclear import functions. In these experiments, vRNP was mixed with 10 molar excess of the peptide and this mixture was injected into the cytoplasm of HeLa cells. Cells were incubated for 10-60 min at

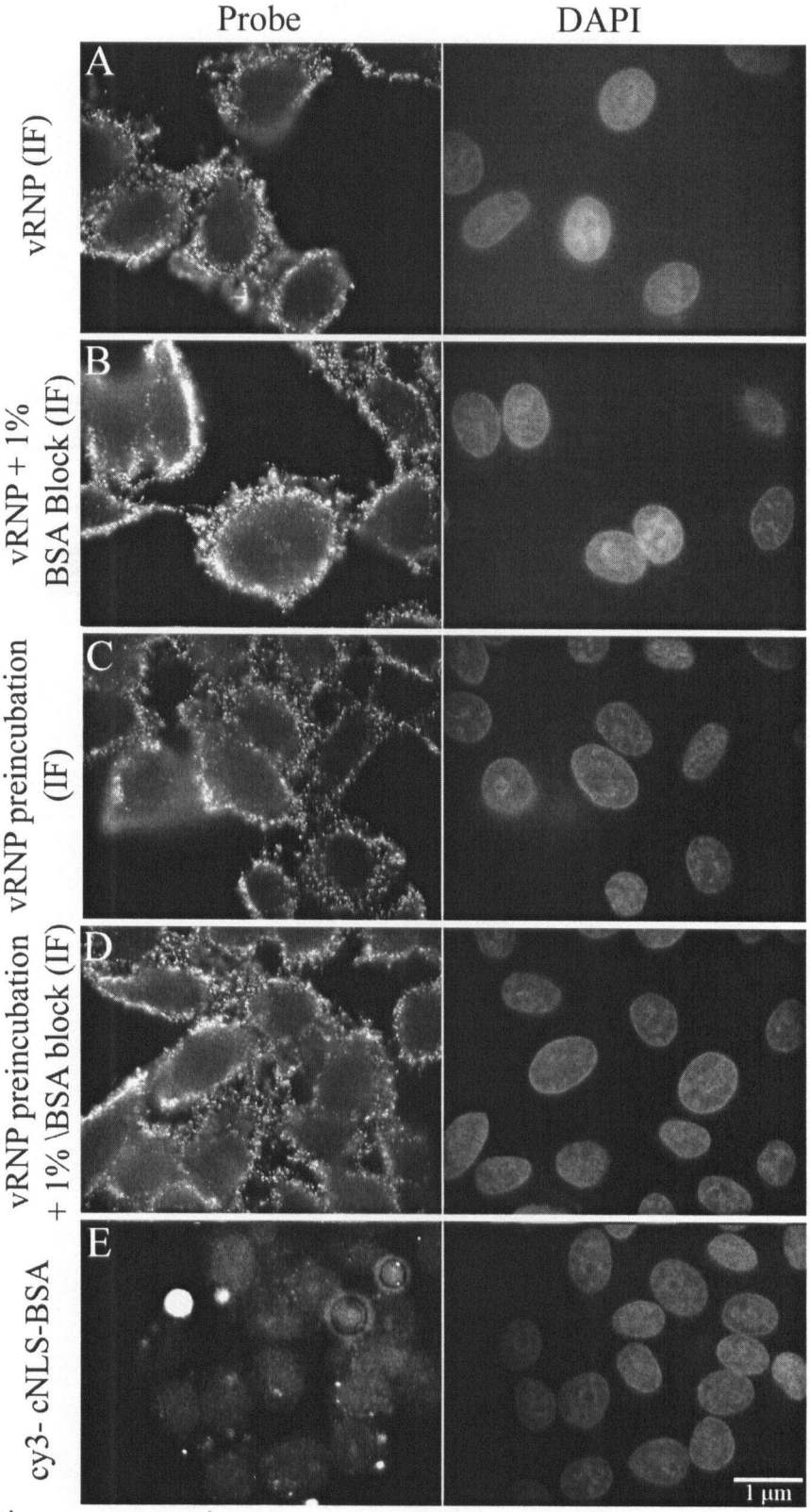

Figure 18 (Caption on next page)

Figure 18: Blocking digitonin-permeabilized HeLa cells with 1% BSA and pre-incubating vRNP with HeLa cytosol prior to nuclear import do not reduce the strong cytosolic-plasma membrane localization of vRNP in the *in vitro* import assays. (A) Fresh vRNP competent in nuclear import was assayed in digitonin-permeabilized HeLa cells in the presence of HC and energy. vRNP was visualized by immunofluorescence microscopy as in Figure 17D. (B) Digitonin-permeabilized HeLa cells were blocked with 1% BSA for three 5-minute intervals before incubated with vRNP as in (A). (C) Fresh vRNP was pre-incubated with HC for 40 min at 37°C and assayed in digitonin-permeabilized HeLa cells as in (A). (D) Fresh vRNP was pre-incubated with HC as in (C) and assayed in BSA-blocked digitonin-permeabilized HeLa cells as in (B). (E) Cy3-cNLS-BSA was incubated in digitonin-permeabilized HeLa cells as in (A) and analyzed by direct fluorescence microscopy.

37°C and the vRNP was visualized by indirect immunofluorescence microscopy using an anti-NP monoclonal antibody.

It was found that both the NPnNLS and the control peptide reduced vRNP nuclear import at 10 molar excess, but the effect of the NPnNLS peptide was stronger (Figure 19). The quantification of the results from three different experiments show that while 96.58% of the cells injected with vRNP alone had predominantly fluorescent nuclei, only 67.39% and 25.00% of the cells co-injected with the control peptide and NPnNLS, respectively, had predominantly fluorescent nuclei. In addition, in the presence of NPnNLS, the majority of the cells had both fluorescent nucleus and cytoplasm (38.89%) (Figure 19B). These data indicated that NPnNLS, at 10 molar excess, could induce a partial inhibition of vRNP nuclear import.

The percentage of cells in each phenotypic class for each competition experiment was found to vary, but the general trend was consistent (see data of three different experiments in Appendix 1). Variability when using the control peptide in the peptide competition experiments was most likely a result from a poor choice of control peptide, because the MVM peptide was later discovered to exhibited heavy nonspecific bindings in cell (data not shown). Consequently, the peptide was found to interfere with vRNP nuclear import (Figure 19 and Appendix 1). To compensate for this, a low peptide:NP ratio was used in the peptide competition experiments and had probably contributed to only a partial inhibition in vRNP nuclear import.

Furthermore, it was found that vRNP nuclear import efficiency dropped with time (data not shown). Thus, the competition experiments, which were done on different days after each vRNP purification, likely had different vRNP nuclear import efficiency. For these reasons, quantitative statistical analysis could not be done for the competition experiments. Alternatively, the primary data from these experiments, which illustrated the range of the different results that was observed, is presented in Appendix 1. This time dependent effect was corrected for the

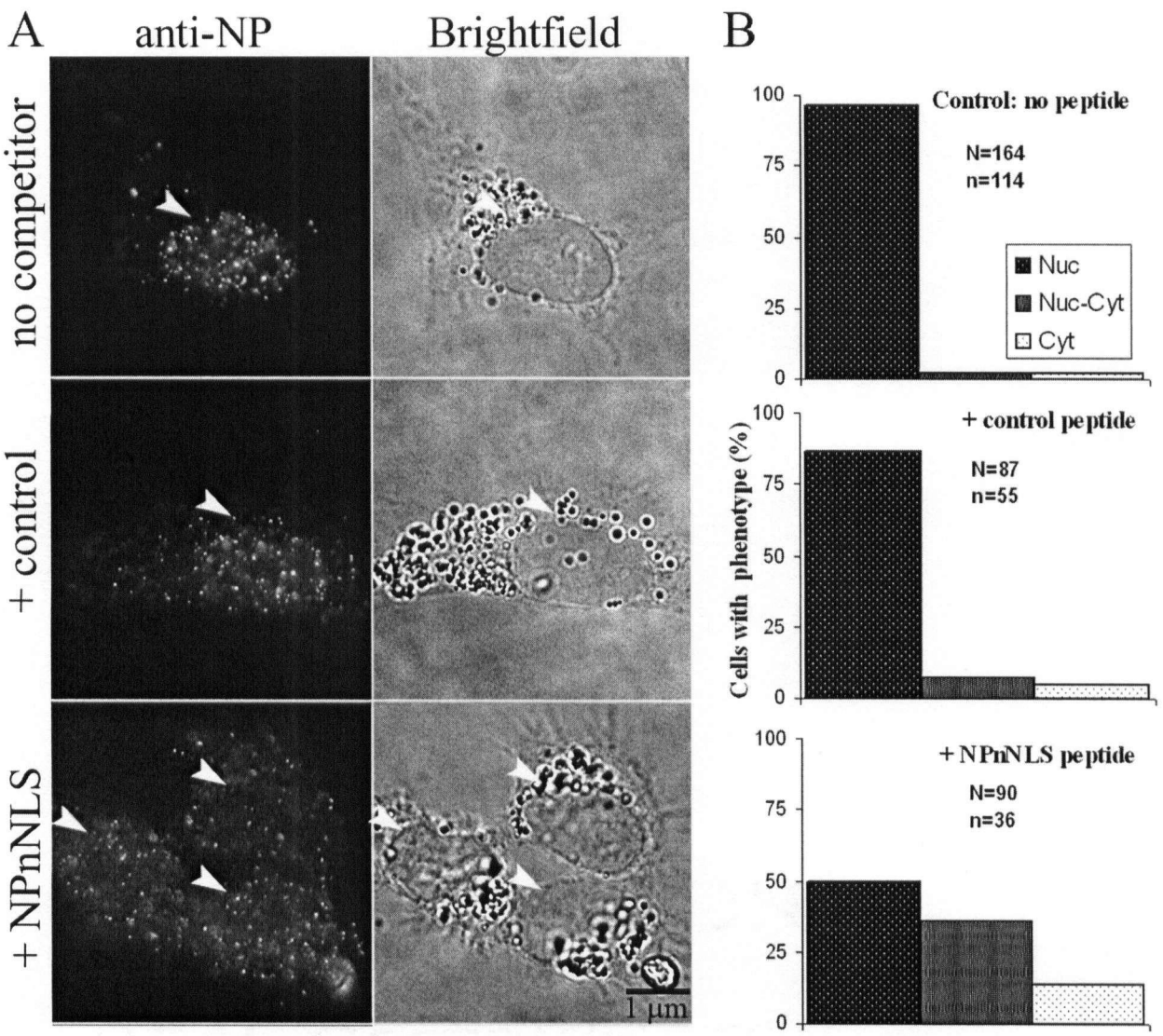

Figure 19: vRNP nuclear import can be partially inhibited by the NPnNLS peptide. Freshly purified vRNP was mixed with ½ volume of PBS (no competitor), control peptide at 10:1 control peptide:NP molar ratio (+ control) or NPnNLS peptide at 10:1 NPnNLS peptide:NP molar ratio (+ NPnNLS), and microinjected into HeLa cells. Injected cells were incubated at 37°C for 10-60 min. Three set of studies using vRNP from three different purifications were analyzed. In all three studies, vRNP + control peptide and vRNP + NPnNLS were microinjected onto cells on the same coverslip and were processed together for immunofluorescence microscopy using an anti-NP antibody.

(A) Representative image of vRNP localization. Fluorescent (left) and bright field (right) image of injected (white arrowheads) cells.

(B) Quantification of vRNP nuclear import. For all three microinjection studies, the percent of fluorescent cells with signals predominantly in the nucleus (Nuc), cytoplasm (Cyt) or equally distributed between the nucleus and the cytoplasm (Nuc-Cyt) were counted and a histogram of their distribution into the three phenotypes are shown. The total number of cells available for analysis (N) and the total number of fluorescent cells (n) were added from all three studies for each condition.

antibody inhibition studies, such that all three experiments were done immediately after purification.

It was found that cells co-injected with NPnNLS showed a two fold reduction in signal when immunolabeled (Figure 19). Out of 92 NPnNLS-vRNP co-injected cells analyzed from three competition studies, only 17 showed fluorescent signals. The nature of this reduction is unknown and is speculated in the discussion.

To our surprise, all competition studies with NPcNLS could not be immunolabeled (Table 2 and Figure 20). None of the four studies using vRNP from three independent purifications produced any fluorescent cells. A total of 352 cells were injected and 224 cells were analyzed. For each study, co-injections of different peptides were performed on adjacent cells. The cells were immunolabeled together, but only cells co-injected with NPcNLS did not show fluorescent signal. The reason for this lack of signal from NPcNLS co-injected cells is not known and is explored in the discussion.

3.5.4 Nuclear import of vRNP in intact HeLa cells is inhibited by the anti-NPnNLS antibody but not by the anti-NPcNLS antibody

To further elucidate the role of the specific signals involved in vRNP nuclear import, antibody inhibition experiments were performed using anti-NPnNLS and anti-NPcNLS specific antibodies. In each inhibition experiment, vRNP was incubated with anti-NPcNLS or anti-NPnNLS antibodies at 1:1 NP:antibody molar ratio or PBS for 1 hour at 4°C before microinjection into the cytoplasm of HeLa cells. The vRNP concentration used for each condition was the same and the injected cells were visualized by indirect immunofluorescence using an anti-NP antibody.

It was found that, under these conditions, the anti-NPnNLS antibody could inhibit vRNP nuclear import *in vivo* efficiently (Figure 21). From an average of three experiments, using vRNP from three different purifications, 90% (SD=17%) of the cells had cytoplasmic vRNP

Table 2: vRNP competition studies using the NPcNLS peptide revealed no NP fluorescent signal after immunofluorescence labeling. Fresh vRNP from three different purifications was mixed with ½ volume of the indicated amount of NPcNLS peptide. The mixture was microinjected into HeLa cells and the cells were immunolabeled using an anti-NP antibody. The number of injected cells ($Total^{inj}$), the number of cells available for analysis (N) and the number of fluorescent cells (n) were counted. For comparison, parallel injections using the same vRNP mixed with the NPnNLS or with BSA were analyzed. The injected cells for the different conditions were in the same coverslip and therefore, were treated in the same way during the immunofluorescence protocol.

Peptide or Protein	Molar Excess of Peptide	vRNP Purification Nº	$Total^{inj}$	N	n
NPcNLS	**10**	**vRNP74B**	132	109	0
	40	**vRNP74A**	69	38	0
	50	**vRNP75A**	86	36	0
	325	**vRNP74A**	65	41	0
BSA	**10**	**vRNP74B**	111	69	40
NPnNLS	**40**	**vRNP74A**	65	20	7
	50	**vRNP75A**	128	39	33
	325	**vRNP74A**	125	65	16

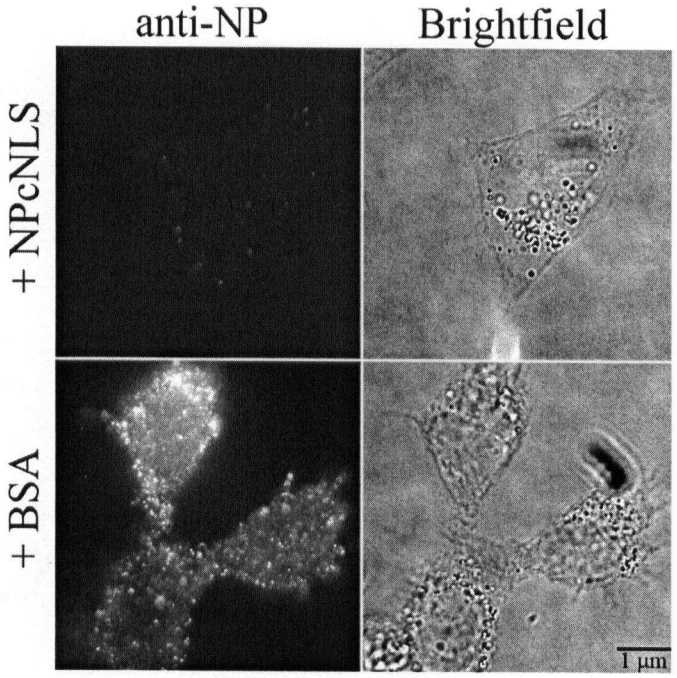

Figure 20: HeLa cells co-injected with vRNP and NPcNLS could not be immunolabelled with the monoclonal anti-NP antibody. Representative images showing cells co-injected with NPcNLS (one cell) or BSA (three cells) and immunolabeled together using an anti-NP antibody. vRNP was mixed with ½ volume of NPcNLS peptide (or BSA) at 10:1 peptide (or protein):NP molar ratio. Injected cells were incubated at 37°C for 10-60 min. Images were captured at the same exposure settings.

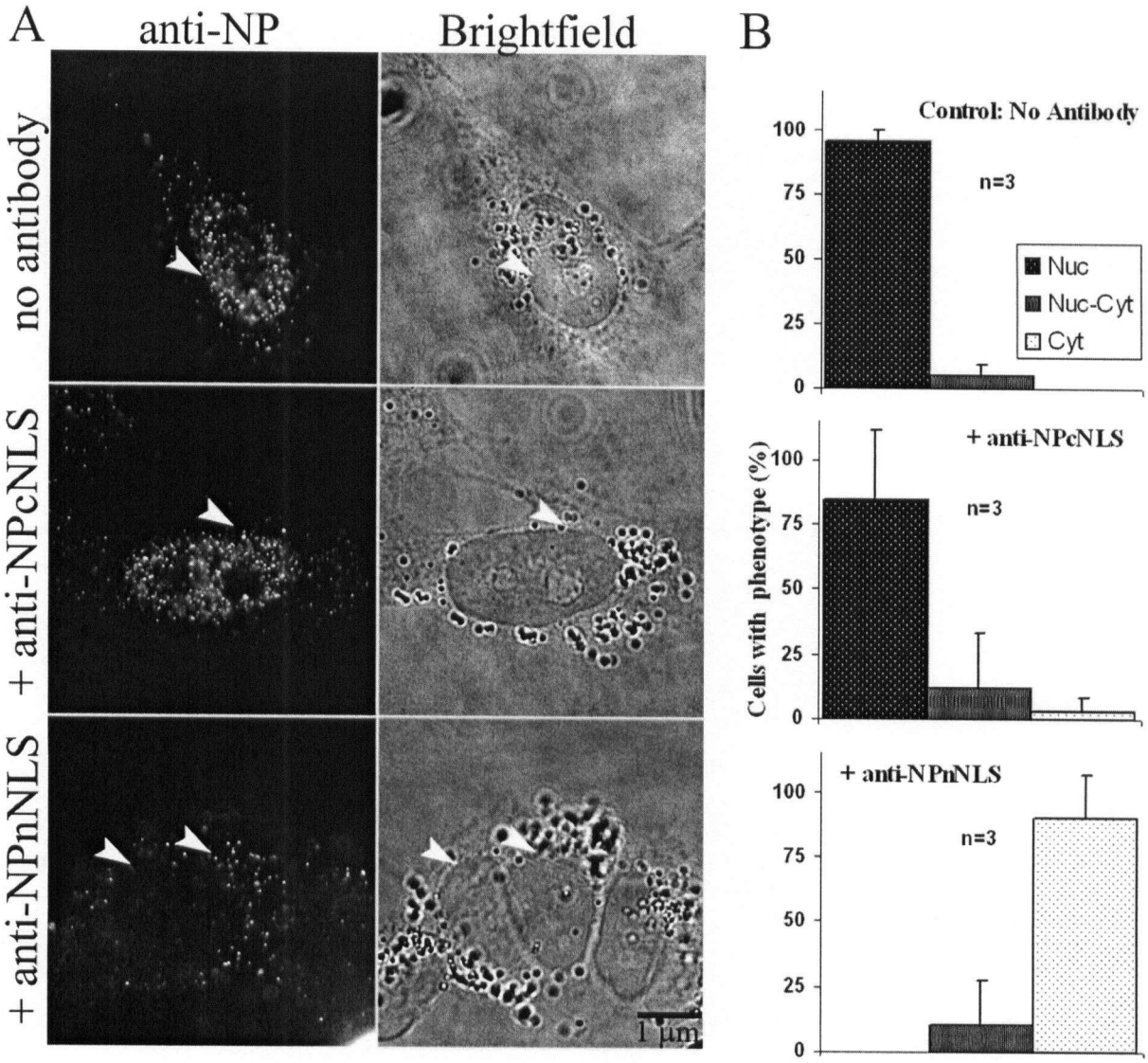

Figure 21: vRNP nuclear import can be inhibited by the anti-NPnNLS but not the anti-NPcNLS antibody. Freshly purified vRNP was incubated at 4°C for 1 hour with 3/5 volumes of PBS (no antibody), affinity purified anti-NPcNLS (+ anti-NPcNLS) or anti-NPnNLS (+ anti-NPnNLS), each at 1:1 antibody:NP molar ratio, and the mixture was microinjected into HeLa cells. The NP and antibody molar concentration was individually predetermined from its absorbance as described in the materials and methods (section 2.3.2). Injected cells were incubated at 37°C for 16-55 min. Three sets of studies (n=3) using vRNP from three different purifications were analyzed. In the three studies, vRNP+PBS, vRNP+anti-NPcNLS antibody and vRNP + anti-NPnNLS antibody were microinjected onto cells on the same coverslip and were processed together for immunofluorescence microscopy using the anti-NP antibody.
(A) Representative image of vRNP localization. Fluorescent (left) and bright field (right) image of injected (white arrowheads) cells for each condition are shown.
(B) Quantification of vRNP nuclear import. For each of the three microinjection studies, the percent fluorescent cells with signals predominantly in the nucleus (Nuc), cytoplasm (Cyt) or equally distributed between the nucleus and the cytoplasm (Nuc-Cyt) were determined. The histograms show the average of the three experiments. The error bars represented the SD

calculated for each phenotype. Numerically, the SD for the Nuc, Nuc-Cyt, Cyt were 4%, 4%, 0%, for the no antibody condition, 26%, 21%, 5%, for the anti-NPcNLS condition, and 0%, 17%, 17%, for the anti-NPnNLS condition, respectively. For each sample, the probability (p) that the average percent of cells in one phenotype is the same as another phenotype is calculated using a two-tailed student t test. For the control, $p<0.0001$ for Nuc=Nuc-Cyt, indicating that the average percent of Nuc is significantly different from Nuc-Cyt; in the presence of anti-NPcNLS antibody, $p=0.0200$ for Nuc=Nuc-Cyt, $p=0.0339$ for Nuc=Cyt, and $p=0.5425$ for Nuc-Cyt=Cyt, indicating that while the average percent of Nuc-Cyt is not significantly different from Cyt, the average percent of Nuc is significantly different from Nuc-Cyt and Cyt; finally, in the presence of anti-NPnNLS antibody, $p=0.0048$ for Nuc-Cyt=Cyt, indicating that the average percent of Nuc-Cyt is significantly different from Cyt.

localization (Figure 21B). The three experiments provided a total of 36 cells that could be visualized by immunofluorescence microscopy, of which, a total of 30 cells showed predominant cytoplasmic vRNP localization. The remaining six cells showed an equal nuclear-cytoplasmic localization and it was found that no cells, from all three studies, showed a predominant nuclear localization.

In contrast, the anti-NPcNLS antibody was found to have little inhibitory effect on vRNP nuclear import. Of the three *independent* microinjection studies performed, it was found that on average, 85% (SD=26%) of the cells had nuclear vRNP localization (Figure 21B). From the three experiments, a total of 45 cells could be visualized by immunofluorescence microscopy, of which, 40 cells showed predominant nuclear vRNP localization. Four cells were found to show equal nuclear-cytoplasmic vRNP localization and only one cell was found to show predominant nuclear localization.

The vRNP localization in the absence of antibody (PBS) was similar to those in the presence of the anti-NPcNLS antibody. For the same three experiments, on average, 95% (SD=4%) of the cells had nuclear vRNP localization (Figure 21B). Out of 120 cells that could be visualized from the three experiments, it was found that 114 cells showed predominant nuclear localization. Only six cells showed equal nuclear-cytoplasmic localization and no cells were found to show predominant cytoplasmic distribution.

The SD for the three anti-NPnNLS antibody inhibition experiments were 0% (nuclear), 17% (equal nuclear and cytoplasmic) and 17% (cytoplasmic) (Figure 21B) and the greatest source of variation came from the first experiment (see data of each experiment in Appendix 2). The low SD in the three antibody inhibition experiments (Figure 21B and Appendix 2) allowed for statistical analysis (Appendix 3). However, there was a major problem. By nature of microinjection studies, the sample size for each experiment was low and using

immunofluorescence to visualize the cells further reduced the sample size.

To address the low sample size in these studies, the nucleocytoplasmic and cytoplasmic phenotypic categories were combined to form the non nuclear category, and the nuclear and non nuclear distribution for the antibody treated sample were individually compared with the PBS control sample. The chi squared (χ^2) likelihood ratio, the χ^2 Pearson, the two-tailed Fisher's exact test, and the two-tailed student t test were calculated for the hypothesis (H_o) that anti-NPnNLS (or anti-NPcNLS) antibodies did not affect vRNP nuclear import (the vRNP localization was the same in the presence or the absence of the antibodies). It was found that in the presence of anti-NPnNLS antibody, the vRNP localization was significantly different from the control (with PBS) ($p<0.0001$, χ^2 likelihood ratio; $p<0.001$, χ^2 Pearson, $p<0.0001$, two-tailed Fisher's exact test, $p<0.0001$, two-tailed student t test; Ho rejected) (Appendix 3). In contrast, the vRNP localization in the presence of anti-NPcNLS antibody was not significantly different from the control ($p<0.1932$, χ^2 likelihood ratio; $p<0.1736$, χ^2 Pearson, $p<0.18$, two-tailed Fisher's exact test, $p=0.5629$, two-tailed student t test; Ho not rejected) (Appendix 3). Furthermore, vRNP localization in the presence of anti-NPnNLS antibody was significantly different from vRNP localization in the presence of anti-NPcNLS antibody ($p=0.0304$, two-tailed student t test).

It was found that in each of the three experiments, vRNP localization in the presence of anti-NPnNLS antibody was significantly different from the control (Appendix 3). However, in the presence of anti-NPcNLS antibody, one experiment was found significantly different from the control, suggesting that some variability was present when anti-NPcNLS antibody was used. This was also evident from a higher SD in anti-NPcNLS antibody inhibition experiments: 26% (nuclear), 21% (equal nuclear and cytoplasmic) and 5% (cytoplasmic) (Figure 21).

Finally, although samples incubated with antibodies showed a slightly reduction in vRNP immunofluorescence labeling efficiency, from 53% to 29% and 20% for the anti-NPcNLS and

anti-NPnNLS antibodies respectively (Figure 21), unlike the peptide inhibition studies, the reduced labeling efficiency was similar for both antibodies.

In conclusion, results from both the peptide competition and the antibody inhibition studies showed that vRNP nuclear import *in vivo* was mediated by the NPnNLS and not by the NPcNLS.

4 DISCUSSION

The goal of this thesis was to identify the NLS used by authentic influenza vRNPs for nuclear import. Supporting previous studies using vRNA-NP complexes assembled *in vitro* (O'Neill et al., 1995; Cros et al., 2005), the results from this thesis demonstrated that authentic influenza vRNPs (purified from influenza A virus; therefore, assembled *in vivo* with NP, PA, PB1 and PB2) also used NP for nuclear import. This protein has two previously characterized NLSs, the NPcNLS and the NPnNLS. After performing both peptide competition and antibody inhibition experiments, the NLS was further pin-pointed to the NPnNLS. For the antibody inhibition experiments, nearly all of the vRNP nuclear import activity was inhibited by a polyclonal peptide antibody against the NPnNLS (Figure 21). In contrast, in the presence of the anti-peptide antibody that specifically recognizes the NPcNLS, little inhibition of vRNP nuclear import was observed (Figure 21). The results provided in this thesis demonstrated, for the first time, that the NPnNLS was the dominating signal for the nuclear import of authentic vRNPs.

Results from the immunogold TEM showed that although both the NPcNLS and the NPnNLS could be located on the outer surfaces of vRNPs. Approximately the same number of NPnNLS could be localized using a 50-fold lower concentration of the anti-NPnNLS antibody, suggesting that more NPnNLS are present on the surface of vRNPs than NPcNLS. These results complement the antibody inhibition studies. In addition, they support the hypothesis that the dominating NLS on authentic vRNPs is NPnNLS, because it is largely exposed on the vRNP surface, and therefore, easily accessible to the host nuclear import receptors.

Furthermore, Western blot experiments showed that the anti-NPnNLS antibody was NP specific, and had no affinity for the PA, PB1 or PB2 NLSs (Figure 7D), but the anti-NPnNLS antibody alone could inhibit the nuclear import of authentic vRNPs. This suggested that NP is

the functional protein responsible for vRNP nuclear import, and that the three polymerases do not play a major role in this process. The possible involvement of the polymerases in this process could not be ruled out based on the results presented in this thesis, because the effects of indirect inhibition, such as steric hindrance, could not be ruled out.

Although the results from both the peptide competition and the antibody inhibition experiments, presented in this thesis, demonstrated that vRNP nuclear import could be inhibited by interfering with the NPnNLS pathway (Figures 19 and 21), the conditions used in the antibody inhibition experiments produced a lower SD and stronger control-experimental difference. For this reason, the methods described for the antibody inhibition studies in this thesis would be the recommended approach for future studies.

When competition experiments were done in the presence of the NPcNLS peptides, it was found that none of the vRNP could be labeled by the monoclonal anti-NP antibody (Table 2). The exact reason for this was not clear. The epitope recognized by the monoclonal NP antibody was not disclosed by the vendor. However, I found the epitope that the monoclonal antibody recognizes is very delicate. Freezing the vRNP at -80°C or disrupting the vRNP with 1% SDS in Western blot analysis prevents NP from being recognized by the antibody (data not shown). These results suggest that the epitope is a 3D structure and not a linear peptide sequence. Thus, one hypothesis is that the NPcNLS peptide associated to the NPs in the competition inhibition experiments, and prevented the anti-NP antibody from binding to the epitope by steric hindrance. Researching the literature showed that the NPcNLS peptide overlaps an NP domain that is involved for NP-NP association (Elton et al., 1999a), holding three key amino acids (R^{199}, R^{204}, R^{213}), including one (R^{199}) that is vital for the association, such that an alanine substitution at R^{199} reduce NP-NP binding by three folds (Figure 5, and Elton et al., 1999a).

Effects from steric hindrance were likely present in the immunofluorescence studies. In the presence of every antibody or peptide tested, a reduction in vRNP labeling efficiency using the anti-NP antibody was observed (section 3.5.3 and 3.5.4). These findings support that the NPcNLS peptide, used at a 10:1 peptide:NP ratio, could be blocking the epitope, preventing anti-NP antibody binding.

Direct visualization of the vRNP by conjugation to a fluorochrome does not suffer from a reduction of fluorescent signal induced by steric hindrance. In fact, visualizing fluorochrome conjugation would be the most direct and convenient method to visualize the trafficking process of macromolecules. However, based on the results in this thesis, it was concluded that the vRNPs lose their nuclear import activity in HeLa cells, *in vivo*, after it was conjugated to the cy3 fluorochrome (Figure 16C). Almost all commercial fluorochromes use primary amines on residues such as K and R for protein conjugation. K and R residues, however, are critical to the proper function of the NLS. Modifying these amino acids can render the signal nonfunctional. Free floating proteins such as the cNLS conjugated BSA, have a coat of amino acids exposed on its surfaces. These amino acids include K and R residues that are not part of the cNLS. Therefore, conjugating fluorochromes such as cy3 to the cNLS-BSA would likely not affect its nuclear import activities (Figure 12D, 13B, 16B, and 17, B and E). In contrast, the NPs in the vRNP were tightly wrapped by the RNA backbone. Consequently, a limited number of amino acids (including K and R residues) are exposed to the environment. For this reason, conjugating the vRNP to cy3 can modify critical K and R residues on NPnNLS (Figure 5), thereby, destroying its function. This was observed (Figure 16), and for this reason, immunofluorescence microscopy was used to visualize vRNP.

Digitonin-permeabilized cell assay would be a powerful tool in this thesis because the treated cells would be selective permeabilized at the plasma membrane but would have an intact

NE; thus, allowing for the specific steps in the nuclear import pathway to be tested (Adam et al., 1990). It was found, however, that digitonin-permeabilized HeLa cells were incompatible with vRNPs isolated from influenza A virus (Figure 17, A and D). A major problem associated with digitonin-permeabilized cells is that they are prone to nonspecific associations. After the plasma membrane is permeabilized and the cytosol removed, many membrane and cytoplasmic sites that are normally hidden are exposed. These sites are recognized by the vRNPs and import is halted. Sometimes the nonspecific binding could be eliminated, but sometimes it could not (Gorlich et al., 1994), and a large effort was made to remove the vRNPs from their nonspecific binding sites (3.4.2), but none of the methods used were successful (Figure 18). For this reason, vRNP nuclear import was studied by microinjection in HeLa cells.

In vitro assembled RNA-NP complexes when assayed in digitonin-permeabilized buffalo rat liver (BRL)-3 A cells did not have this problem (O'Neill et al., 1995, Cros et al., 2005) and neither did vRNP complexes that have been kept at 4°C for few months (Figure 13, 14 and 15). One explanation is that features in the *in vitro* assembled vRNA-NP complexes, such as the low NP:RNA ratio, prevent the vRNA-NP complexes from forming all of its normal structural domains, including the regions involved in nonspecific binding to digitonin-permeabilized HeLa cells, suggesting that vRNA-NP complexes and the vRNPs isolated from the influenza virus differ on an ultrastructural level. Similarly, as purified vRNP age and gradually disassemble at 4°C, these nonspecific binding domains can be lost. Without these nonspecific binding regions, vRNPs kept at 4°C for a few months are freed from its nonspecific binding sites. This hypothesis is supported, at least in part from experiments using vRNPs from several other purifications that after being stored at 4°C for a few months, these vRNPs diffused into the nucleus of digitonin-permeabilized HeLa cells (data not shown). These results supported that when vRNPs are kept in

4°C for a few months, they had, in fact, underwent modifications/degradation. One example of such modification is protease degradation resulted from microbial contamination.

While the work described in this thesis was underway, two manuscripts characterizing influenza vRNP nuclear import were published (Babcock et al., 2004; Cros et al., 2005). The first group, Babcock et al. (2004), characterized vRNP nuclear import in real time by microinjecting vRNP in BS-C-1 cells, an African green monkey kidney epithelial cell line. In contrast to the results presented in this thesis, Babcock et al. (2004) was able to show that the majority of the cy3-labeled vRNP purified from influenza virus entered the nucleus of BS-C-1 cells within 15 min after injection (Figure 16, and Babcock et al., 2004). The purification and labeling protocols used by these authors were similar to those used in this thesis, with the exception that Babcock et al. (2004) labeled the vRNPs at a cy3:protein ratio of 1, (i.e., a cy3:vRNP ratio of 36-94). I used a cy3:protein ratio in the range of 0.1 (section 3.4.2) to minimize modification to the NPnNLS and to ensure that every vRNP but not every vRNP protein was theoretically labeled. One hypothesis that explains for the contrasting results between Babcock et al. (2004) and that of this thesis is that HeLa cells and BS-C-1 cells have different importin α expression patterns. A difference in importin α expression pattern have been reported for cells derived from different human tissues (Kohler et al., 2002) and cells from derived different mouse tissues (Tsuji et al., 1997). In particular, it has been demonstrated that in HeLa cells, the absolute overall levels of importin α protein expression is considerably lower than other human cells such as endothelial cells, Matu breast cancer cells, or Jurkat T cells (Kohler et al., 2002). This is particular evident for the importin α1 levels, which has been shown to be involved in NP nuclear import (O'Neill et al., 1995; Cros et al., 2005). No information is available to date on the importin α expression patterns of the BS-C-1 cells; however, judging from the unusually weak importin α expression

patterns in HeLa cells, BS-C-1 cells are likely to have a stronger importin α expression pattern than HeLa cells. This high concentration of importin α in BS-C-1 cells can compromise for the modifications in vRNP NLSs by cy3, while the low concentration of importin α in HeLa cells cannot.

The above hypothesis, namely, a difference in importin α expression in HeLa cells (used in this thesis) and BS-C-1 cells (used by Babcock et al. (2004)) contribute to a difference in cy3-vRNP nuclear import profiles, can be tested through a series of experiments. First, the expression levels of importin α1 and α5 in HeLa cell lysate and BS-C-1 can be compared by taking lysate from HeLa cells and BS-C-1 cells, and performing a Western blot using anti-importin α1 and anti-importin α5 specific antibodies. If the hypothesis is true, then more importin α1 and or α5 will be found in the lysate of BS-C-1 cells compared to HeLa cells. Next, the effects of importin α expression levels on cy3-vRNP importin α association can be directly evaluated in a binding assay, such that the cy3-vRNP, functioning here as a bait, can be used to pull down importin αs from the lysate of HeLa cells and BS-C-1 cells. Cy3-vRNP bound importin αs can be purified in a glycerol gradient by ultracentrifugation followed by fractionation, or by affinity chromatography. The identity of each importin α can be confirmed using specific anti-importin α antibodies, or by mass spectroscopy. Levels of importin αs present can be quantified digitally or in a luminescent analysis. If the results indicate a significant higher level of importin α is pulled from BS-C-1 cells by cy3-vRNP as compared to that pulled from HeLa cells, then it can be concluded that a difference in importin α expression pattern in HeLa cells and BS-C-1 contributes to a difference in cy3-vRNP-importin α binding in the two cell types. Finally, the effect of importin α concentration on cy3-vRNP nuclear import can be tested by elevating, through transfection, the expression levels of importin α in HeLa cells. If it is shown that HeLa

cells with a higher importin α expression level can support cy3-vRNP nuclear import, then the hypothesis that a difference in cy3-vRNP nuclear import profile in HeLa cells and BS-C-1 cells is due to a difference in importin α expression levels, can be demonstrated to be true.

In the second manuscript, Cros et al. (2005) showed that vRNA-NP complexes entered the nucleus of digitonin-permeabilized cells in a mechanism that is dependent of the NPnNLS. Their findings were consistent with, and supported the findings described in this thesis (Figure 14, 15 and 21). The group also found that the NPnNLS was the predominant NLS on NP, and in contrast to previous studies (Weber et al., 1998), that NPcNLS did not play a role in NP nuclear import. Finally, their competition experiments using NPnNLS and SV40 cNLS peptides suggested that although both NPnNLS and SV40 cNLS used importin α5 for nuclear import, they bound to importin αs at different sites.

Putting together the data collected from this thesis and what was known in the current literature, a model for the nuclear import of influenza vRNP could be compiled (Figure 22). This would become the second model, after U snRNP (Fischer et al., 1993; Bordonne, 2000), to show that the nuclear import of a RNP complex, was mediated by the NLS on one of its proteins. In this model, upon released into the host cytoplasm, the influenza vRNP becomes dissociated from most, although likely not all of its associating M1. Recall, from section 3.1.1 and 3.2 that a low concentration of M1 can be tolerated without largely compromising the nuclear import properties of vRNPs. With the majority of M1 dissociated, a large portion of surface NPnNLS becomes exposed (Figure 22, step 1). The NPnNLS is recognized by host adaptor molecules importin α1 or importin α5 (Figure 22, step 2), and is joined to the host importin β via either of these adaptor molecules (Figure 22, step 3). Importin β brings the importin α-vRNP to the FG repeats on the NPC and transports the vRNP complex into the nucleus. Once inside the nucleus, the vRNP

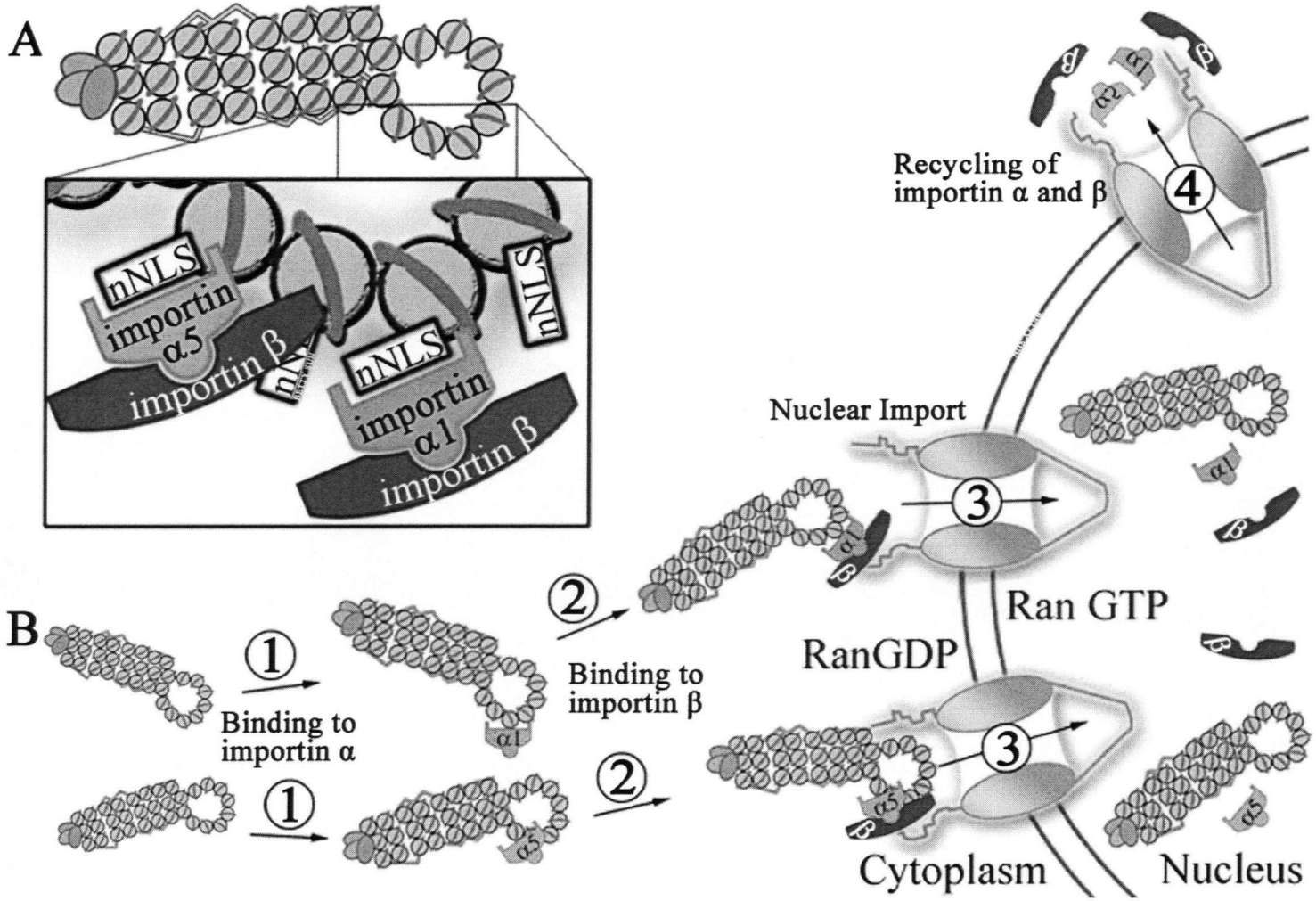

Figure 22: A model for authentic vRNP nuclear import. (A) Schematic diagram of the binding of importin α and importin β to the NPnNLS on authentic vRNP. (B) Steps in the vRNP nuclear import pathway (see text for details). Note: A colored copy of this figure is available in the department of zoology at the University of British Columbia on 6270 University Boulevard, Vancouver, British Columbia, V6T 1Z4.

dissociates from the importins in the presence of Ran GTP and viral mRNA synthesis starts. Like any other cNLS import pathway, the importins are then exported from the nucleus to allow for further rounds of nuclear import (Figure 22, step 4).

One application arisen from the research presented in this thesis is the ability to design anti-virals against the influenza virus. I have demonstrated that purified anti-NPnNLS antibodies can effectively inhibit vRNP nuclear import in intact cells. Therefore, I propose to inhibit the influenza viral replication by inhibiting the vRNP nuclear import via the NPnNLS pathway. This strategy is particularly attractive for two reasons. First, influenza vRNP nuclear import takes place early in the viral life cycle. By inhibiting vRNP nuclear import, all subsequent steps in the viral life cycle, such as RNA replication, protein synthesis, viral assembly and budding will not take place, thereby reducing viral induced damages on the host cell, and increasing the chance of rescuing the host cell. Second, NP also uses the NPnNLS for nuclear import; therefore, inhibiting the NPnNLS pathway can also inhibit NP nuclear import, and in turn, preventing vRNP assembly, and reducing the number of viable vRNP and mature viruses. Ideally, this inhibition will cause an overload to the host protein synthesis system that apoptosis would take place before any virus can be released. More importantly, the proposed anti-viral therapy will attack the influenza A virus on two essential replication steps: vRNP nuclear import and NP nuclear import.

Presently, two immediate hurdles need to be addressed before an effective antiviral can be tested: one involves drug delivery, and the other, inhibitor design. Efficient drug delivery, involving target specificity and vessel design is particularly important in this anti-viral therapy because the target is an intracellular process. Therefore, the inhibitor must be able to enter the infected cell specifically and efficiently. Active research is currently being conducted on an array

of drug delivery systems, including proteoliposomes, which is a promising vessel to deliver inhibitors of the NPnNLS nuclear import pathway. In particular, I envision a proteoliposome inserted with HA and M2, and encasing the anti-viral, undergoing endocytosis and internalization, to release the antiviral into the cytosol. Due to its influenza derived characteristics, I will call these proteoliposomes "mini-influenza like anti-influenza".

The second hurdle involves designing the anti-viral itself. Viruses rely on host machineries such as the importin family nuclear import receptors for replication. Nuclear import receptors, however, are essential to the normal functions of the host cell. Therefore, inhibition of the nuclear receptors is deleterious to the host cell. A good anti-viral, then, must achieve viral inhibition while minimize adversity. For this reason, I believe, the influenza vRNPs is a better target for anti-viral design than host nuclear import receptors, and I have identified in this thesis, a novel target site on the vRNP, the NPnNLS.

However, in order to impose a minimal adverse effect to the host cell, the anti-viral must be highly specific. This is difficult to achieve because the NPnNLS is recognized by importin α1, an important nuclear import adaptor that recognizes other host cell cNLS. All NLSs recognized by importin α1 share similar characteristics; therefore, an inhibitor with an affinity for the NPnNLS will likely have an affinity for other cNLSs. Furthermore, even if large effort is expended to create an NPnNLS specific inhibitor, I can foresee a quick viral mutation take in place, allowing the virus to escape the effects of the inhibitor. For these reasons, I believe the key to designing a good antiviral is to targeting unique and essential viral traits.

Two of such essential characteristics are found in the vRNPs. They are: (1) exposed NPnNLS—the NPnNLS must be exposed for the vRNP to be functional and (2) NP bound vRNA--the vRNA must bind to NP for it to be nuclear imported. Therefore, I envision the anti-

viral to be an inhibitor with the ability to utilize both of these characteristics (that is, having two binding sites), such that optimum binding efficiency takes place when both the NPnNLS and the vRNA are bound. The overall effect is the ability to achieve target specificity while minimizing host cell adversity.

5 CONCLUSION REMARKS

To conclude, the results from this thesis demonstrated that vRNPs isolated from influenza A virus use NP for nuclear import. More specifically, vRNPs, which have densely distributed NPnNLS on their surfaces, bind nuclear import receptors using the NPnNLS, and are taken into the nucleus via the cNLS nuclear import pathway. The results from this thesis in combination with previous studies provide evidence that the NPnNLS is used by the influenza A virus at two independent occasions: for the nuclear import of incoming vRNPs (this thesis) and of newly synthesized NPs (Neumann et al., 1997; Wang et al., 1997; Weber et al., 1998). This is a good strategy that is both efficient and economical for the virus. The ability to use one NLS for two import processes increases the chance for a successful viral replication, because a host cell that expresses the import receptors for the NPnNLS ensures that both vRNP and NP nuclear import are successful. This also provides yet another example of how multi-functionality is used to achieve a complex viral process, while not compromising the virus' compact size. Furthermore, because it has been demonstrated in this thesis that authentic vRNP uses NPnNLS for nuclear import, future studies can explore the possibility of fluorescently labeling the vRNA of vRNPs in order to visualize the nuclear import process directly. Finally, knowing that the NPnNLS is critical for authentic vRNP nuclear import provides a novel target for anti-viral therapy, and knowing that blocking the NPnNLS with an anti-NPnNLS antibody can efficiently inhibit nuclear import suggests that the anti-viral therapy can be accomplished using small proteins, with the high affinity for the NPnNLS.

REFERENCES

Adam, S. A., Marr, R. S., and Gerace, L. (1990). Nuclear protein import in permeabilized mammalian cells requires soluble cytoplasmic factors. J Cell Biol *111*, 807-816.

Akey, C. W., and Radermacher, M. (1993). Architecture of the Xenopus nuclear pore complex revealed by three-dimensional cryo-electron microscopy. J Cell Biol *122*, 1-19.

Albo, C., Valencia, A., and Portela, A. (1995). Identification of an RNA binding region within the N-terminal third of the influenza A virus nucleoprotein. J Virol *69*, 3799-3806.

Allen, T. D., Cronshaw, J. M., Bagley, S., Kiseleva, E., and Goldberg, M. W. (2000). The nuclear pore complex: mediator of translocation between nucleus and cytoplasm. J Cell Sci *113 (Pt 10)*, 1651-1659.

Area, E., Martin-Benito, J., Gastaminza, P., Torreira, E., Valpuesta, J. M., Carrascosa, J. L., and Ortin, J. (2004). 3D structure of the influenza virus polymerase complex: localization of subunit domains. Proc Natl Acad Sci U S A *101*, 308-313.

Arrese, M., and Portela, A. (1996). Serine 3 is critical for phosphorylation at the N-terminal end of the nucleoprotein of influenza virus A/Victoria/3/75. J Virol *70*, 3385-3391.

Babcock, H. P., Chen, C., and Zhuang, X. (2004). Using single-particle tracking to study nuclear trafficking of viral genes. Biophys J *87*, 2749-2758.

Baudin, F., Bach, C., Cusack, S., and Ruigrok, R. W. (1994). Structure of influenza virus RNP. I. Influenza virus nucleoprotein melts secondary structure in panhandle RNA and exposes the bases to the solvent. Embo J *13*, 3158-3165.

Baudin, F., Petit, I., Weissenhorn, W., and Ruigrok, R. W. (2001). In vitro dissection of the membrane and RNP binding activities of influenza virus M1 protein. Virology *281*, 102-108.

Bauerle, M., Doenecke, D., and Albig, W. (2002). The requirement of H1 histones for a heterodimeric nuclear import receptor. J Biol Chem *277*, 32480-32489.

Beck, M., Forster, F., Ecke, M., Plitzko, J. M., Melchior, F., Gerisch, G., Baumeister, W., and Medalia, O. (2004). Nuclear pore complex structure and dynamics revealed by cryoelectron tomography. Science *306*, 1387-1390.

Bordonne, R. (2000). Functional characterization of nuclear localization signals in yeast Sm proteins. Mol Cell Biol *20*, 7943-7954.

Bui, M., Myers, J. E., and Whittaker, G. R. (2002). Nucleo-cytoplasmic localization of influenza virus nucleoprotein depends on cell density and phosphorylation. Virus Res *84*, 37-44.

Bui, M., Whittaker, G., and Helenius, A. (1996). Effect of M1 protein and low pH on nuclear transport of influenza virus ribonucleoproteins. J Virol *70*, 8391-8401.

Bullido, R., Gomez-Puertas, P., Albo, C., and Portela, A. (2000). Several protein regions contribute to determine the nuclear and cytoplasmic localization of the influenza A virus nucleoprotein. J Gen Virol *81*, 135-142.

Cronshaw, J. M., Krutchinsky, A. N., Zhang, W., Chait, B. T., and Matunis, M. J. (2002). Proteomic analysis of the mammalian nuclear pore complex. J Cell Biol *158*, 915-927.

Cros, J. F., Garcia-Sastre, A., and Palese, P. (2005). An unconventional NLS is critical for the nuclear import of the influenza A virus nucleoprotein and ribonucleoprotein. Traffic *6*, 205-213.

Davey, J., Dimmock, N. J., and Colman, A. (1985). Identification of the sequence responsible for the nuclear accumulation of the influenza virus nucleoprotein in Xenopus oocytes. Cell *40*, 667-675.

Dingwall, C., and Laskey, R. A. (1998). Nuclear import: a tale of two sites. Curr Biol *8*, R922-924.

Doms, R. W., Helenius, A., and White, J. (1985). Membrane fusion activity of the influenza virus hemagglutinin. The low pH-induced conformational change. J Biol Chem *260*, 2973-2981.

Elster, C., Larsen, K., Gagnon, J., Ruigrok, R. W. H., and Baudin, F. (1997). Influenza virus M1 protein binds to RNA through its nuclear localization signal. Journal of General Virology *78*, 1589-1596.

Elton, D., Medcalf, E., Bishop, K., and Digard, P. (1999a). Oligomerization of the influenza virus nucleoprotein: identification of positive and negative sequence elements. Virology *260*, 190-200.

Elton, D., Medcalf, L., Bishop, K., Harrison, D., and Digard, P. (1999b). Identification of amino acid residues of influenza virus nucleoprotein essential for RNA binding. J Virol *73*, 7357-7367.

Fahrenkrog, B., and Aebi, U. (2003). The nuclear pore complex: nucleocytoplasmic transport and beyond. Nat Rev Mol Cell Biol *4*, 757-766.

Fahrenkrog, B., Koser, J., and Aebi, U. (2004). The nuclear pore complex: a jack of all trades? Trends Biochem Sci *29*, 175-182.

Fischer, U., and Luhrmann, R. (1990). An essential signaling role for the m3G cap in the transport of U1 snRNP to the nucleus. Science *249*, 786-790.

Fischer, U., Sumpter, V., Sekine, M., Satoh, T., and Luhrmann, R. (1993). Nucleo-cytoplasmic transport of U snRNPs: definition of a nuclear location signal in the Sm core domain that binds a transport receptor independently of the m3G cap. Embo J *12*, 573-583.

Fodor, E., and Brownlee, G. G. (2002). Influenza virus replication. In Influenza, C. W. Potter, ed. (Elsevier Science B V), pp. 1-29.

Fried, H., and Kutay, U. (2003). Nucleocytoplasmic transport: taking an inventory. Cell Mol Life Sci *60*, 1659-1688.

Garcia-Sastre, A. (2001). Inhibition of interferon-mediated antiviral responses by influenza A viruses and other negative-strand RNA viruses. Virology *279*, 375-384.

Goldfarb, D. S., Corbett, A. H., Mason, D. A., Harreman, M. T., and Adam, S. A. (2004). Importin alpha: a multipurpose nuclear-transport receptor. Trends Cell Biol *14*, 505-514.

Gorlich, D., and Kutay, U. (1999). Transport between the cell nucleus and the cytoplasm. Annu Rev Cell Dev Biol *15*, 607-660.

Gorlich, D., Prehn, S., Laskey, R. A., and Hartmann, E. (1994). Isolation of a protein that is essential for the first step of nuclear protein import. Cell *79*, 767-778.

Harris, A., Forouhar, F., Qiu, S., Sha, B., and Luo, M. (2001). The crystal structure of the influenza matrix protein M1 at neutral pH: M1-M1 protein interfaces can rotate in the oligomeric structures of M1. Virology *289*, 34-44.

Hsu, M. T., Parvin, J. D., Gupta, S., Krystal, M., and Palese, P. (1981). Influenza virus, an RNA virus, synthesizes its messenger RNA in the nucleus of infected cells. Cell *26*, 391-400.

Huang, X., Liu, T., Muller, J., Levandowski, R. A., and Ye, Z. (2001). Effect of influenza virus matrix protein and viral RNA on ribonucleoprotein formation and nuclear export. Virology *287*, 405-416.

Huber, J., Cronshagen, U., Kadokura, M., Marshallsay, C., Wada, T., Sekine, M., and Luhrmann, R. (1998). Snurportin1, an m3G-cap-specific nuclear import receptor with a novel domain structure. Embo J *17*, 4114-4126.

Jakel, S., Albig, W., Kutay, U., Bischoff, F. R., Schwamborn, K., Doenecke, D., and Gorlich, D. (1999). The importin beta/importin 7 heterodimer is a functional nuclear import receptor for histone H1. Embo J *18*, 2411-2423.

Jakel, S., and Gorlich, D. (1998). Importin beta, transportin, RanBP5 and RanBP7 mediate nuclear import of ribosomal proteins in mammalian cells. Embo J *17*, 4491-4502.

Jennings, P. A., Finch, J. T., Winter, G., and Robertson, J. S. (1983). Does the higher order structure of the influenza virus ribonucleoprotein guide sequence rearrangements in influenza viral RNA? Cell *34*, 619-627.

Kemler, I., Whittaker, G., and Helenius, A. (1994). Nuclear import of microinjected influenza virus ribonucleoproteins. Virology *202*, 1028-1033.

Kohler, M., Fiebeler, A., Hartwig, M., Thiel, S., Prehn, S., Kettritz, R., Luft, F. C., and Hartmann, E. (2002). Differential expression of classical nuclear transport factors during cellular proliferation and differentiation. Cell Physiol Biochem *12*, 335-344.

Macara, I. G. (2001). Transport into and out of the nucleus. Microbiol Mol Biol Rev *65*, 570-594, table of contents.

Martin, K., and Helenius, A. (1991a). Nuclear transport of influenza virus ribonucleoproteins: the viral matrix protein (M1) promotes export and inhibits import. Cell *67*, 117-130.

Martin, K., and Helenius, A. (1991b). Transport of incoming influenza virus nucleocapsids into the nucleus. J Virol *65*, 232-244.

Martin-Benito, J., Area, E., Ortega, J., Llorca, O., Valpuesta, J. M., Carrascosa, J. L., and Ortin, J. (2001). Three-dimensional reconstruction of a recombinant influenza virus ribonucleoprotein particle. EMBO Rep *2*, 313-317.

Matlin, K. S., Reggio, H., Helenius, A., and Simons, K. (1981). Infectious entry pathway of influenza virus in a canine kidney cell line. J Cell Biol *91*, 601-613.

Medcalf, L., Poole, E., Elton, D., and Digard, P. (1999). Temperature-sensitive lesions in two influenza A viruses defective for replicative transcription disrupt RNA binding by the nucleoprotein. J Virol *73*, 7349-7356.

Melen, K., Fagerlund, R., Franke, J., Kohler, M., Kinnunen, L., and Julkunen, I. (2003). Importin alpha nuclear localization signal binding sites for STAT1, STAT2, and influenza A virus nucleoprotein. J Biol Chem *278*, 28193-28200.

Mukaigawa, J., and Nayak, D. P. (1991). Two signals mediate nuclear localization of influenza virus (A/WSN/33) polymerase basic protein 2. J Virol *65*, 245-253.

Murti, K. G., Webster, R. G., and Jones, I. M. (1988). Localization of RNA polymerases on influenza viral ribonucleoproteins by immunogold labeling. Virology *164*, 562-566.

Nagata, K., Takizawa, N., Haruki, H., Mibayashi, M., and Watanabe, K. (2002). Nuclear import and export of influenza virus ribonucleoprotein complexes. In Recent advances in influenza virus research, Y. Hayase, ed. (Research Signpost), pp. 15-43.

Nath, S. T., and Nayak, D. P. (1990). Function of two discrete regions is required for nuclear localization of polymerase basic protein 1 of A/WSN/33 influenza virus (H1 N1). Mol Cell Biol *10*, 4139-4145.

Neumann, G., Castrucci, M. R., and Kawaoka, Y. (1997). Nuclear import and export of influenza virus nucleoprotein. J Virol *71*, 9690-9700.

Neumann, G., Hughes, M. T., and Kawaoka, Y. (2000). Influenza A virus NS2 protein mediates vRNP nuclear export through NES-independent interaction with hCRM1. Embo J *19*, 6751-6758.

Nieto, A., de la Luna, S., Barcena, J., Portela, A., and Ortin, J. (1994). Complex structure of the nuclear translocation signal of influenza virus polymerase PA subunit. J Gen Virol *75 (Pt 1)*, 29-36.

O'Neill, R. E., Jaskunas, R., Blobel, G., Palese, P., and Moroianu, J. (1995). Nuclear import of influenza virus RNA can be mediated by viral nucleoprotein and transport factors required for protein import. J Biol Chem *270*, 22701-22704.

O'Neill, R. E., Talon, J., and Palese, P. (1998). The influenza virus NEP (NS2 protein) mediates the nuclear export of viral ribonucleoproteins. Embo J *17*, 288-296.

Pante, N. (2004). Nuclear pore complex structure: unplugged and dynamic pores. Dev Cell *7*, 780-781.

Pante, N., and Aebi, U. (1994). Toward the molecular details of the nuclear pore complex. J Struct Biol *113*, 179-189.

Pante, N., and Aebi, U. (1996a). Molecular dissection of the nuclear pore complex. Crit Rev Biochem Mol Biol *31*, 153-199.

Pante, N., and Aebi, U. (1996b). Toward the molecular dissection of protein import into nuclei. Curr Opin Cell Biol *8*, 397-406.

Pante, N., and Kann, M. (2002). Nuclear pore complex is able to transport macromolecules with diameters of about 39 nm. Mol Biol Cell *13*, 425-434.

Paschal, B. M., and Gerace, L. (1995). Identification of NTF2, a cytosolic factor for nuclear import that interacts with nuclear pore complex protein p62. J Cell Biol *129*, 925-937.

Pemberton, L. F., and Paschal, B. M. (2005). Mechanisms of receptor-mediated nuclear import and nuclear export. Traffic *6*, 187-198.

Pollard, V. W., Michael, W. M., Nakielny, S., Siomi, M. C., Wang, F., and Dreyfuss, G. (1996). A novel receptor-mediated nuclear protein import pathway. Cell *86*, 985-994.

Pons, M. W., Schulze, I. T., and Hirst, G. K. (1969). Isolation and characterization of the ribonucleoprotein of influenza virus. Virology *39*, 250-259.

Rochovansky, O. M. (1976). RNA synthesis by ribonucleoprotein-polymerase complexes isolated from influenza virus. Virology *73*, 327-338.

Rout, M. P., Aitchison, J. D., Suprapto, A., Hjertaas, K., Zhao, Y., and Chait, B. T. (2000). The yeast nuclear pore complex: composition, architecture, and transport mechanism. J Cell Biol *148*, 635-651.

Sekimoto, T., Imamoto, N., Nakajima, K., Hirano, T., and Yoneda, Y. (1997). Extracellular signal-dependent nuclear import of Stat1 is mediated by nuclear pore-targeting complex formation with NPI-1, but not Rch1. Embo J *16*, 7067-7077.

Sieczkarski, S. B., and Whittaker, G. R. (2002). Influenza virus can enter and infect cells in the absence of clathrin-mediated endocytosis. J Virol *76*, 10455-10464.

Stoffler, D., Feja, B., Fahrenkrog, B., Walz, J., Typke, D., and Aebi, U. (2003). Cryo-electron tomography provides novel insights into nuclear pore architecture: implications for nucleocytoplasmic transport. J Mol Biol *328*, 119-130.

Toyoda, T., Hara, K., Kashiwagi, T., Iwahashi, J., Yoshino, H., and Hamada, N. (2002). Molecular dissection of the transcription and replication machinery of influenza virus. In Recent advances in influenza virus research, Y. Hayase, ed. (Research Signpost), pp. 1-13.

Tsuji, L., Takumi, T., Imamoto, N., and Yoneda, Y. (1997). Identification of novel homologues of mouse importin alpha, the alpha subunit of the nuclear pore-targeting complex, and their tissue-specific expression. FEBS Lett *416*, 30-34.

Wang, P., Palese, P., and O'Neill, R. E. (1997). The NPI-1/NPI-3 (karyopherin alpha) binding site on the influenza a virus nucleoprotein NP is a nonconventional nuclear localization signal. J Virol *71*, 1850-1856.

Weber, F., Kochs, G., Gruber, S., and Haller, O. (1998). A classical bipartite nuclear localization signal on Thogoto and influenza A virus nucleoproteins. Virology *250*, 9-18.

Wente, S. R. (2000). Gatekeepers of the nucleus. Science *288*, 1374-1377.

Whittaker, G., Bui, M., and Helenius, A. (1996a). Nuclear trafficking of influenza virus ribonuleoproteins in heterokaryons. J Virol *70*, 2743-2756.

Whittaker, G., Bui, M., and Helenius, A. (1996b). The role of nuclear import and export in influenza virus infection. Trends Cell Biol *6*, 67-71.

Yang, Q., Rout, M. P., and Akey, C. W. (1998). Three-dimensional architecture of the isolated yeast nuclear pore complex: functional and evolutionary implications. Mol Cell *1*, 223-234.

Ye, Z., Liu, T., Offringa, D. P., McInnis, J., and Levandowski, R. A. (1999). Association of influenza virus matrix protein with ribonucleoproteins. J Virol *73*, 7467-7473.

APPENDIX

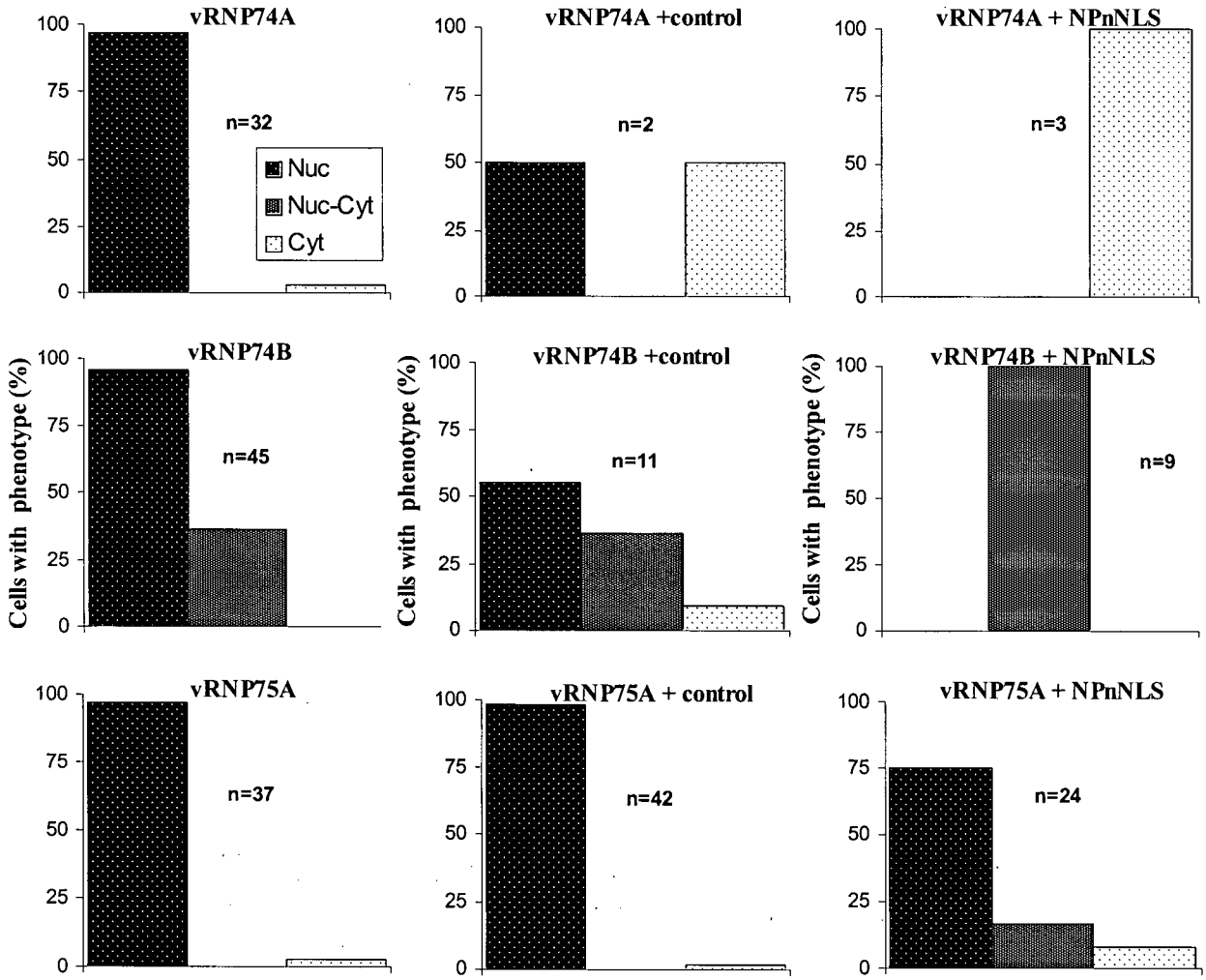

Appendix 1: Nuclear import distribution of vRNP for the competition inhibition experiments, for three independent experiments. vRNP nuclear import in the presence of PBS (vRNP) or specific competitors: control peptide (vRNP + control) and NPnNLS peptide (vRNP + NPnNLS) were studied by microinjection in live HeLa cells and visualized by immunofluorescence microscopy using a NP monoclonal antibody. Peptides were mixed with vRNP at 10:1 peptide:NP molar ratio. Three independent experiments were done, using vRNP from three different purifications (purification N^{o} 74A, 74B, and 75A). Experiments using the same vRNP purification were done together, with cells seeded onto the same coverslip. vRNP localization was quantified for each experiment. vRNPs were found either predominantly in the nucleus (Nuc), equally distributed between the nucleus and the cytoplasm (Nuc-Cyt) or predominantly distributed in the cytoplasm (Cyt). The number of cells that could be visualized by immunofluorescence microscopy is indicated (n).

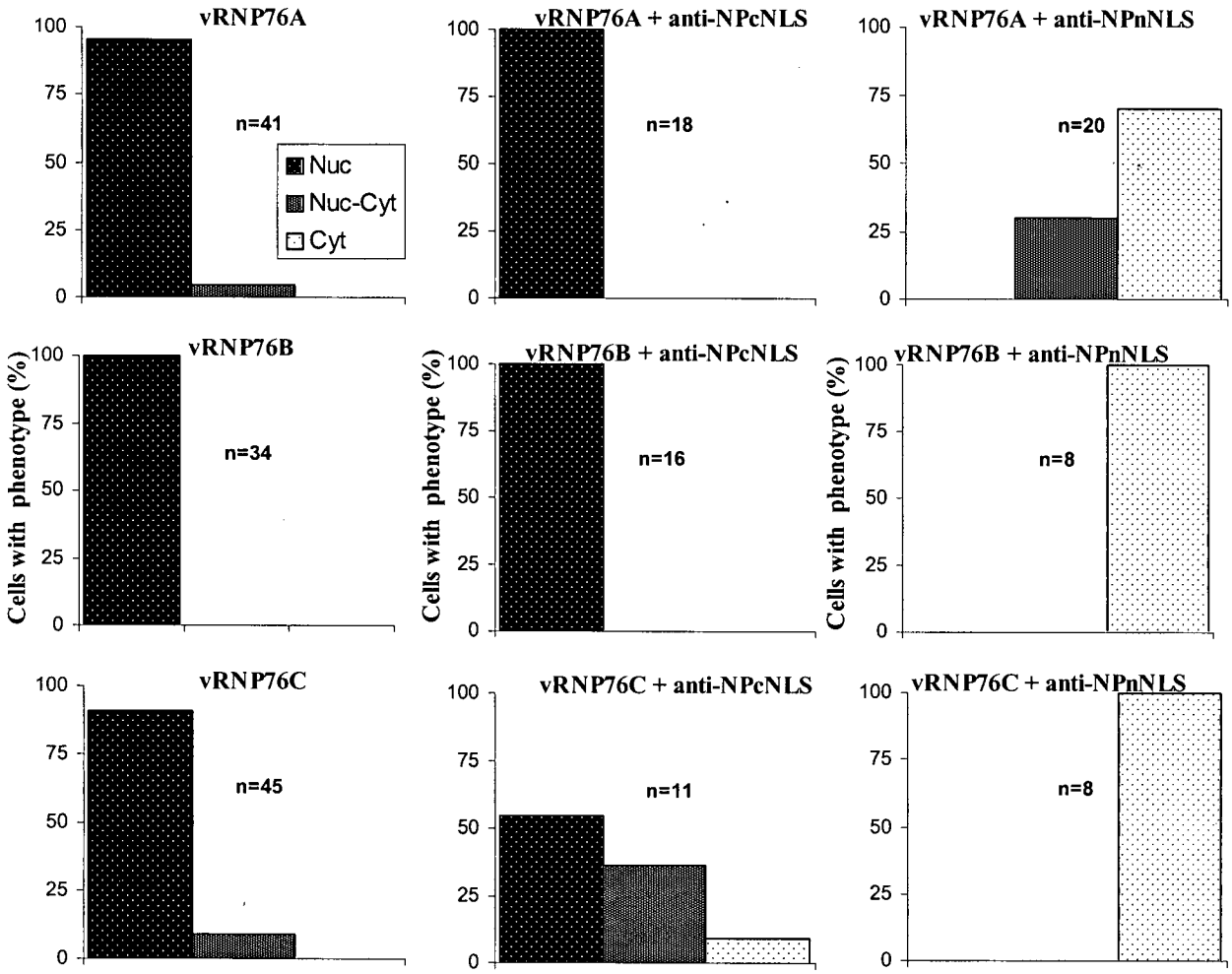

Appendix 2: Nuclear import distribution of vRNP for the antibody inhibition experiments, for three independent experiments. vRNP nuclear import in the presence of PBS (vRNP) or specific antibodies: anti-NPcNLS antibodies (vRNP + anti-NPcNLS) and anti-NPnNLS antibodies (vRNP + anti-NPnNLS) were studied by microinjection in live HeLa cells and visualized by immunofluorescence microscopy using a NP monoclonal antibody. Antibodies were incubated with vRNP at 1:1 antibody:NP molar ratio at 4°C for 1 hour. Three independent experiments were done, using vRNP from three different purifications (purification N° 76A, 76B, and 76C). Experiments using the same vRNP purification were done together, with cells seeded onto the same coverslip. vRNP localization was quantified for each experiment. vRNPs were found either predominantly in the nucleus (Nuc), equally distributed between the nucleus and the cytoplasm (Nuc-Cyt) or predominantly distributed in the cytoplasm (Cyt). The number of cells that could be visualized by immunofluorescence microscopy is indicated (n).

Appendix 3: Statistics analysis of antibody inhibition experiments. Quantitative data from three antibody inhibition experiments (Experiment 1-3) were each compared with the control: anti-NPnNLS antibody with PBS (left) and anti-NPcNLS antibody with PBS (right). The cell phenotypes were re-categorized into two phenotypes, nuclear and non nuclear, and the frequency of cells falling into the two phenotypes are indicated. Chi squared (χ^2) likelihood ratio test, χ^2 Pearson test, two-tailed Fisher's exact test were performed and their calculated values along with their probability (p) are reported. A two-tailed student t test was also tested for the average of all three experiments. The hypothesis (Ho): cell phenotypes were the same for vRNPs in the presence or the absence of the specified antibody, was tested. The result determined for each hypothesis is reported.

Experiment 1

	Nuclear	Non Nuclear	N
PBS	0.95	0.05	41
Anti-NPnNLS	0.00	1.00	20
N	39	22	61

χ^2 Likelihood Ratio	χ^2 Pearson	$p>\chi^2$ Likelihood Ratio	$p>\chi^2$ Pearson
63.78	52.749	<0.0001	<0.001

Two-tailed Fisher's Exact Test: <0.0001

H_o rejected

Experiment 2

	Nuclear	Non Nuclear	N
PBS	1.00	0.00	34
Anti-NPnNLS	0.00	1.00	8
N	34	8	42

χ^2 Likelihood Ratio	χ^2 Pearson	$p>\chi^2$ Likelihood Ratio	$p>\chi^2$ Pearson
40.90	42	<0.0001	<0.001

Two-tailed Fisher's Exact Test: <0.0001

H_o rejected

Experiment 3

	Nuclear	Non Nuclear	N
PBS	0.91	0.09	45
Anti-NPnNLS	0.00	1.00	8
N	41	12	53

χ^2 Likelihood Ratio	χ^2 Pearson	$p>\chi^2$ Likelihood Ratio	$p>\chi^2$ Pearson
29.70	32.193	<0.0001	<0.001

Two-tailed Fisher's Exact Test: <0.0001

H_o rejected

All Experiments

	Nuclear	Non Nuclear	N
PBS	0.95	0.00	120
Anti-NPnNLS	0.05	1.00	36
N	114	42	156

χ^2 Likelihood Ratio	χ^2 Pearson	$p>\chi^2$ Likelihood Ratio	$p>\chi^2$ Pearson
134.09	127.029	<0.0001	<0.001

Two-tailed Fisher's Exact Test: <0.0001

Two-tailed student T Test: <0.0001 H_o rejected

Experiment 1

	Nuclear	Non Nuclear	N
PBS	0.95	0.05	41
Anti-NPcNLS	1.00	0.00	18
N	57	2	59

χ^2 Likelihood Ratio	χ^2 Pearson	$p>\chi^2$ Likelihood Ratio	$p>\chi^2$ Pearson
1.49	0.909	0.2228	0.3404

Two-tailed Fisher's Exact Test: 1.00

H_o not rejected

Experiment 2

	Nuclear	Non Nuclear	N
PBS	1.00	0.00	34
Anti-NPcNLS	1.00	0.00	17
N	51	0	51

χ^2 Likelihood Ratio	χ^2 Pearson	$p>\chi^2$ Likelihood Ratio	$p>\chi^2$ Pearson
0.00	0	0.00	0.00

Two-tailed Fisher's Exact Test: Division of 0

Experiment 3

	Nuclear	Non Nuclear	N
PBS	0.91	0.09	45
Anti-NPcNLS	0.55	0.45	11
N	47	9	56

χ^2 Likelihood Ratio	χ^2 Pearson	$p>\chi^2$ Likelihood Ratio	$p>\chi^2$ Pearson
7.22	8.762	0.0072	0.0031

Two-tailed Fisher's Exact Test: 0.01

H_o rejected

All Experiments

	Nuclear	Non Nuclear	N
PBS	0.95	0.00	120
Anti-NPcNLS	0.89	0.11	46
N	155	11	166

χ^2 Likelihood Ratio	χ^2 Pearson	$p>\chi^2$ Likelihood Ratio	$p>\chi^2$ Pearson
1.69	1.852	0.1932	0.1736

Two-tailed Fisher's Exact Test: 0.18

Two-tailed student T Test: 0.56 H_o not rejected